The Abdus Salam International Centre for Theoretical Physics

United Nations Educational, Scientific and Cultural Organization

IAEA International Atomic Energy Agency

2354-5

Summer School on Cosmology

16 - 27 July 2012

Large-scale Structure - Lecture Note 1

R. Scoccimarro

NYU, New York

Large-Scale Structure Lectures:

- Brief comments on shape of primordial spectrum
- Linear evolution of fluctuations
- Nonlinear Standard Perturbation Theory (SPT)
- Generation of non-Gaussianity (tree-level) and loop corrections in P(k)
- Problems with SPT, Renormalized PT (RPT)
- Galaxy Bias (local and nonlocal), Redshift-Space distortions

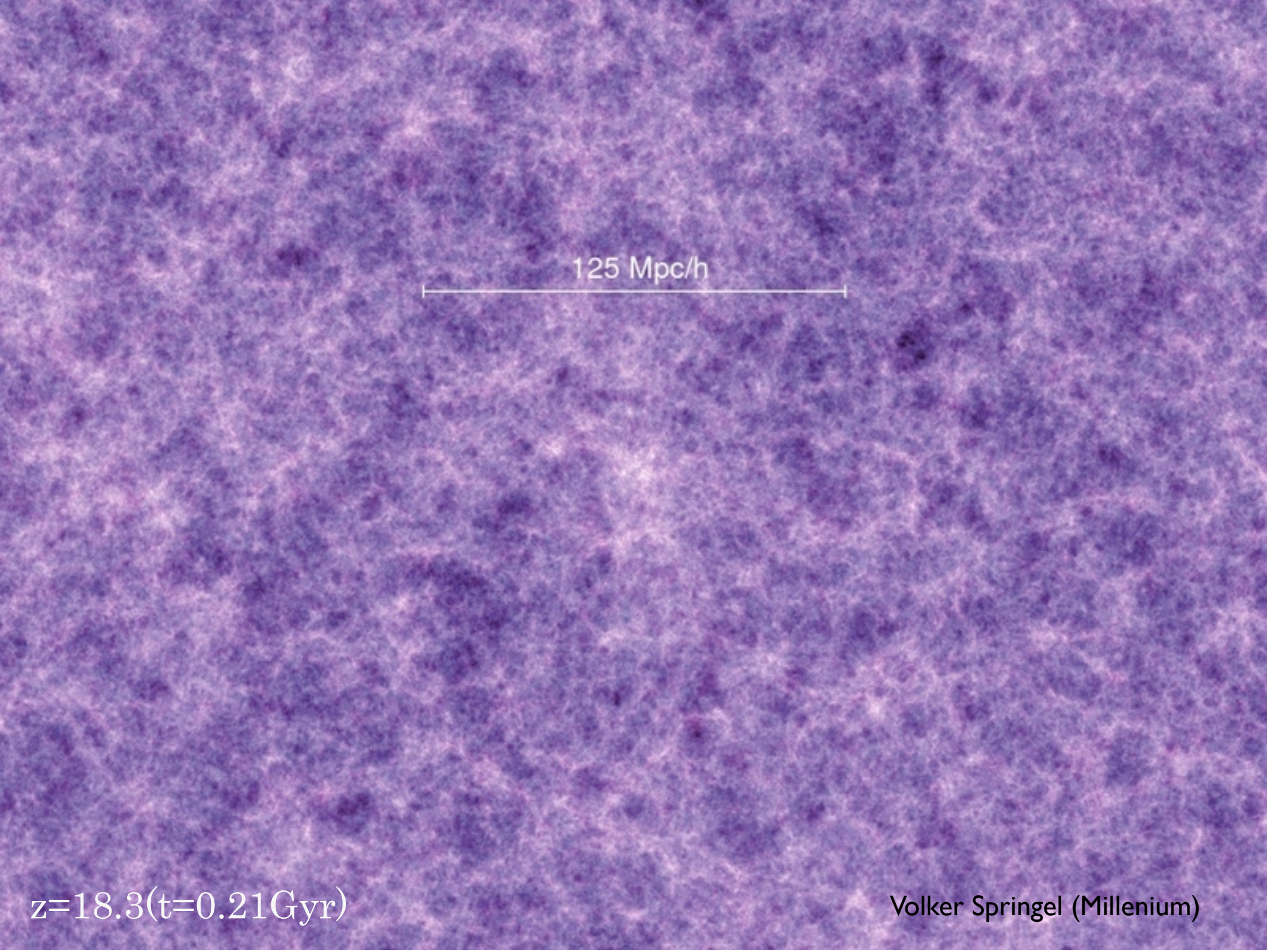
125 Mpc/h
z=18.3(t=0.21Gyr)
Volker Springel (Millenium)

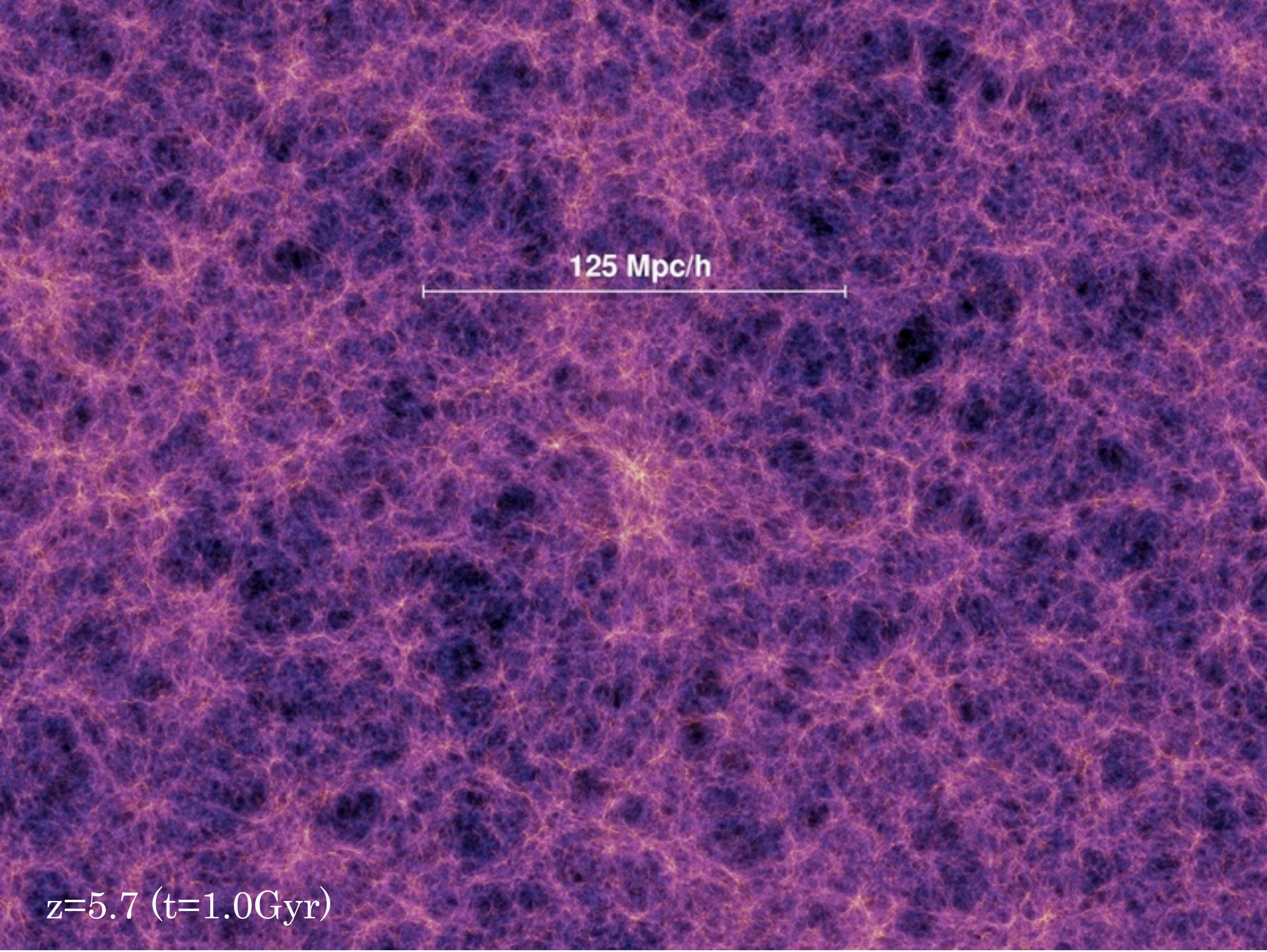
125 Mpc/h
z=5.7 (t=1.0Gyr)

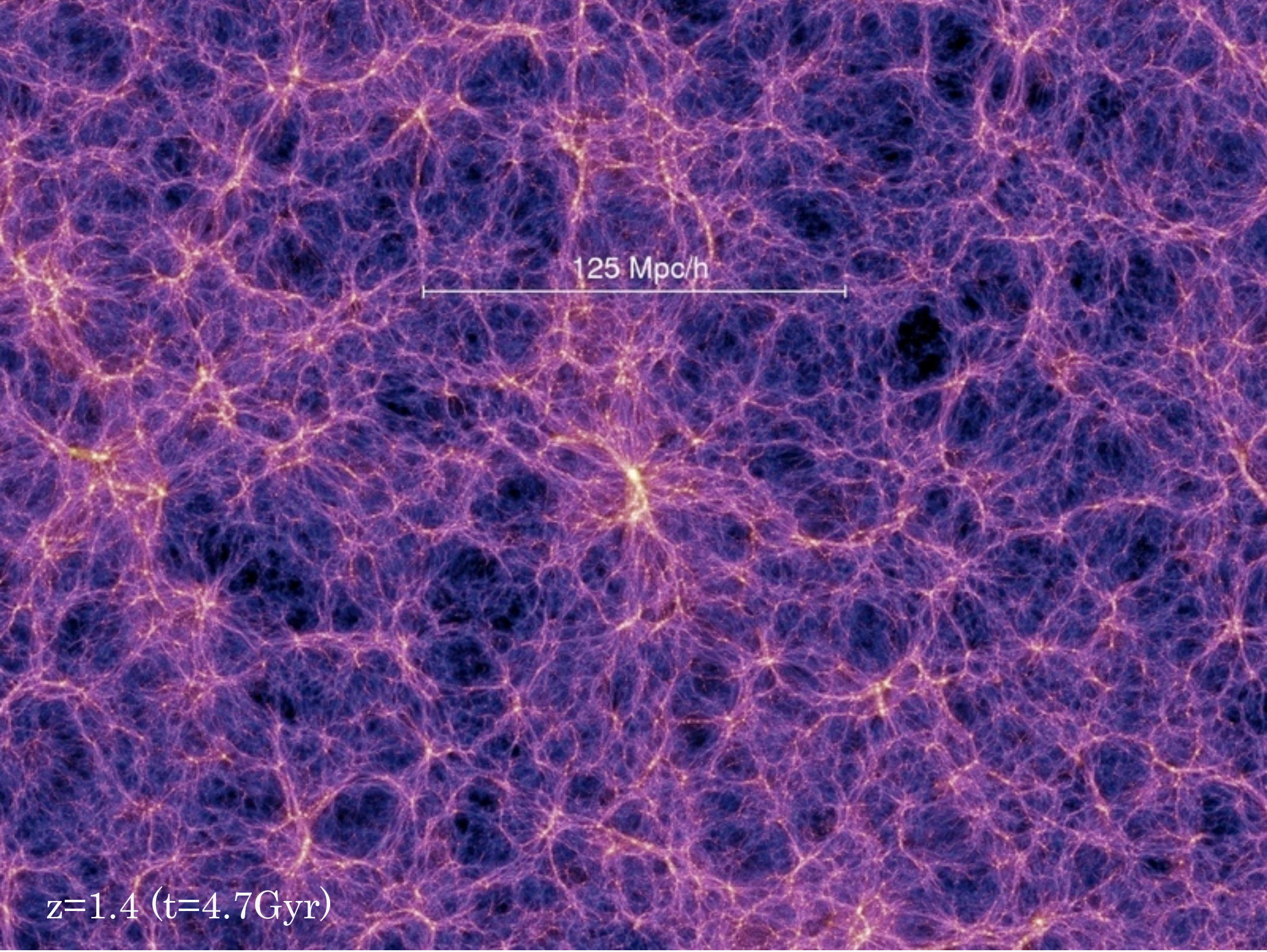
125 Mpc/h
z=1.4 (t=4.7Gyr)

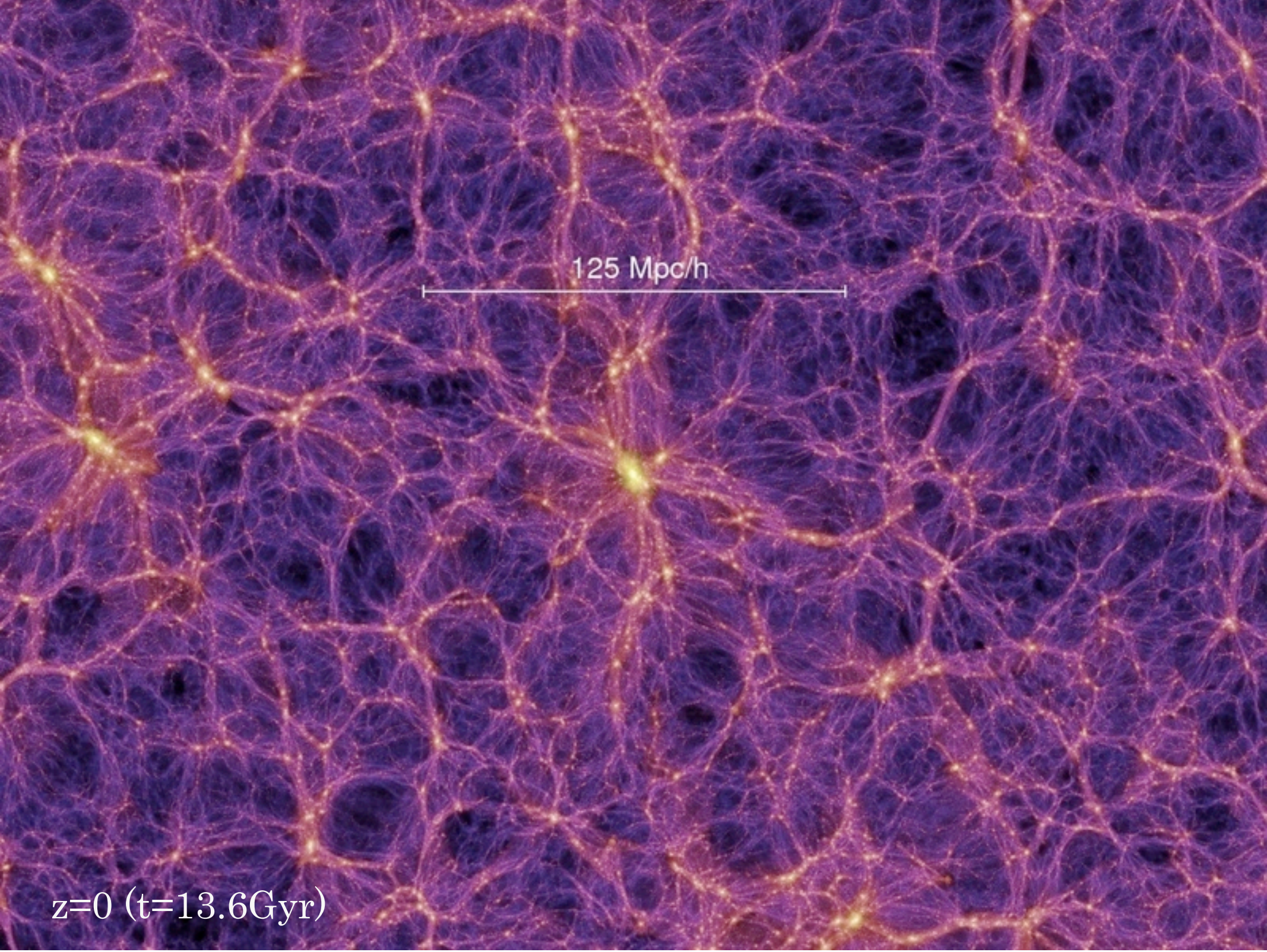
125 Mpc/h
z=0 (t=13.6Gyr)

Gaussian Fluctuations become non-Gaussian

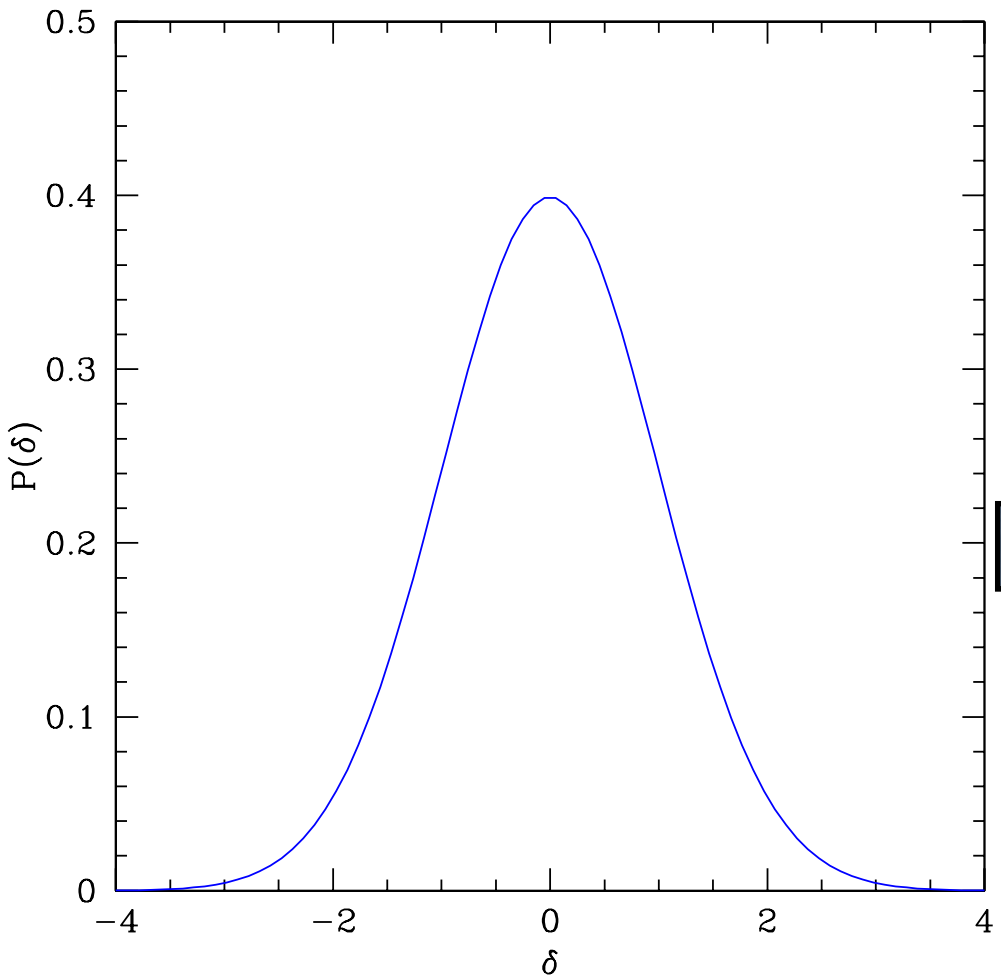

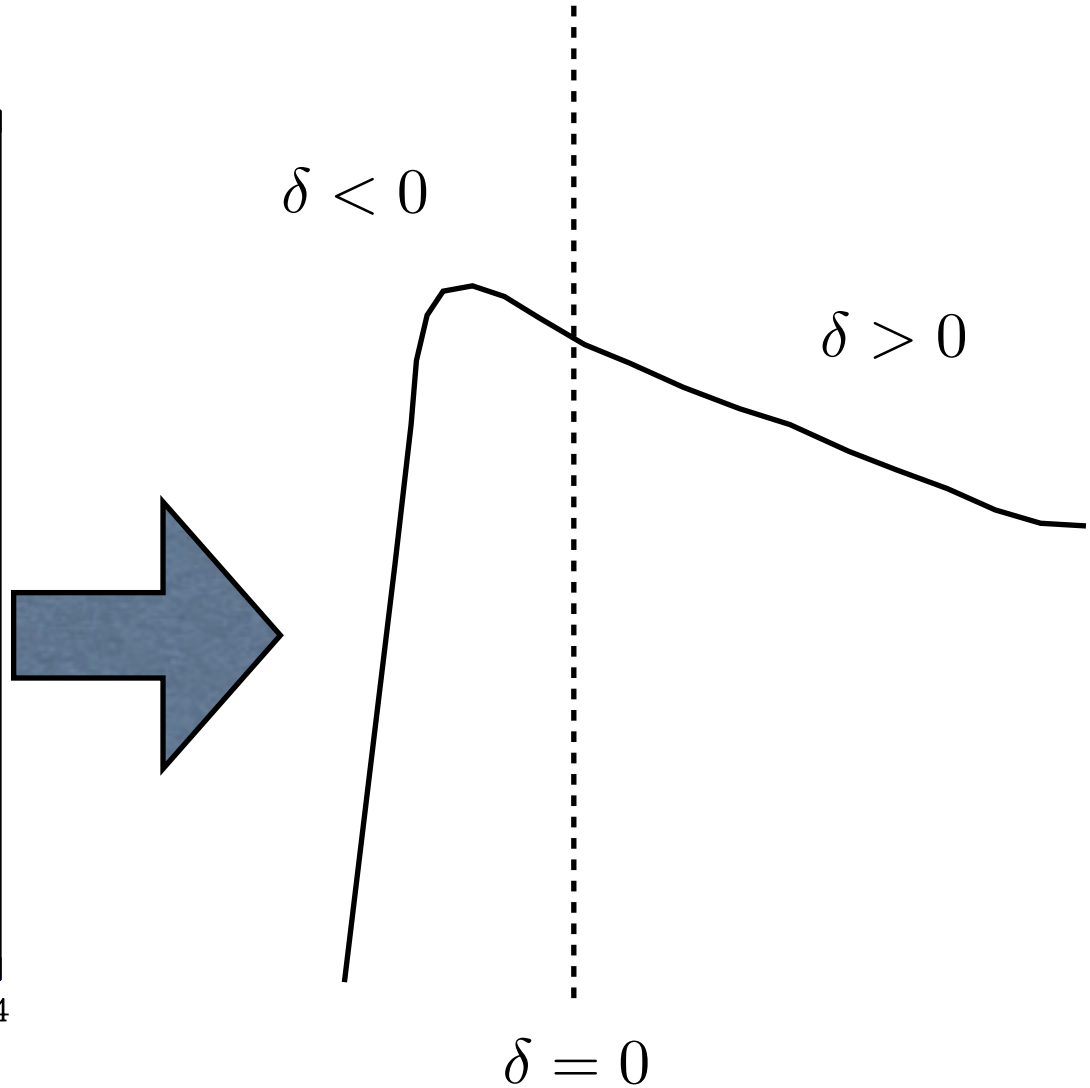

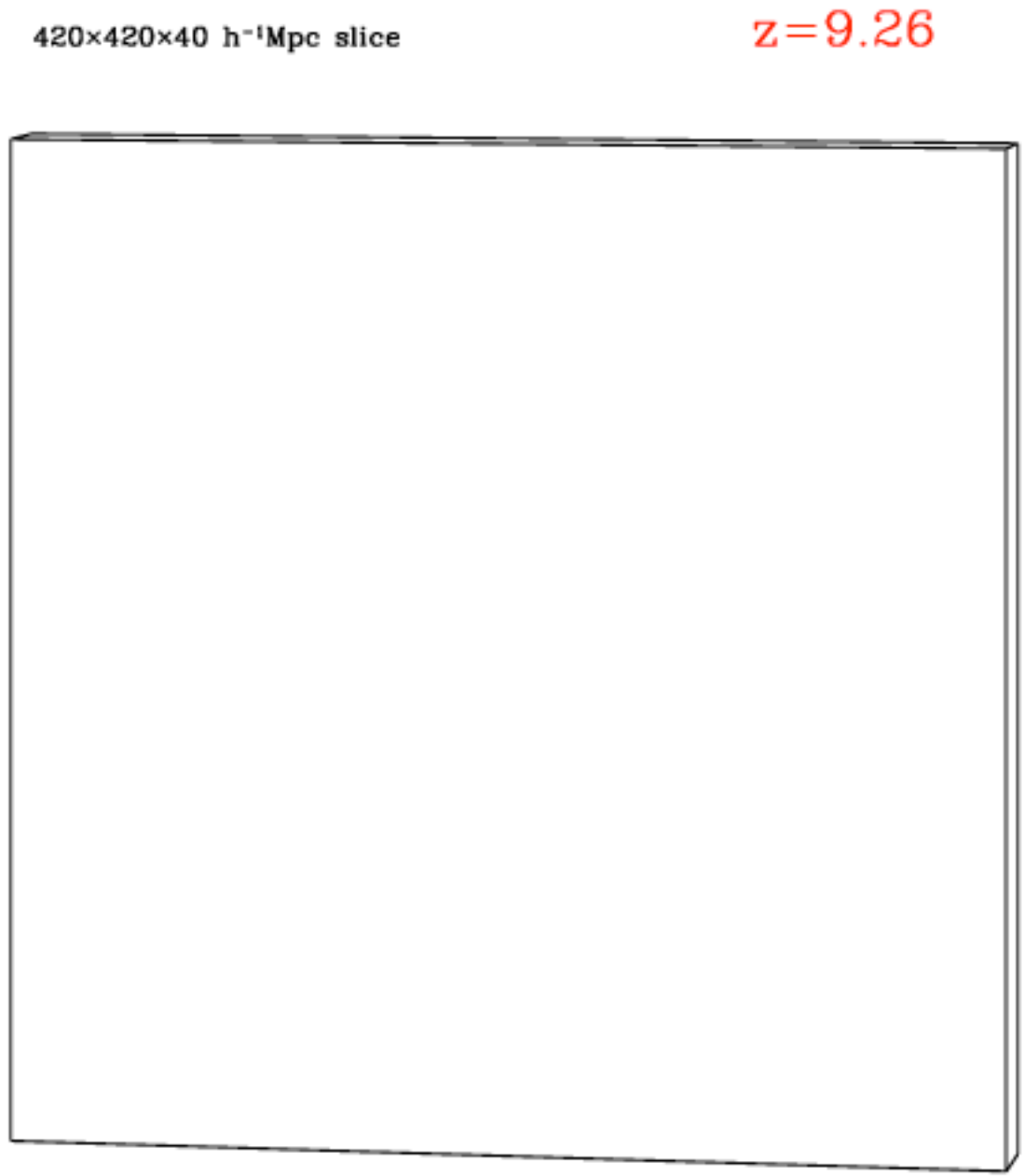

Andreas Berlind (Las Damas)

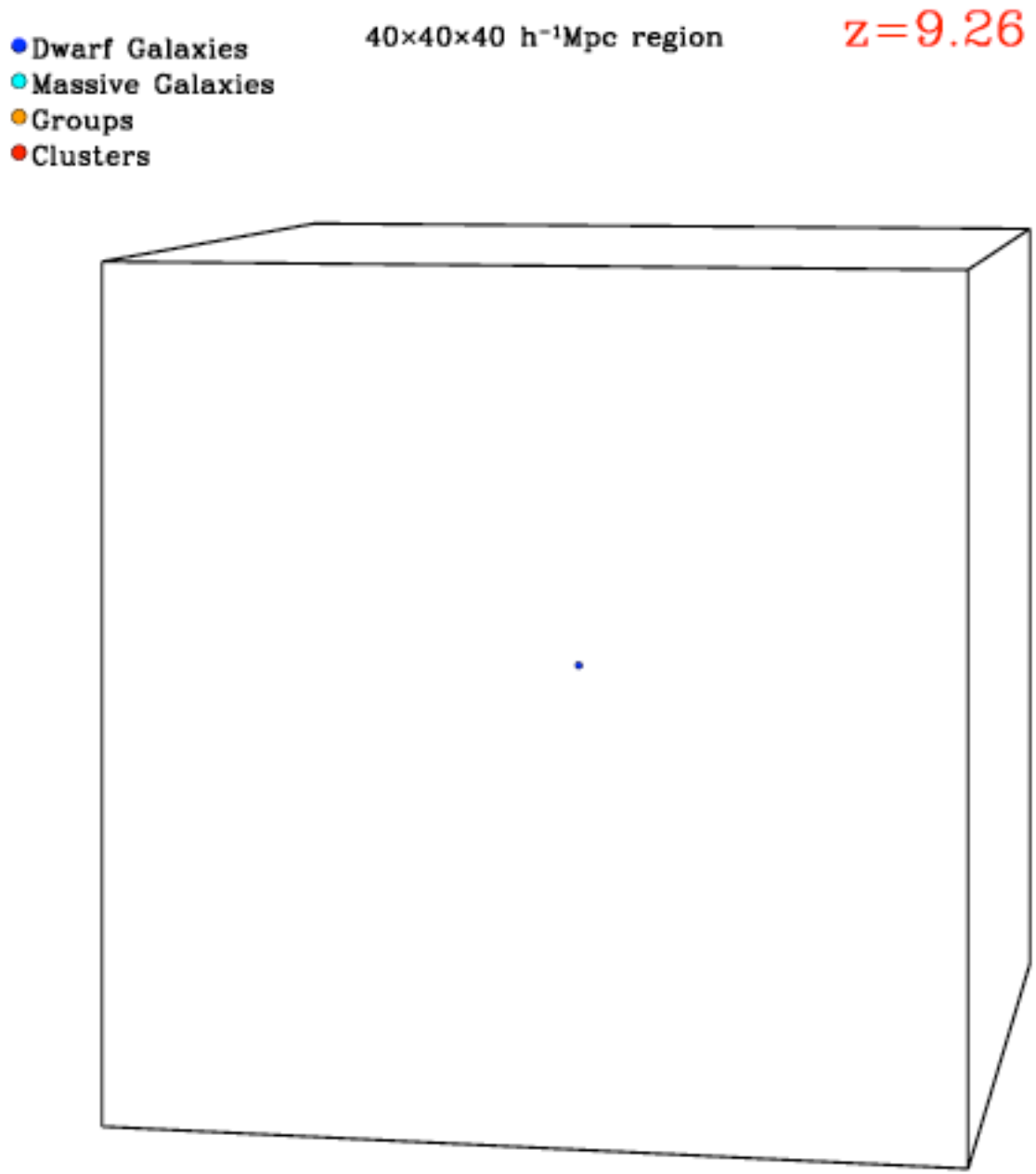

Andreas Berlind (Las Damas)

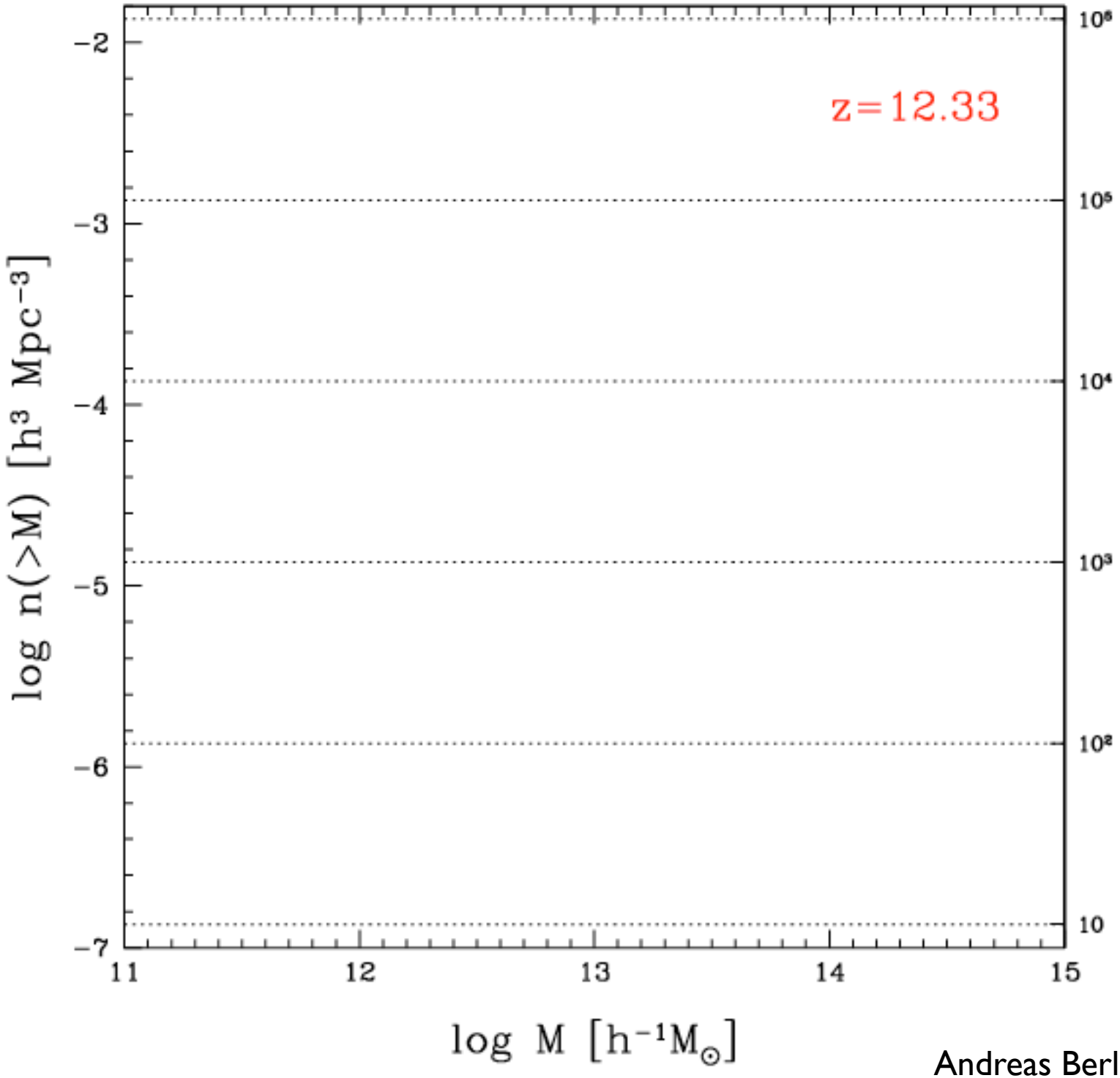

Andreas Berlind (Las Damas)

Homogeneous and Isotropic Universe

Coordinates:

$$\mathbf{r}_{\rm phys} = a(t)\ \mathbf{r}$$

Physical Coordinate

Scale Factor

Comoving Coordinate

Friedmann Equations

Metric:

$$ds^2 = dt^2 - a^2(t)\left[\frac{dr^2}{1-kr^2} - r^2 d\Omega\right] = a^2(\tau)\left[d\tau^2 - \frac{dr^2}{1-kr^2} - r^2 d\Omega\right]$$

Conformal Time

$k = 0(\text{flat}), 1(\text{closed}), -1(\text{open})$

Symmetries (plus no bulk viscosity) require for each component a stress-energy (in rest frame of fluid):

$$T^{\mu}_{\nu} = \mathrm{diag}(\rho, -p, -p, -p)$$

"Equation of state": $p = w\ \rho$

Friedmann Equations

$$\left(\frac{\dot{a}}{a}\right)^2 = H^2 = \frac{8\pi G}{3}\Big(\rho_{\mathrm{DM}} + \rho_{\mathrm{DE}} + \rho_{\mathrm{RAD}}\Big)$$

$$\frac{\ddot{a}}{a} = -\frac{4\pi G}{3}\sum_i (\rho + 3p)_i$$

Stress-Energy Conservation I. Background

$$T^{\mu\nu}_{;\nu} = 0 \quad \Rightarrow \quad d(\rho a^3) = -p d(a^3)$$

$$\rho \propto a^{-3(1+w)}$$

$$\text{RAD}: \quad w = \frac{1}{3} \qquad \rho \propto a^{-4}$$

$$\text{DM}: \quad w = 0 \qquad \rho \propto a^{-3}$$

$$\text{VAC}: \quad w = -1 \qquad \rho \propto \text{const.}$$

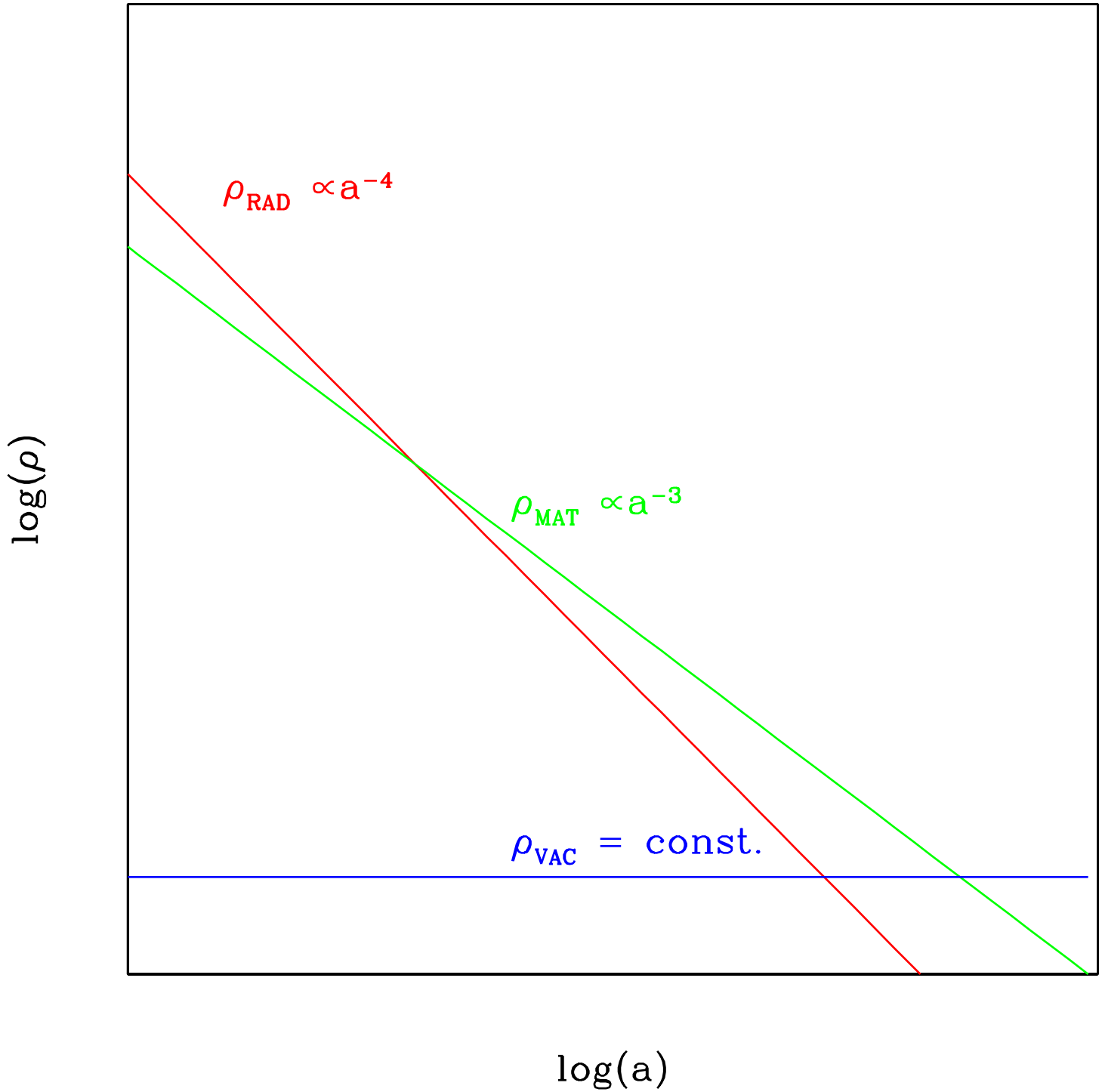
$\rho_{RAD} \propto a^{-4}$
$\rho_{MAT} \propto a^{-3}$
ρ_{VAC} = const.
log(ρ)
log(a)

$$\text{RAD}: \quad \rho \propto a^{-4} \rightarrow H^2 \propto a^{-4} \rightarrow a(t) \propto t^{1/2}$$

$$\text{Hubble time/radius} = H^{-1} \propto \frac{1}{t} \propto a^2(t)$$

$$\text{MAT}: \quad \rho \propto a^{-3} \rightarrow H^2 \propto a^{-3} \rightarrow a(t) \propto t^{2/3}$$

$$H^{-1} \propto \frac{1}{t} \propto a^{3/2}(t)$$

$$\text{VAC}: \quad H^{-1} = \text{const.} \rightarrow a(t) \propto \mathrm{e}^{Ht}$$

Describing Fluctuations at Sub-Horizon Scales

Density Field:

$$\rho(\mathbf{x}, t) = \bar{\rho}(t)\ [1 + \delta(\mathbf{x}, t)]$$

Spatial average

Fluctuations

Stress-Energy Conservation

Velocity Field:

$$\mathbf{V} = H(t)\,\mathbf{r} + \mathbf{v}(\mathbf{x}, t)$$

Hubble Flow

Fluctuations

Stress-Energy Conservation II. Fluctuations

$$\delta T^{\mu\nu}_{;\nu} = 0$$

$$\frac{\partial \delta}{\partial \tau} + \nabla \cdot [(1+\delta)\mathbf{v}] = 0$$

$$\frac{\partial \mathbf{v}}{\partial \tau} + \mathcal{H}\mathbf{v} + \mathbf{v} \cdot \nabla \mathbf{v} = -\nabla \Phi$$

$$\text{Poisson } (\Omega_m = 1): \quad \nabla^2 \Phi = \frac{3}{2}\mathcal{H}^2 \delta$$

$$\nabla \cdot \mathbf{v} \equiv -\mathcal{H}\Theta, \qquad \mathcal{H} \equiv Ha$$

Linear Evolution of Fluctuations

Linearize in perturbation amplitudes

$$\Psi_a \equiv \begin{pmatrix} \delta \\ \Theta \end{pmatrix} = G_{ab}\ \phi_b$$

$$G_{ab} = \frac{a}{5}\begin{pmatrix} 3 & 2 \\ 3 & 2 \end{pmatrix} - \frac{a^{-3/2}}{5}\begin{pmatrix} -2 & 2 \\ 3 & -3 \end{pmatrix}$$

The two eigenmodes correspond to growing and decaying modes

During RAD era, equations for the DM fluctuations can be obtained from MAT by changing,

$$\bar{\rho} \longrightarrow \bar{\rho} + \bar{p}$$

The presence of substantial radiation makes the universe expand so fast that density perturbations only grow as

$$\delta(\mathbf{k}) \sim \ln(a)$$

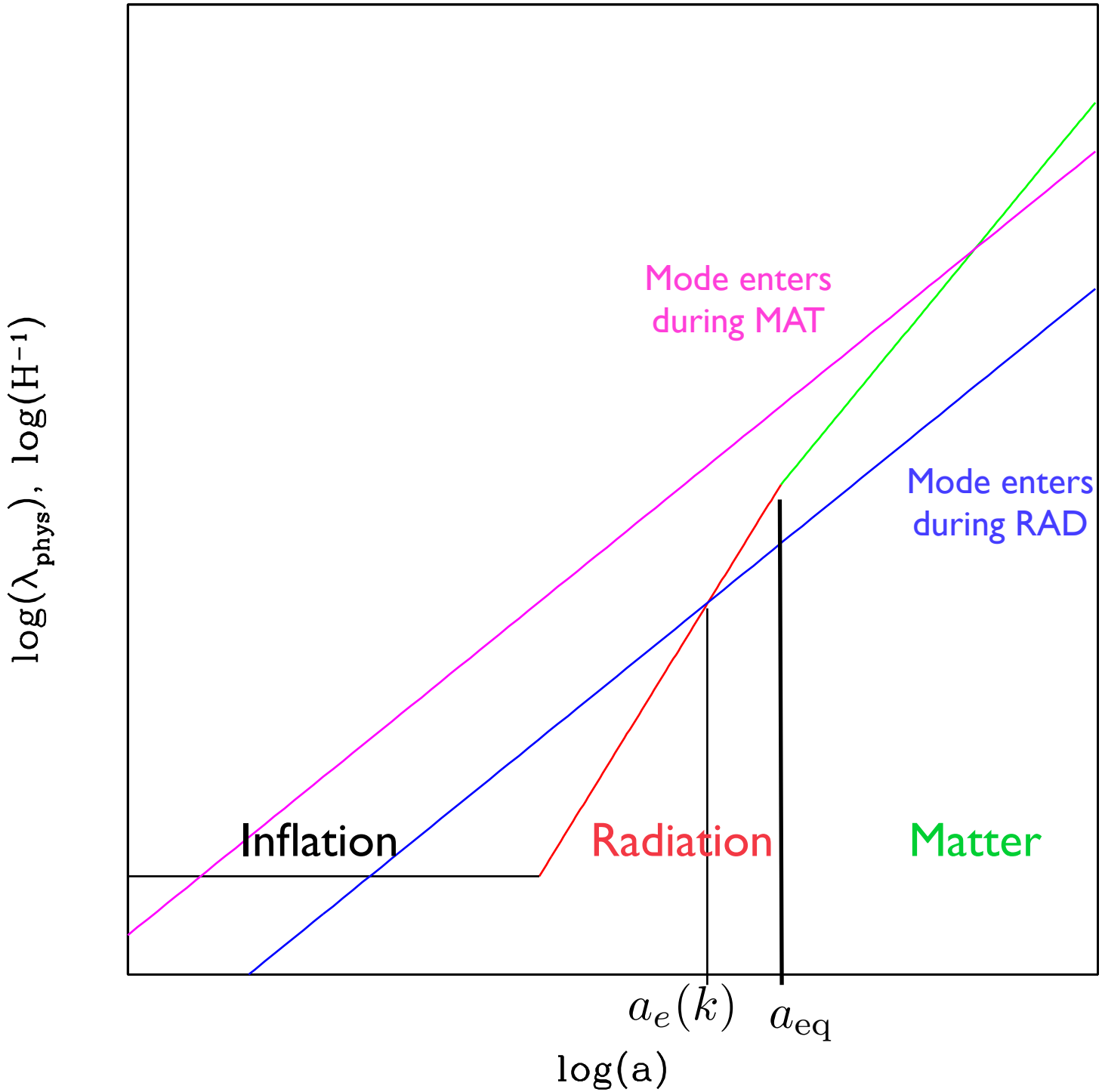
Mode enters
during MAT
Mode enters
during RAD
Inflation
Radiation
Matter
$a_e(k)$
$a_{\rm eq}$
$\log(a)$
$\log(\lambda_{\rm phys}),\ \log(H^{-1})$

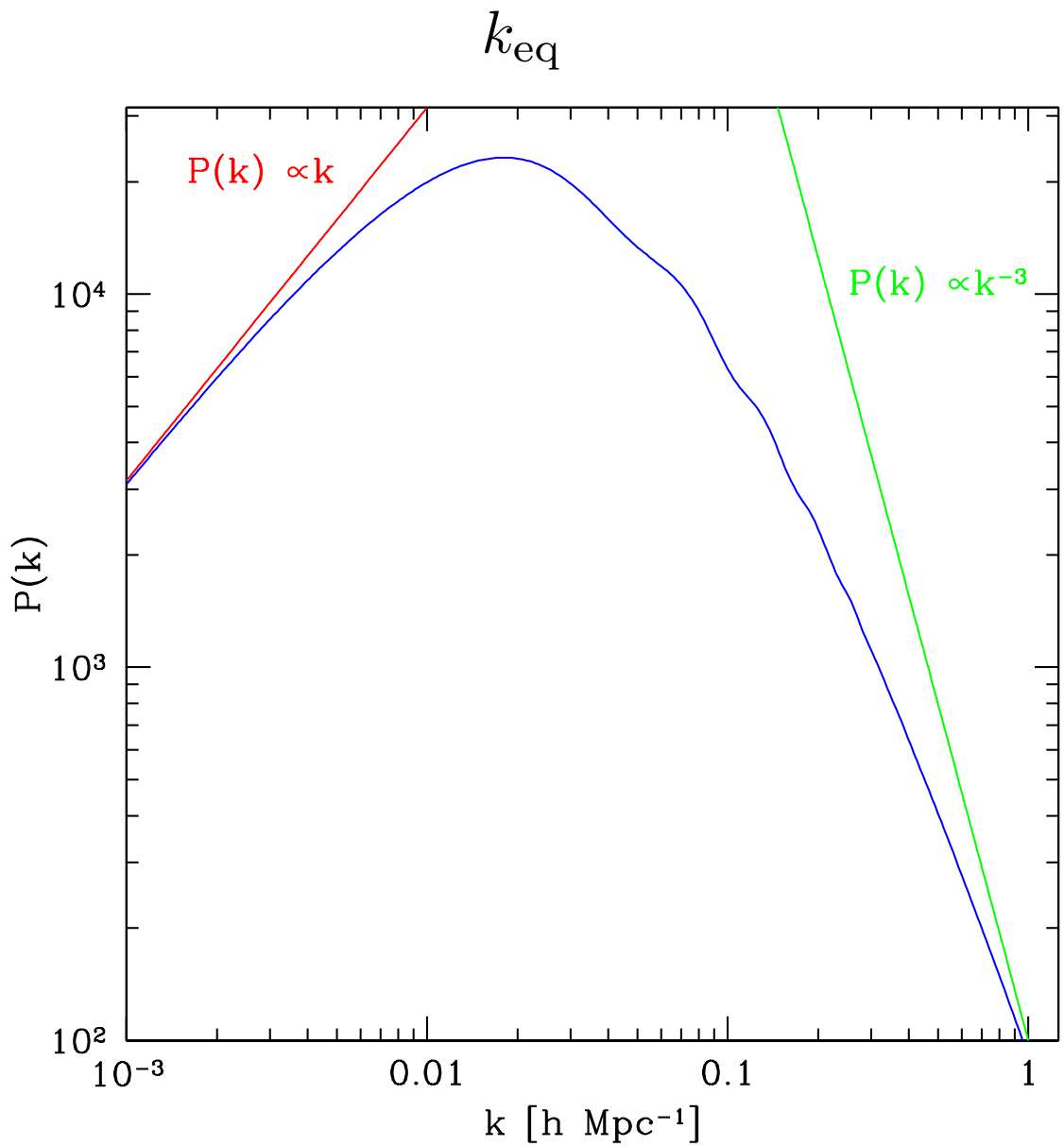
$k_{\rm eq}$
P(k) ∝k
P(k) ∝k⁻³
10⁴
10³
10²
P(k)
10⁻³
0.01
0.1
1
k [h Mpc⁻¹]

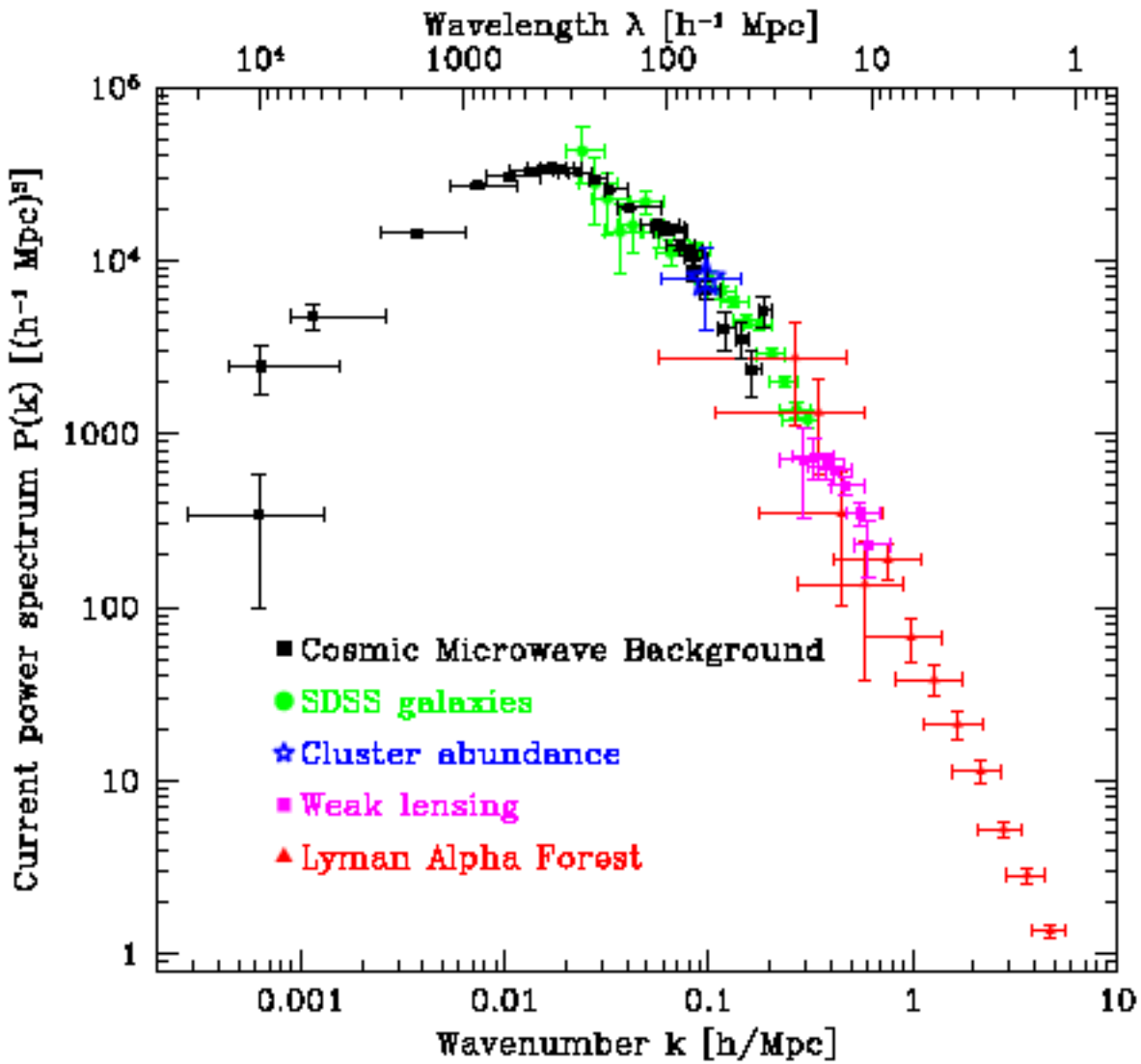

Tegmark et al. (2003)

To get a feeling for what the shape of the power spectrum means in practice, remember that it just measures the square amplitude of Fourier coefficients as a function of wavenumber. Say, if

$$P(k) \sim k^n$$

If spectral index is "negative", then distribution is dominated by long wavelengths

If spectral index is "positive", then distribution is dominated by small wavelengths

One realization of n=-2 one-dimensional Gaussian Random Field

First 25 Fourier modes

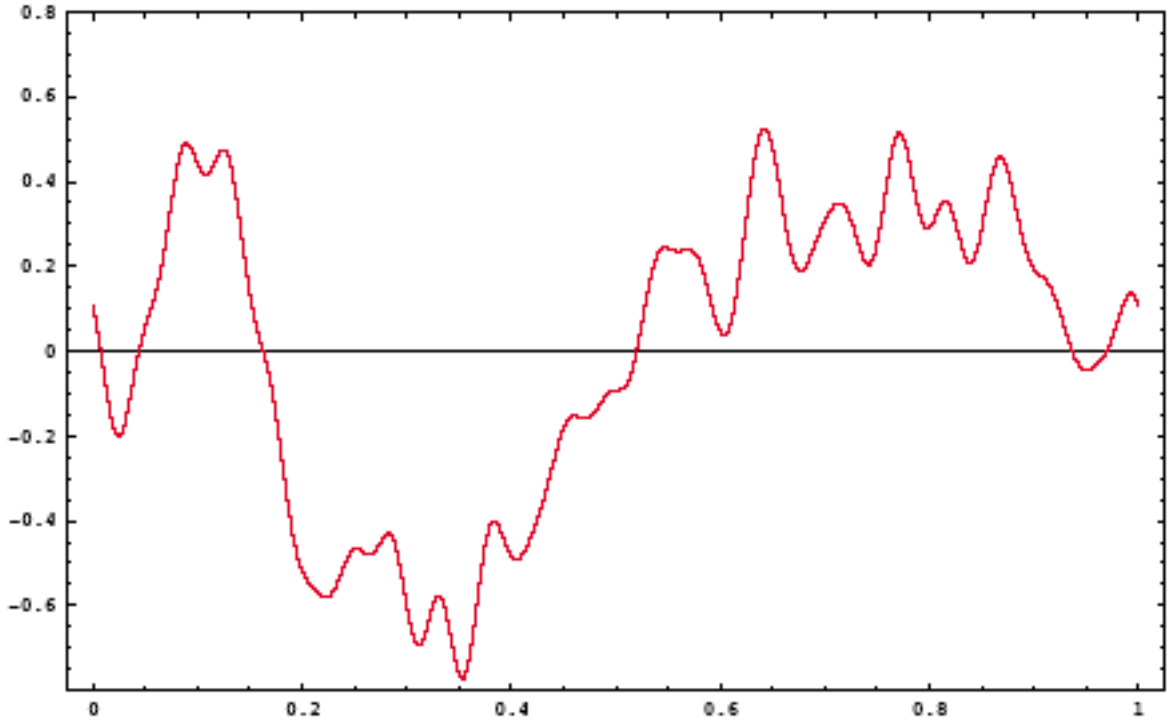

First 50 Fourier modes

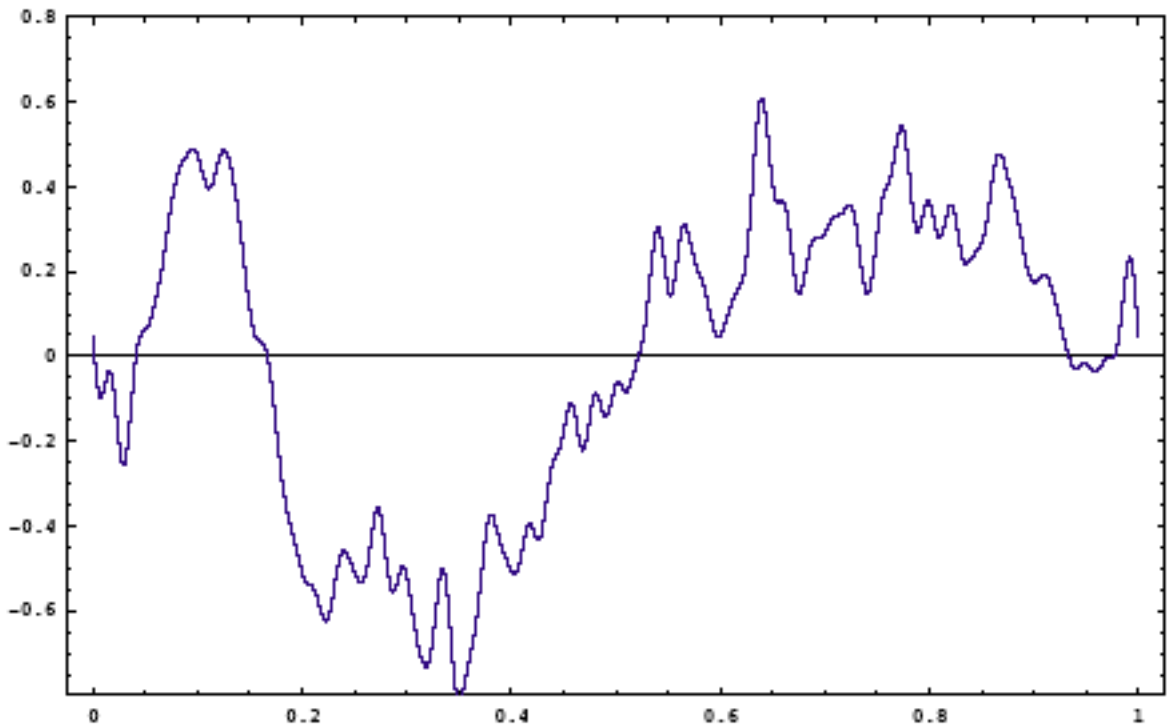

One realization of n=0 one-dimensional Gaussian Random Field

First 25 Fourier modes

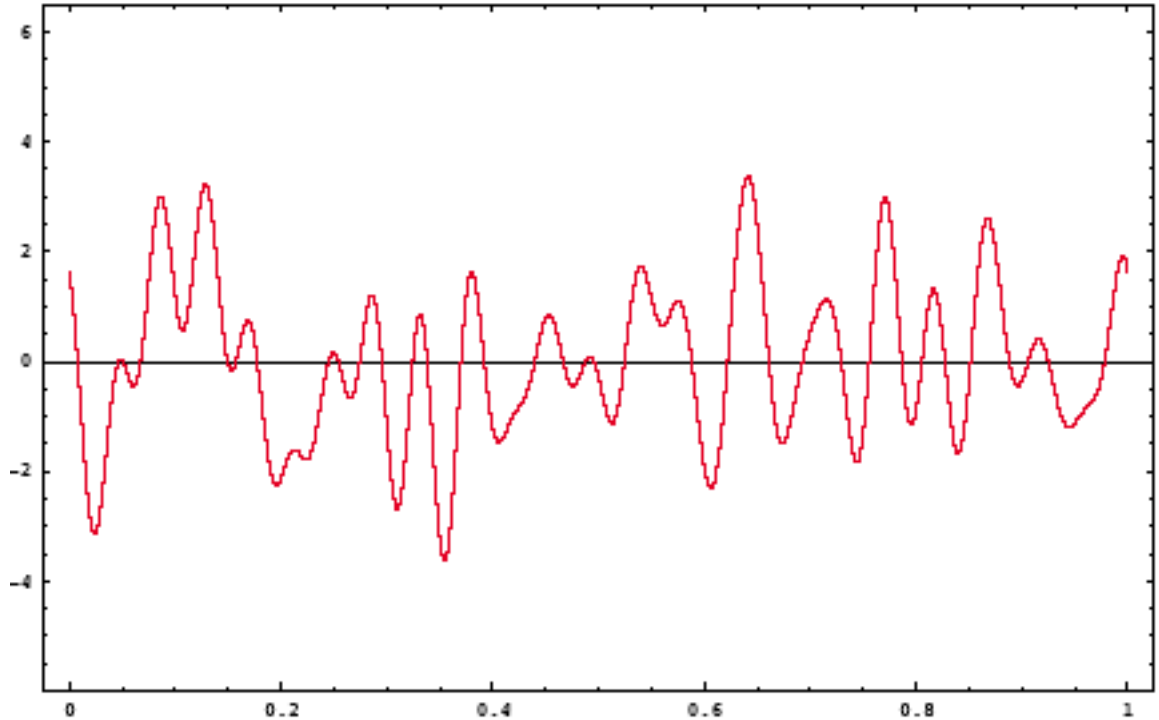

First 50 Fourier modes

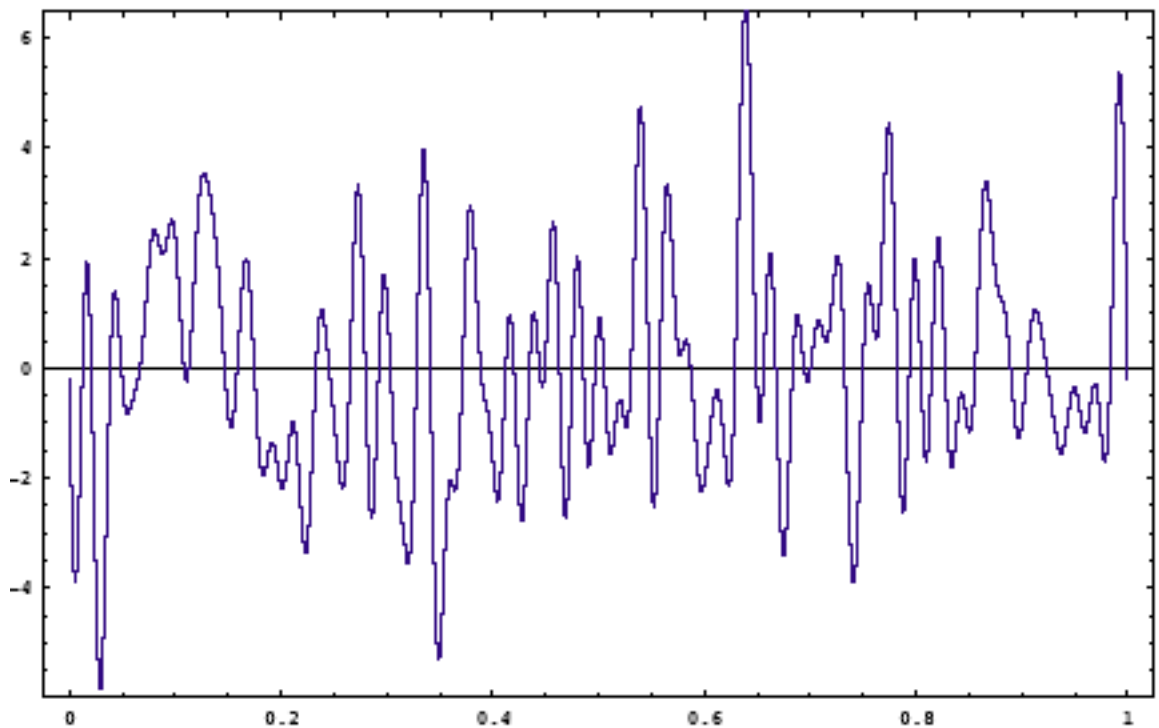

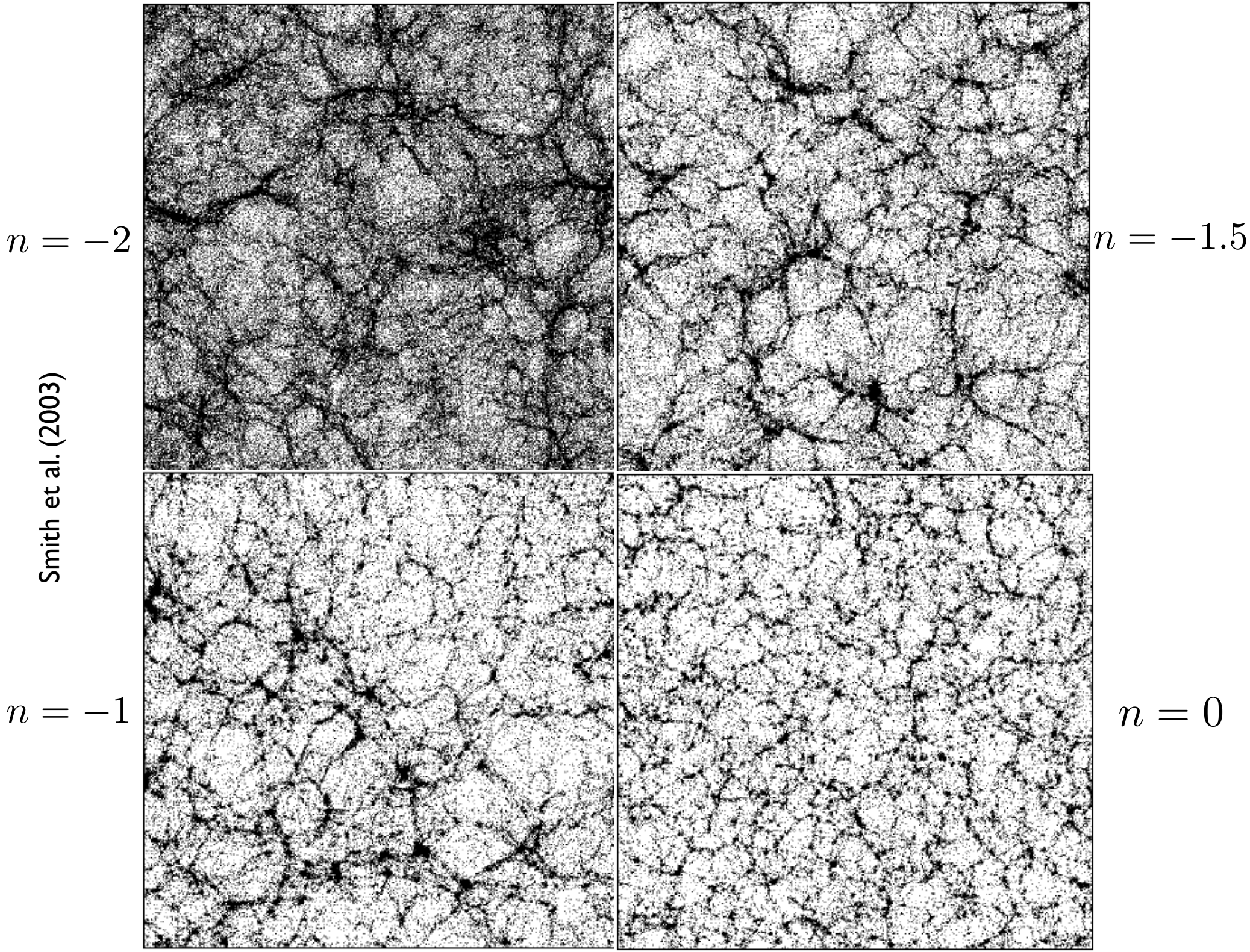
$n = -2$
$n = -1.5$
$n = -1$
$n = 0$
Smith et al. (2003)

Gaussian vs Non-Gaussian Information

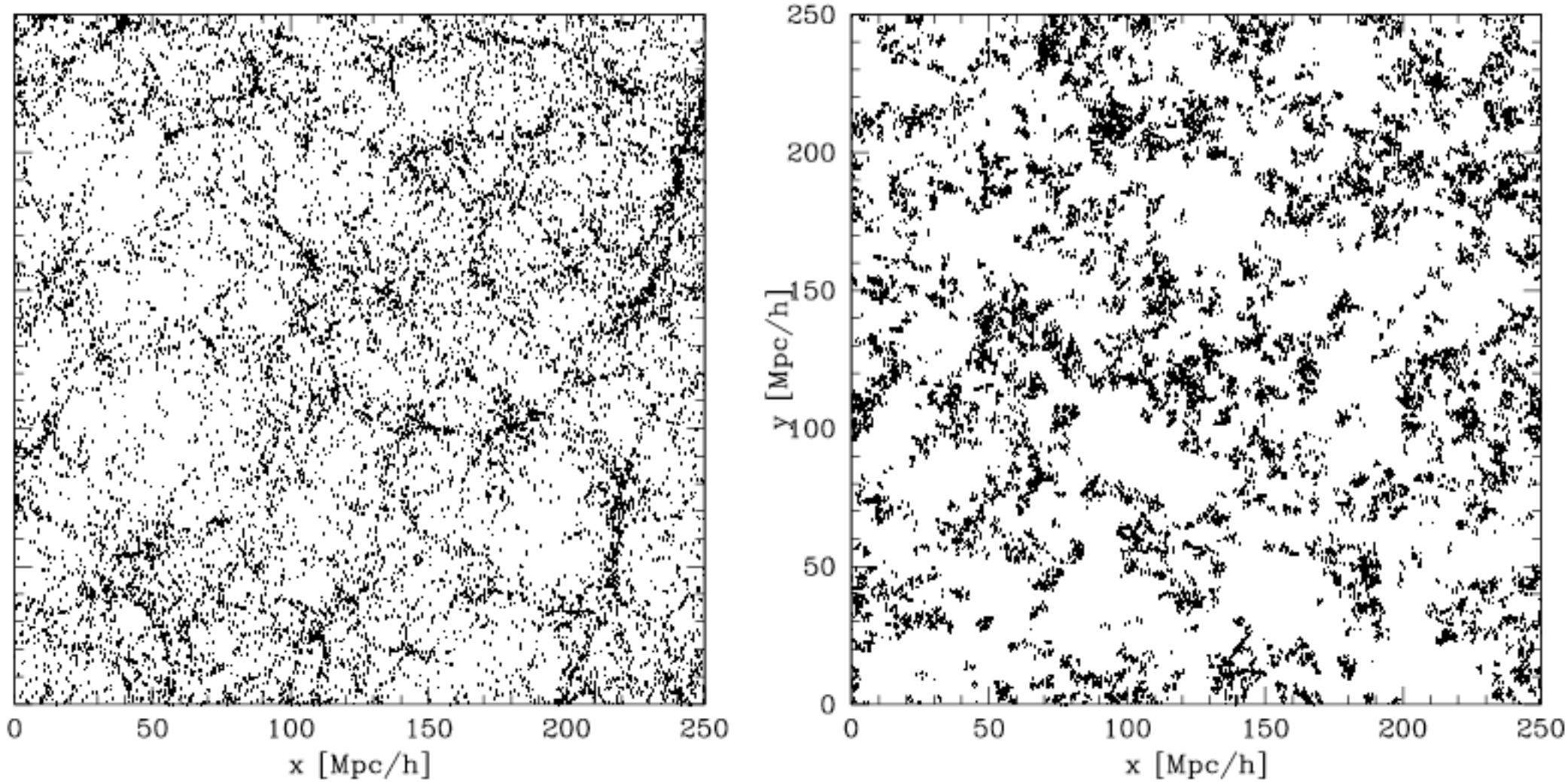

The two distributions have about the same Power Spectrum!

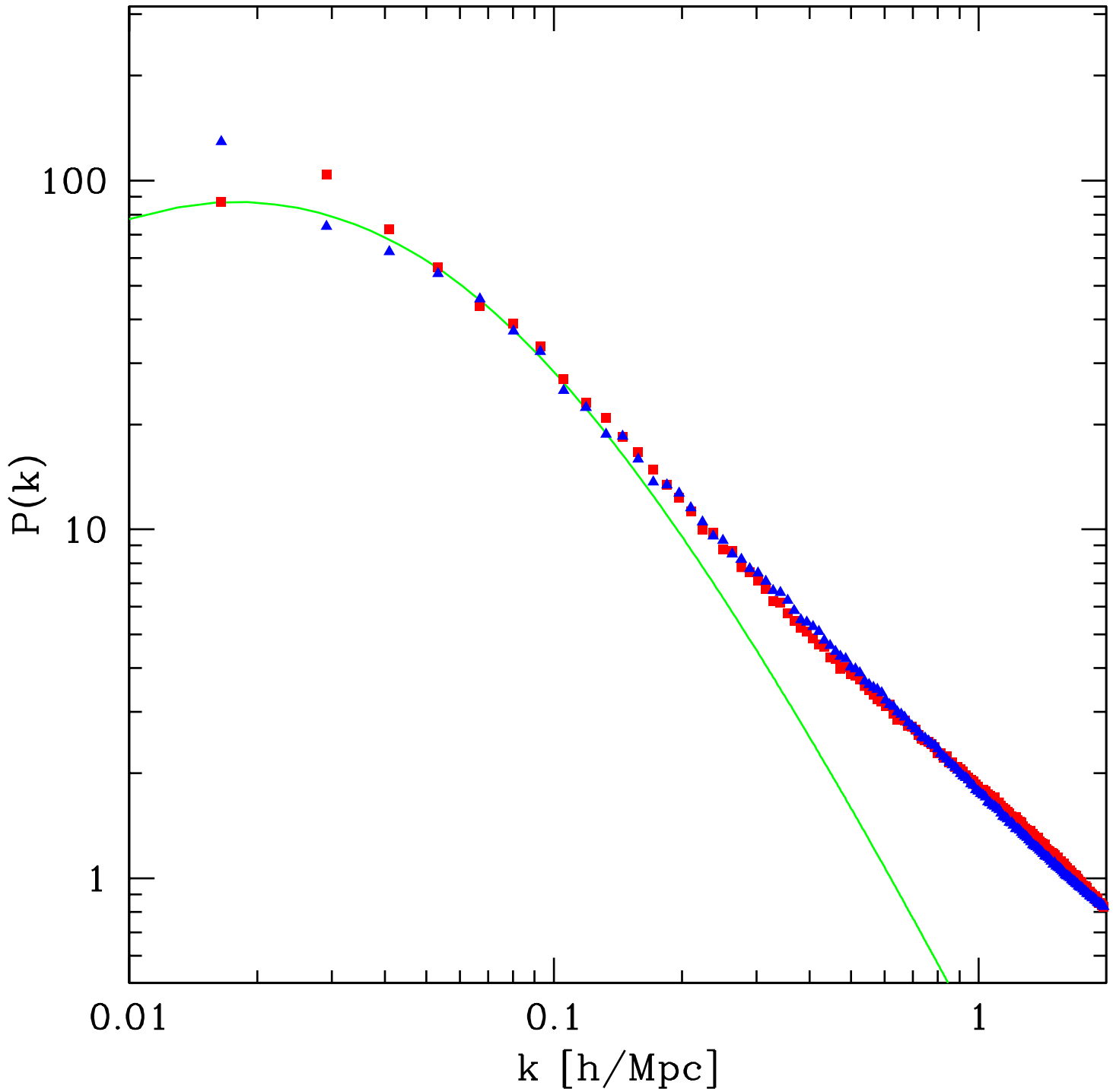

Three-point statistics are the lowest order measure of the shape of structures (filaments, walls, halos) generated by gravitational instability.

- Indeed, with two points one can only form a single shape: a line

- Three-points form a triangle, so we got different triangle shapes we can compare, for example collinear triangles with equilateral triangles,

If filamentary structures are predominant, then the three-point amplitude (Q) should be larger for collinear triangles than equilateral (or isosceles).

- A limitation of three-point statistics is that three points always form a plane. In order to better probe the "three-dimensional" shape of structures, one needs to go to the four-point function.

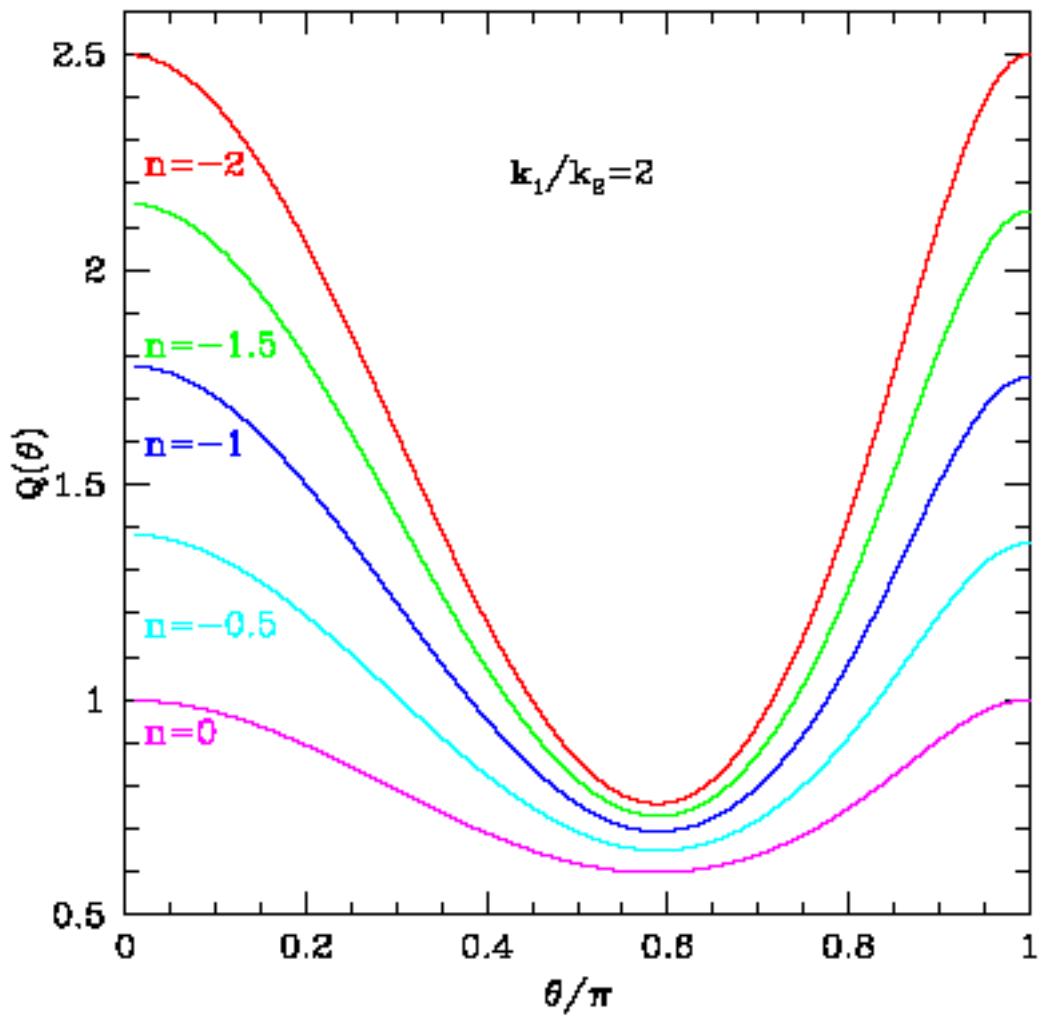
2.5
2
1.5
1
0.5
Q(θ)
n=−2
n=−1.5
n=−1
n=−0.5
n=0
k1/k2=2
0
0.2
0.4
0.6
0.8
1
θ/π

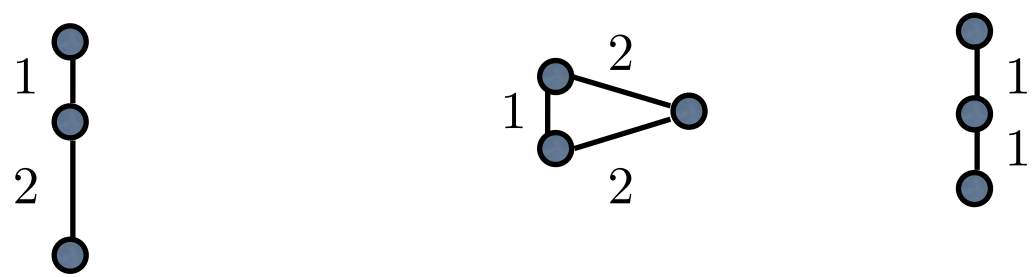
1
2
2
1
2
1
1

The two distributions can be distinguished easily by higher-order correlations!

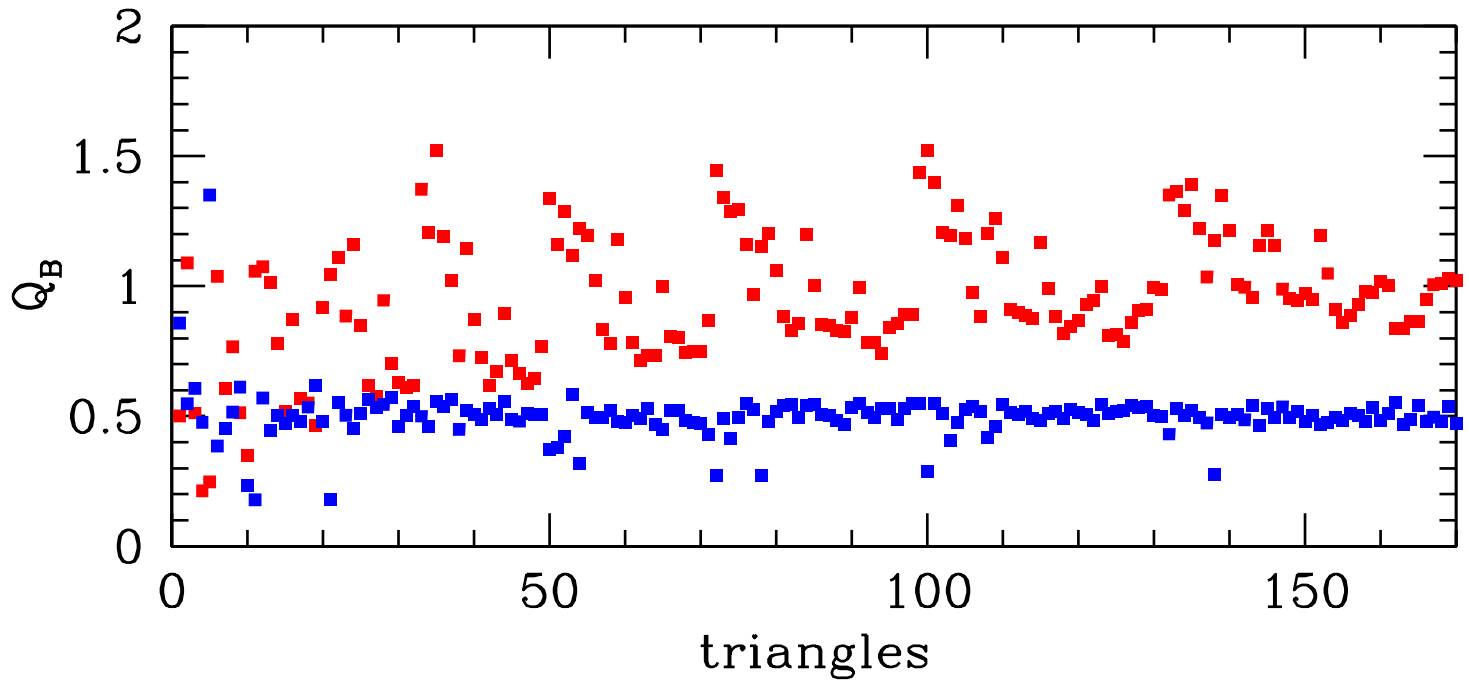

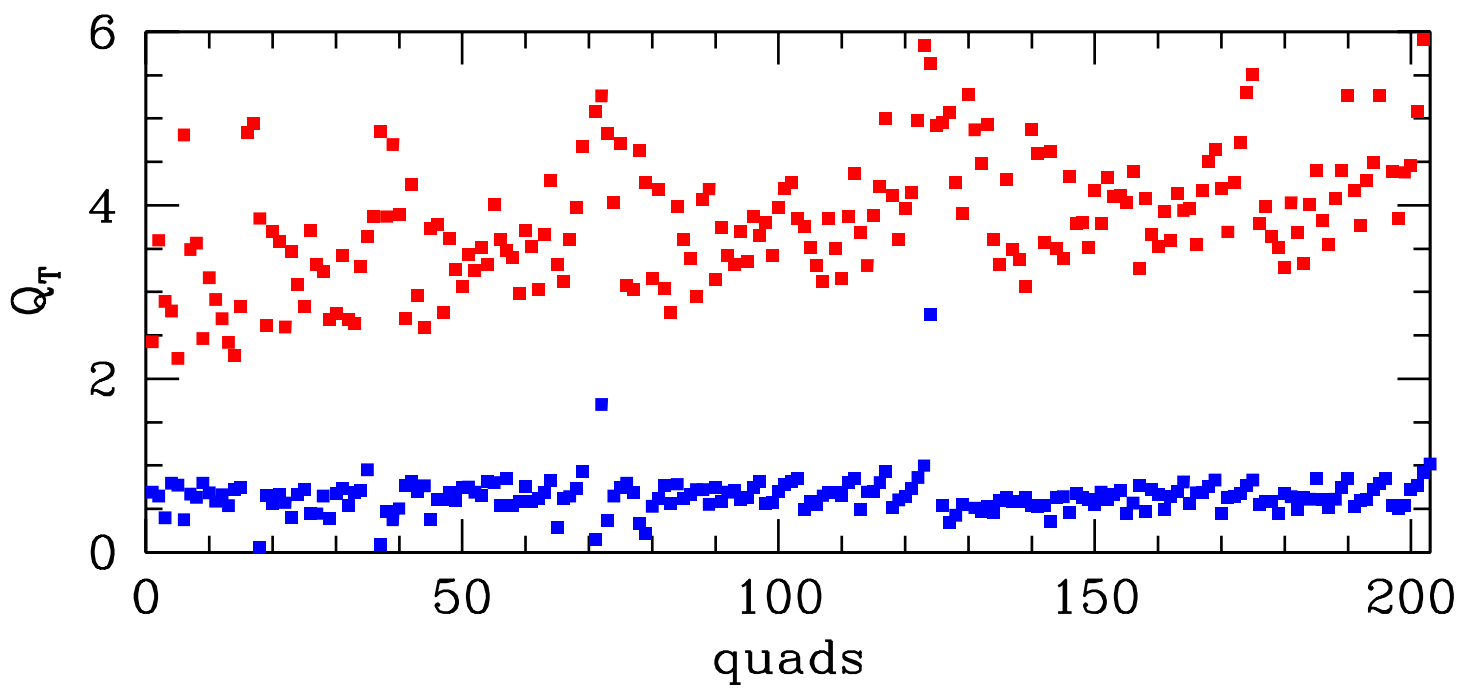

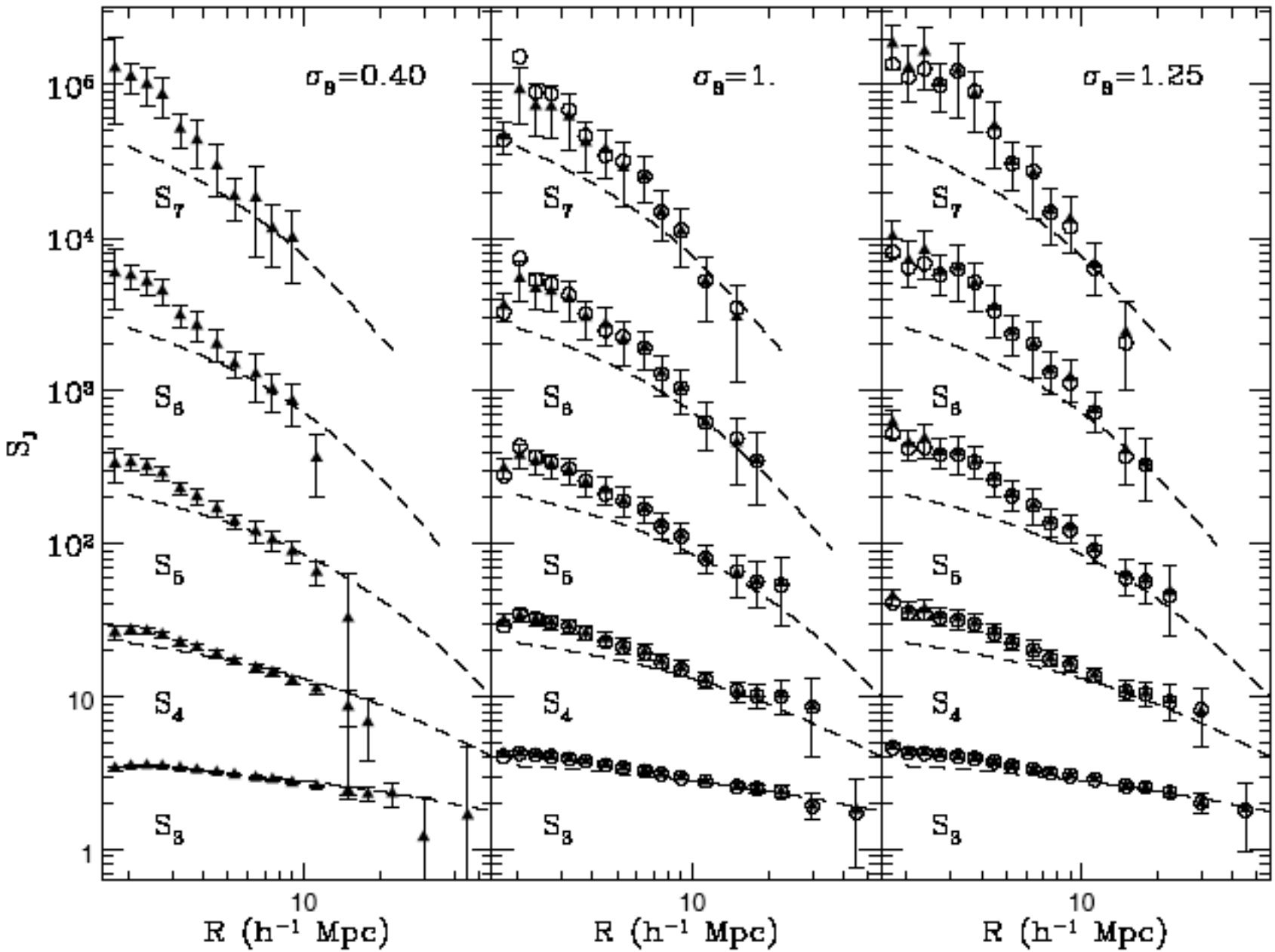

Baugh, Gaztanaga and Efstathiou (1995)

Bernardeau (1994)

$$\delta_{\max} \approx -\frac{S_3}{2}\,\sigma^2$$

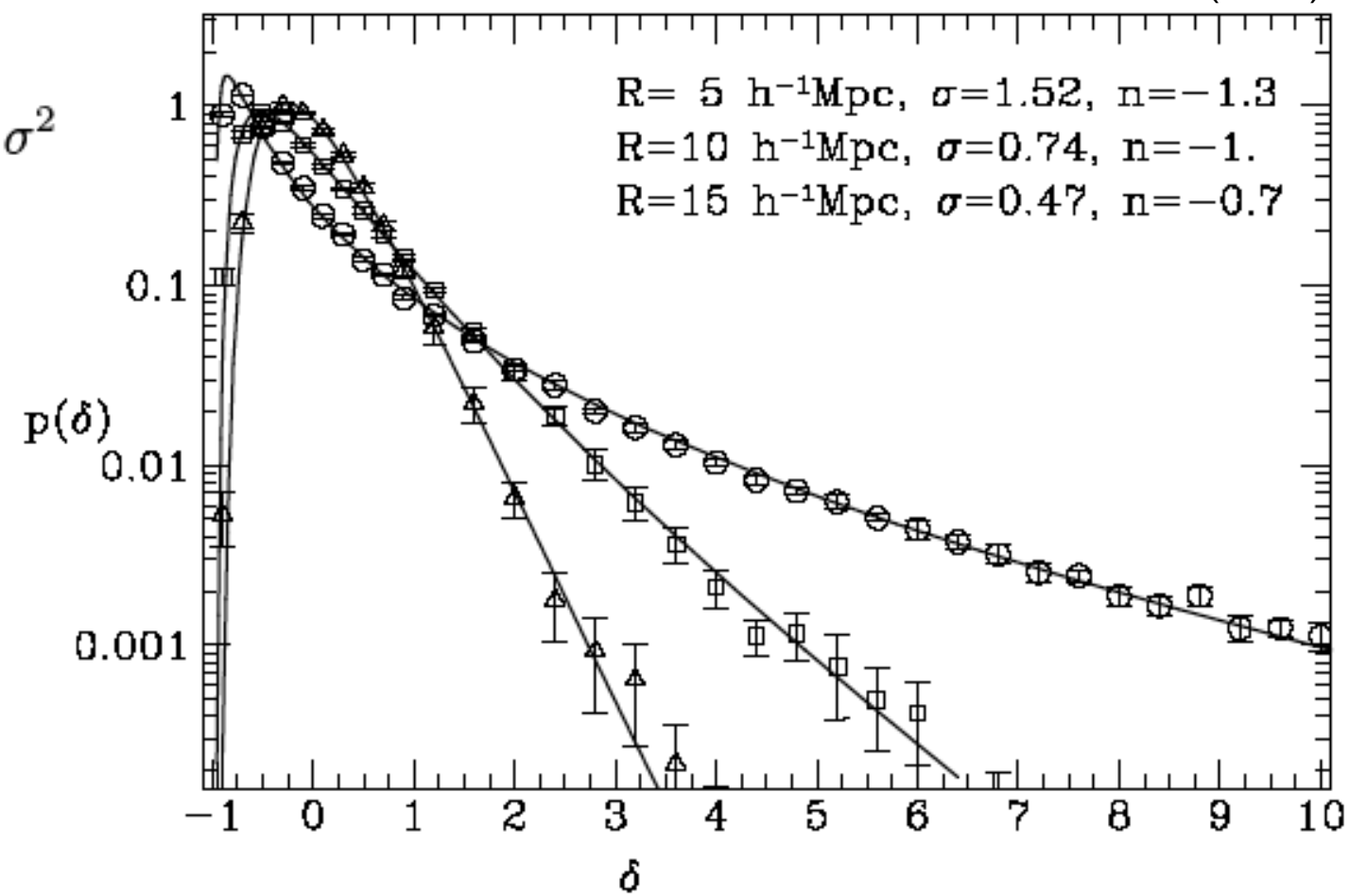

Another application is to calculate non-linear corrections to the power spectrum due to mode-mode coupling,

$$P(k,\tau) = P^{(0)}(k,\tau) + P^{(1)}(k,\tau) + \ldots,$$

$$P^{(0)}(k,\tau) = [D_1^{(+)}]^2 \; P_L(k),$$ (just an overall scaling)

$$P^{(1)}(k,\tau) = P_{22}(k,\tau) + P_{13}(k,\tau),$$ (changes the shape)

$$P_{22}(k,\tau) \equiv 2 \int [F_2^{(s)}(\mathbf{k}-\mathbf{q},\mathbf{q})]^2 P_L(|\mathbf{k}-\mathbf{q}|,\tau) P_L(q,\tau) \mathrm{d}^3\mathbf{q},$$
$$P_{13}(k,\tau) \equiv 6 \int F_3^{(s)}(\mathbf{k},\mathbf{q},-\mathbf{q}) P_L(k,\tau) P_L(q,\tau) \mathrm{d}^3\mathbf{q}.$$

These corrections become important at scales where density perturbations of order unity, i.e.

$$\Delta(k) \equiv 4\pi k^3 P(k) \simeq 1$$

However, it depends strongly on spectral index and it differs for velocities...

"linear" (large) scales

non-linear regime

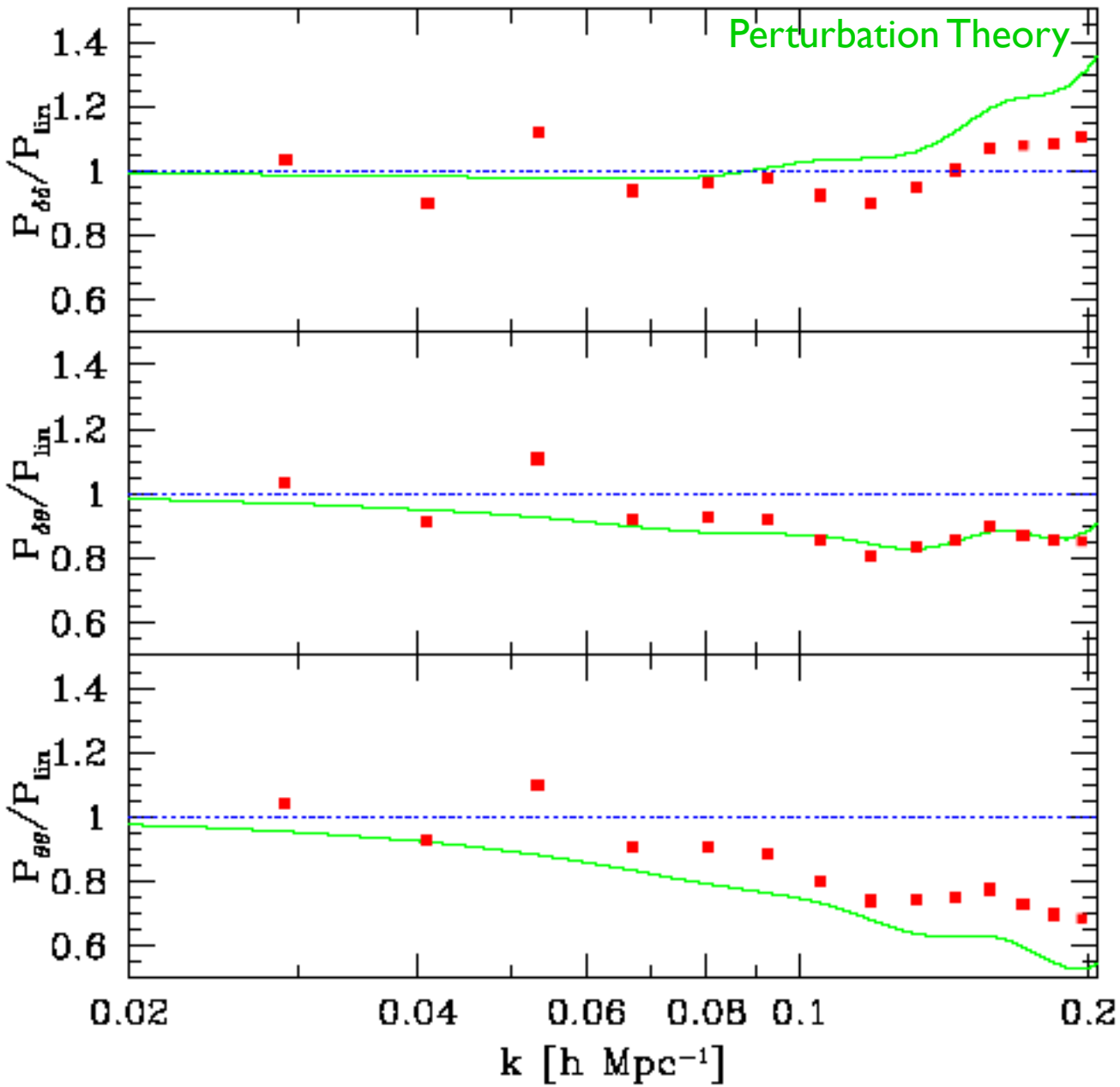

At high-z nonlinearities are strong (density field power)

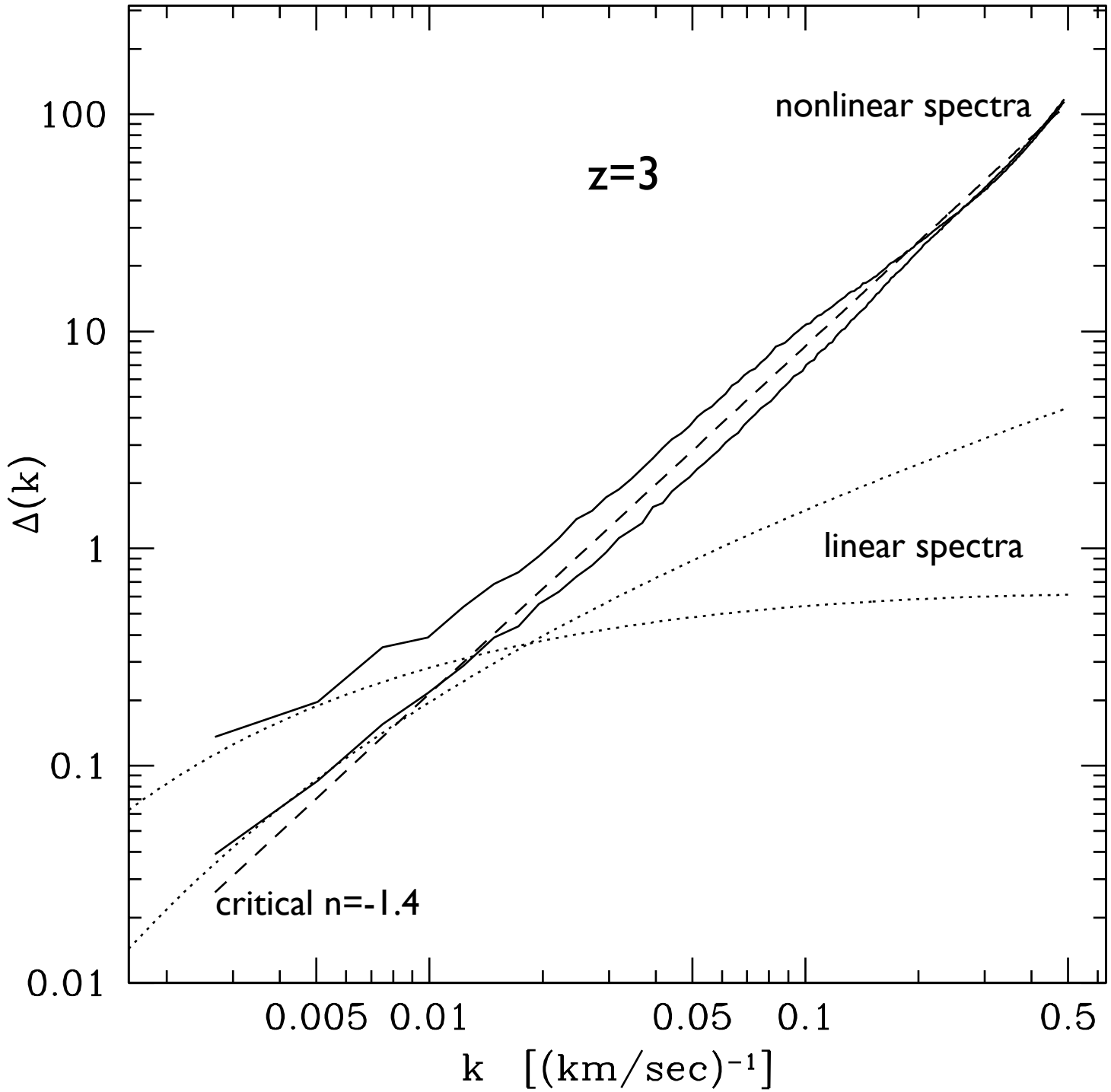

For sufficiently positive n, nonlinear growth is always SMALLER than linear!

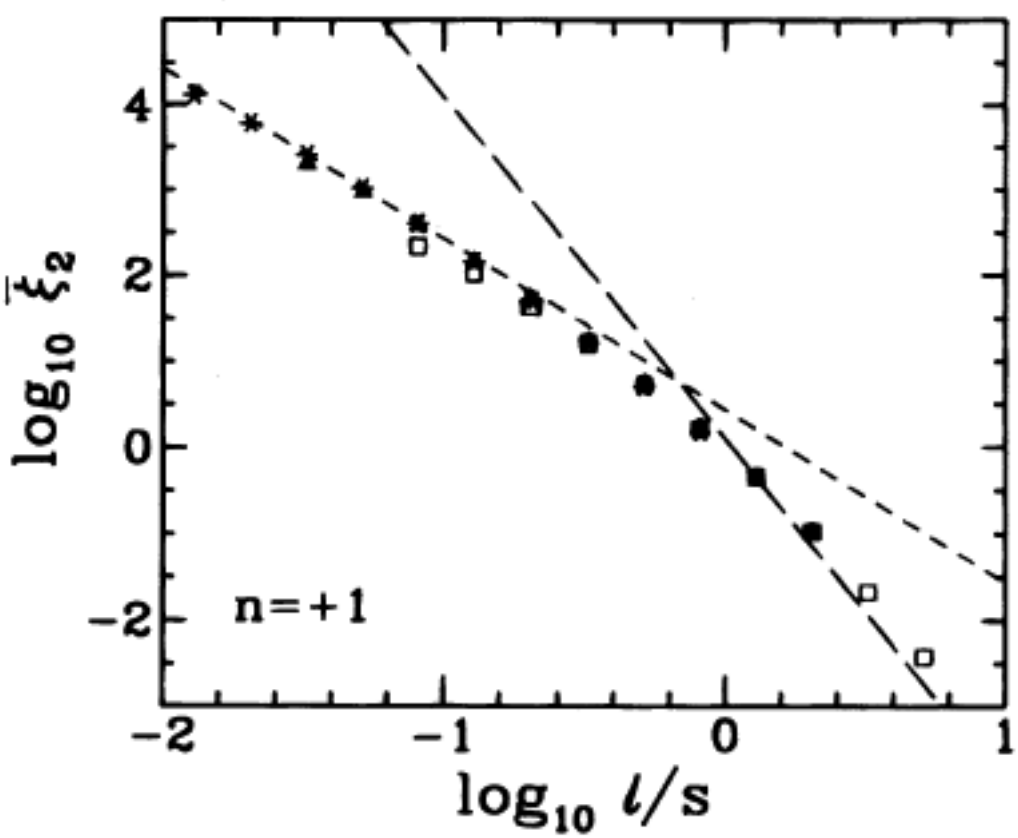

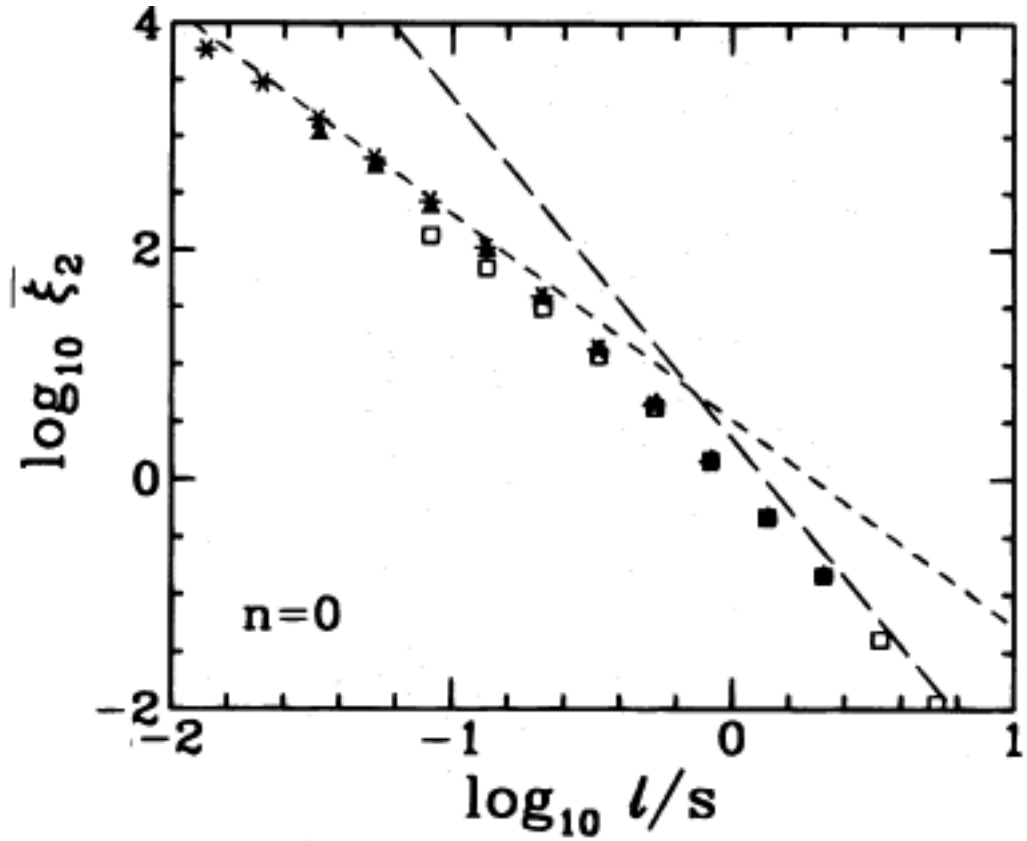

Colombi, Bouchet and Hernquist (1996)

Standard Perturbative Approach to Gravitational Clustering

- The Universe is homogeneous at large (Hubble) scales. Fluctuations become larger as small scales are approached.

- In standard perturbation theory (PT), one expands in the amplitude of density perturbations.

- This is well justified when looking for asymptotic behavior at large-scales, where fluctuations become small. PT at these scales is successful in predicting N-point correlation functions.

- In diagrammatic language, where a given topology uniquely describes the size of contributions in terms of the amplitude of fluctuations, such calculations are obtained by "tree" diagrams.

power spectrum: linear PT vs. N-body simulations

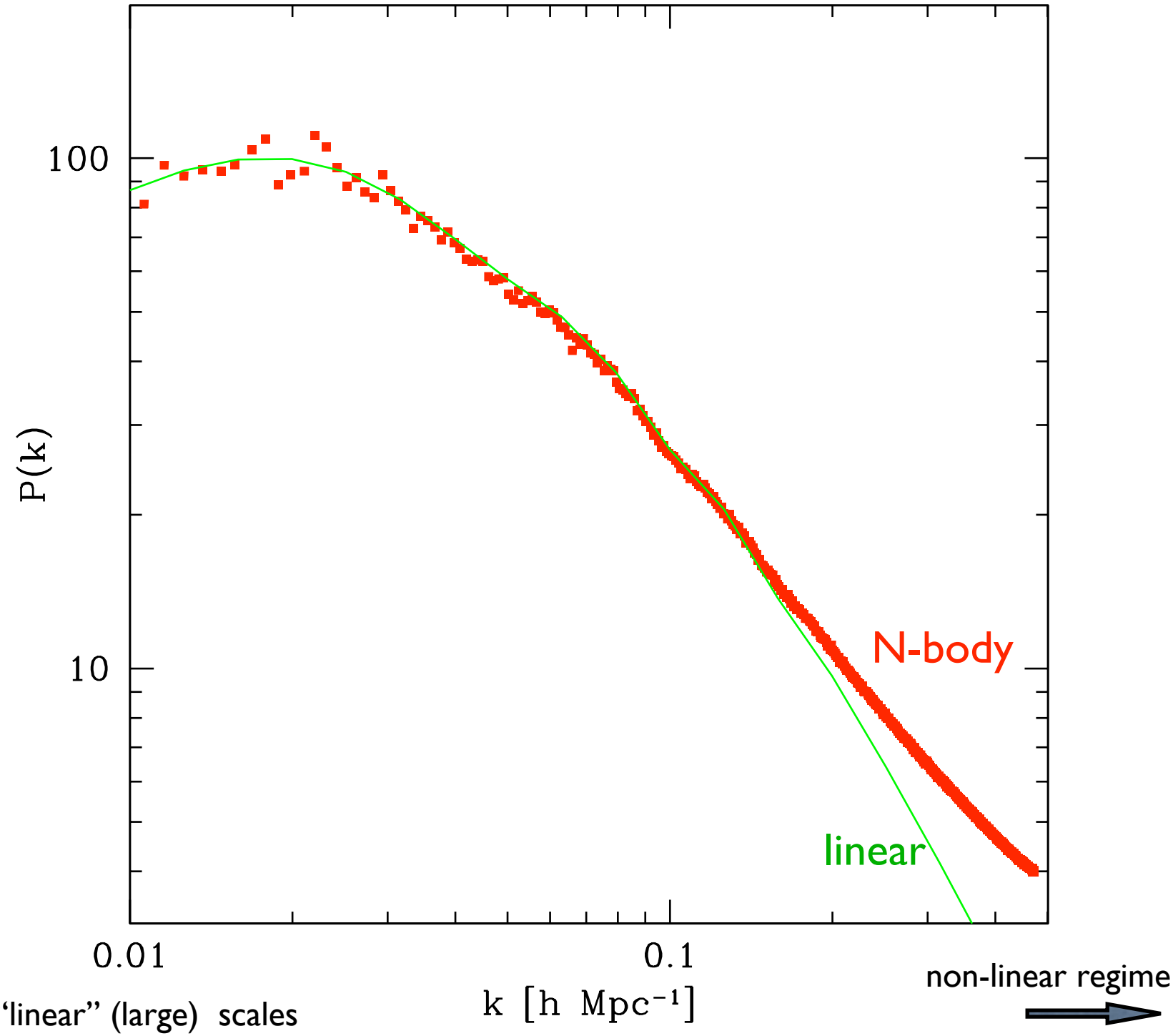

- How about nonlinear corrections ("loop" diagrams) to tree-level results?

- Once these become important, one basically needs to sum up all orders in PT (i.e. number of loops) to obtain meaningful answers, since the expansion parameter becomes of order unity or larger.

$$P(k,z) = D_+^2(z)\, P_0(k) + P_{1\mathrm{loop}}(k,z) + P_{2\mathrm{loop}}(k,z) + \ldots$$

$$P_{1\mathrm{loop}} \sim \mathcal{O}(P_{\mathrm{lin}}\, \Delta_{\mathrm{lin}}), \qquad P_{2\mathrm{loop}} \sim \mathcal{O}(P_{\mathrm{lin}}\, \Delta_{\mathrm{lin}}^2), \qquad \Delta_{\mathrm{lin}} \equiv 4\pi k^3 P_{\mathrm{lin}}$$

- For the power spectrum (N=2), taking into account just one-loop corrections to the linear spectrum works well for steep spectra but not so well for CDM spectra at z=0.

- Similar results hold for the bispectrum (N=3).

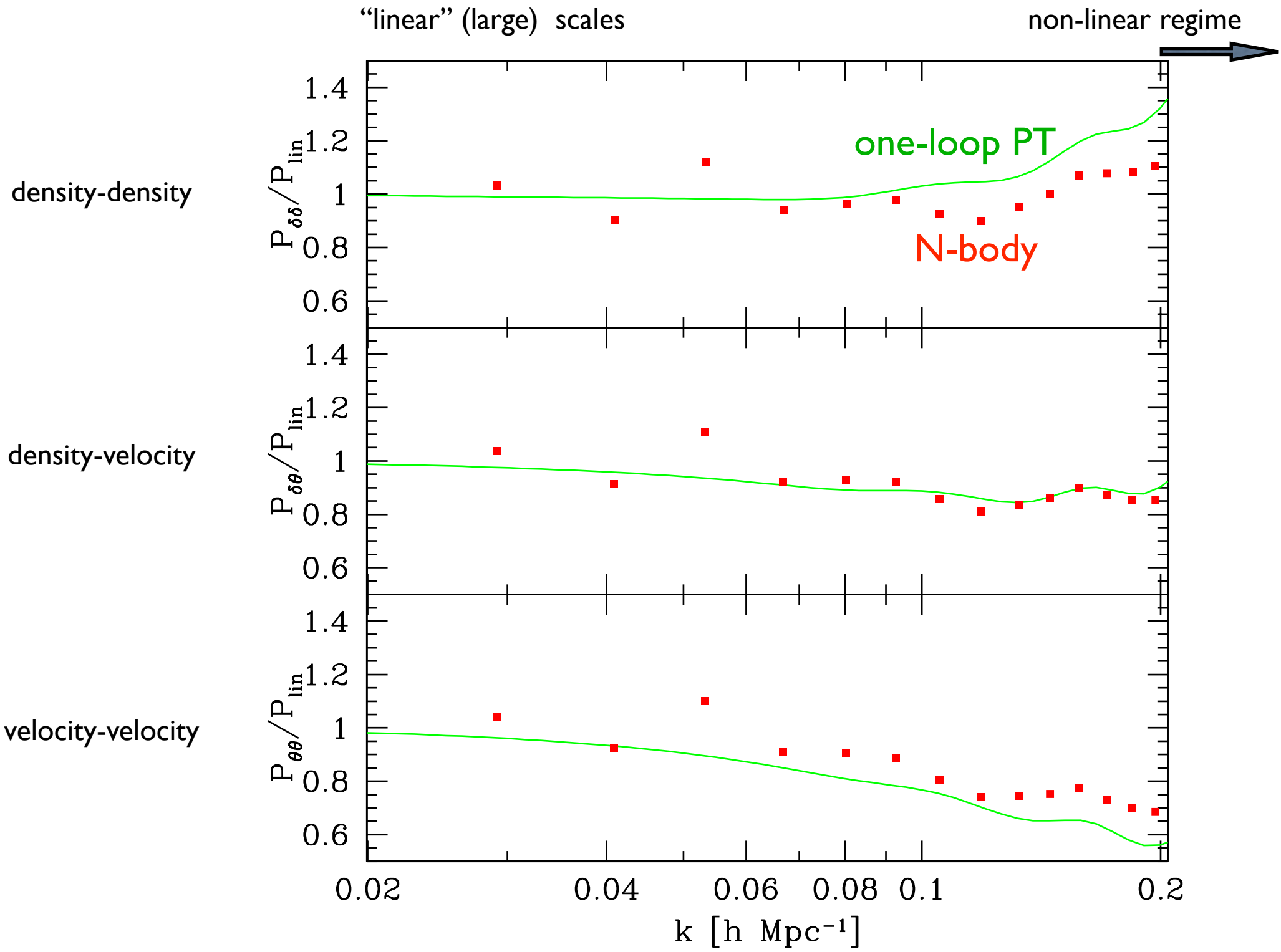
"linear" (large) scales
non-linear regime
density-density
density-velocity
velocity-velocity
one-loop PT
N-body
$P_{\delta\delta}/P_{lin}$
$P_{\delta\theta}/P_{lin}$
$P_{\theta\theta}/P_{lin}$
1.4
1.2
1
0.8
0.6
0.02
0.04
0.06
0.08
0.1
0.2
k [h Mpc^{-1}]

Why do we care? : Extracting cosmological information requires understanding of nonlinearities

- Knowledge of the transition to the nonlinear regime helps significantly in constraining the growth factor and therefore e.g. constraints dark energy or modifications of general relativity.

- Studies of baryon acoustic oscillations imprinted on the dark matter power spectrum can be used to determine the angular diameter distance, which constraints the expansion history of the universe. However, these acoustic signatures are modified by weakly nonlinear evolution.

- Nonlinearities play an important role in the determination of cosmological parameters from large-scale structure surveys. Our inability to model them accurately puts a limit to the cosmological information we can extract.

Why not just use N-Body simulations?

Simulations are extremely useful and rely on approximations that do not assume small fluctuations. However, there are benefits in having a complementary approach:

- Successful comparison reinforces validity of both, and differences lead to understanding of limitations of one method over another.

- Interplay between simulations and analytic results (e.g. as in fitting formulae)

- Physical insight and understanding of details difficult to extract from complex simulations.

- Computational cost is large for scanning over cosmological parameter space.

- Simulations make truncations of dynamics: finite box size and particle number, generation of initial conditions.

Renormalized Perturbation Theory (RPT)

- In RPT, one looks at the infinite series of diagrams in PT for correlation functions and sees how they organize themselves into a few characteristic physical quantities, the most important of which is the propagator

Final density / velocity div.

$$G_{ab}(k,\eta)\ \delta_{\rm D}(\mathbf{k}-\mathbf{k}') \equiv \left\langle \frac{\delta\Psi_a(\mathbf{k},\eta)}{\delta\phi_b(\mathbf{k}')} \right\rangle$$

Initial Conditions

where

$$\Psi_a(\mathbf{k},\eta) \equiv \left(\delta(\mathbf{k},\eta),\ -\theta(\mathbf{k},\eta)/\mathcal{H}\right), \qquad \eta \equiv \ln a(\tau).$$

$$\phi_a(\mathbf{k}) = \Psi_a(\mathbf{k},\eta=0)$$

Equations of motion can be written as,

$$\partial_\eta \Psi_a(\mathbf{k},\eta) + \Omega_{ab}\Psi_b(\mathbf{k},\eta) = \gamma_{abc}(\mathbf{k},\mathbf{k}_1,\mathbf{k}_2)\Psi_b(\mathbf{k}_1,\eta)\Psi_c(\mathbf{k}_2,\eta)$$

Laplace transform in time variable, $(\sigma^{-1}_{ab}(\omega) \equiv \omega\delta_{ab} + \Omega_{ab})$

$$\sigma^{-1}_{ab}(\omega)\ \Psi_b(\mathbf{k},\omega) = \phi_a(\mathbf{k}) + \gamma^{(\mathrm{s})}_{abc}(\mathbf{k},\mathbf{k}_1,\mathbf{k}_2) \oint \frac{d\omega_1}{2\pi i}\ \Psi_b(\mathbf{k}_1,\omega_1)\Psi_c(\mathbf{k}_2,\omega-\omega_1),$$

Initial Conditions

then going back to time,

$$\Psi_a(\mathbf{k},\eta) = g_{ab}(\eta)\phi_b(\mathbf{k}) + \int_0^\eta d\eta' g_{ab}(\eta-\eta')\gamma^{(\mathrm{s})}_{bcd}(\mathbf{k},\mathbf{k}_1,\mathbf{k}_2)\Psi_c(\mathbf{k}_1,\eta')\Psi_d(\mathbf{k}_2,\eta')$$

Diagrammatically:

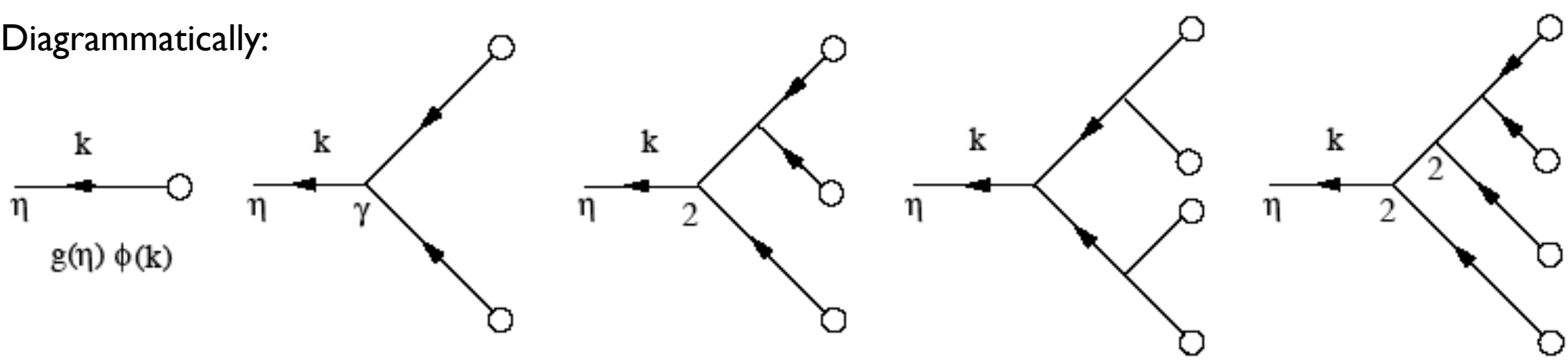

The propagator is a measure of the memory of initial conditions, and reduces to the usual growth factors in linear theory,

$$g_{ab}(\eta) = \frac{\mathrm{e}^{\eta}}{5}\begin{bmatrix} 3 & 2 \\ 3 & 2 \end{bmatrix} - \frac{\mathrm{e}^{-3\eta/2}}{5}\begin{bmatrix} -2 & 2 \\ 3 & -3 \end{bmatrix},$$

growing mode
$\phi_a(\mathbf{k}) \propto (1,1)$

decaying mode
$\phi_a(\mathbf{k}) \propto (1,-3/2)$

At smaller scales this receives nonlinear corrections that drive the propagator to zero (the final condition "does not remember" the initial condition).

Once these terms are resummed into the nonlinear propagator, the rest of the diagrams (still an infinite number) can be thought of as the effects of mode-coupling,

- they measure generation of structure at small scales

- they dominate in a narrow range of scales, drastically improving convergence

Measuring the Propagator from Numerical Simulations

A. From the Cross-Corrrelation:

For Gaussian initial conditions, the nonlinear propagator can be related to the cross-correlation between initial and final conditions,

$$G_{ab}(k,\eta)\,\langle\phi_b(\mathbf{k})\phi_c(\mathbf{k}')\rangle = \langle\Psi_a(\mathbf{k},\eta)\,\phi_c(\mathbf{k}')\rangle.$$

In this sense the propagator measures the memory of perturbations to their initial conditions.

B. From the Functional Derivative:

The definition involves,

$$\frac{\delta\Psi_a(\mathbf{k})}{\delta\phi_b(\mathbf{k}')} = \lim_{\epsilon\to 0}\,\frac{\Psi_a[\phi_b(\mathbf{k})+\epsilon\,\delta_{\rm D}(\mathbf{k}-\mathbf{k}')]-\Psi_a[\phi_b(\mathbf{k})]}{\epsilon}.$$

This is impractical, but doable assuming ergodicity.

Both methods give the same answer!

O : cross-correlation

× : functional derivative

$$(G_\delta, G_\theta) = G_{ab}\,(1,1)_b = (G_{11} + G_{12}, G_{21} + G_{22})$$

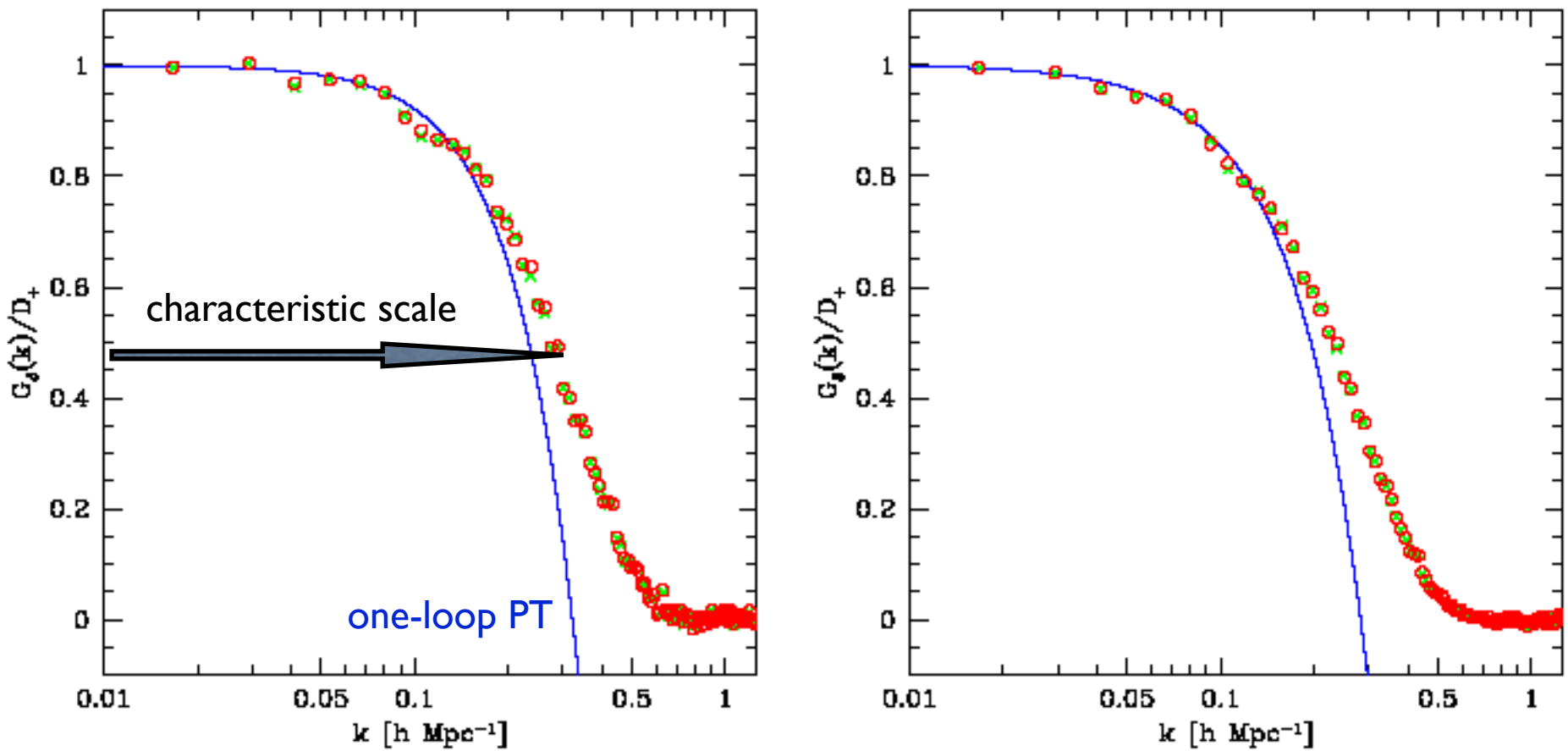

FIG. 4: The density (left panel) and velocity divergence (right panel) propagators at redshift $z = 0$ from initial conditions at $z = 5$ (corresponding to $D_+ = 4.68$). The symbols represent measurement in numerical simulations, from implementation of the functional derivative (crosses) and from the relation to the cross-correlation coefficient (circles). The solid lines show the predictions of one-loop PT, Eq. (28).

Calculating the Propagator in RPT

In the exact dynamics the resummation of the propagator can be calculated, though it is much more difficult than in ZA.

Let me just sketch how it is done.

Diagramatically, the PT expansion looks like:

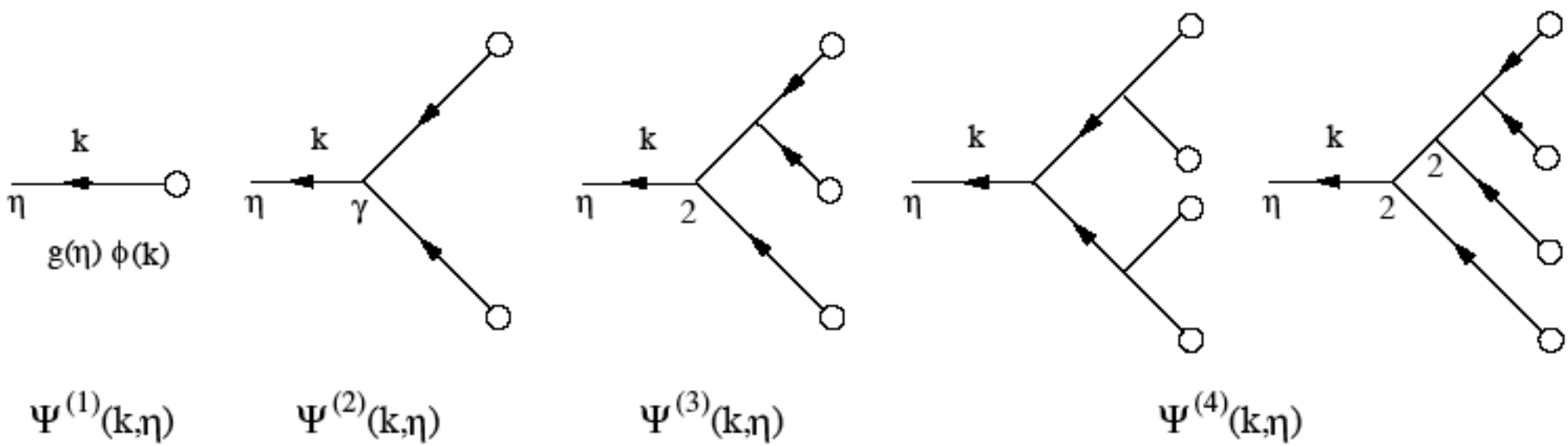

FIG. 3: Diagrams up to order $n = 4$ in the series expansion of $\Psi(\mathbf{k}, \eta)$.

Power Spectrum

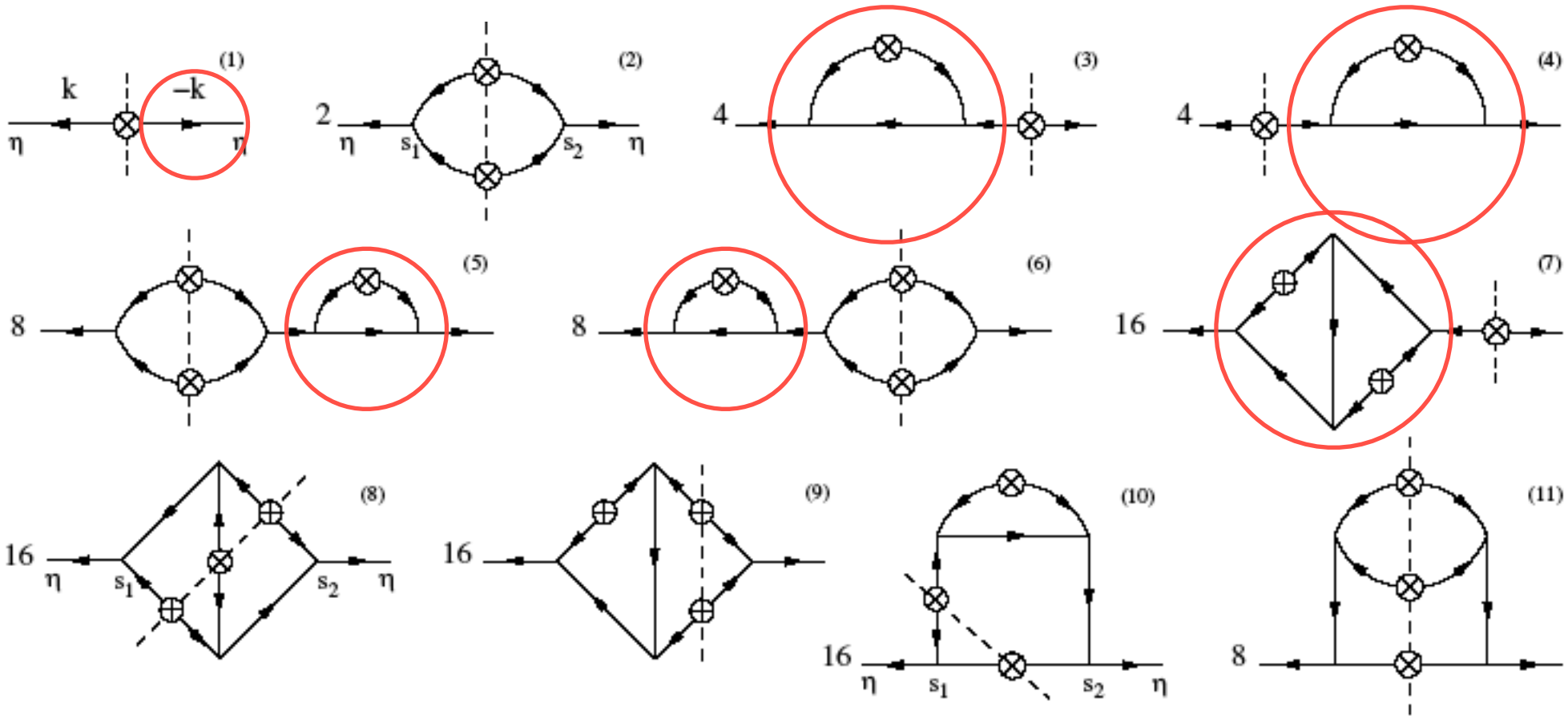

FIG. 5: Diagrams for the correlation function $P_{ab}(\mathbf{k},\eta)$ up to two-loops (only 7 out of 29 two-loop diagrams a
hown here). The dashed lines represent the points at which the two trees representing perturbative solutions to Ψ
nd Ψ_b have been glued together.

Propagator

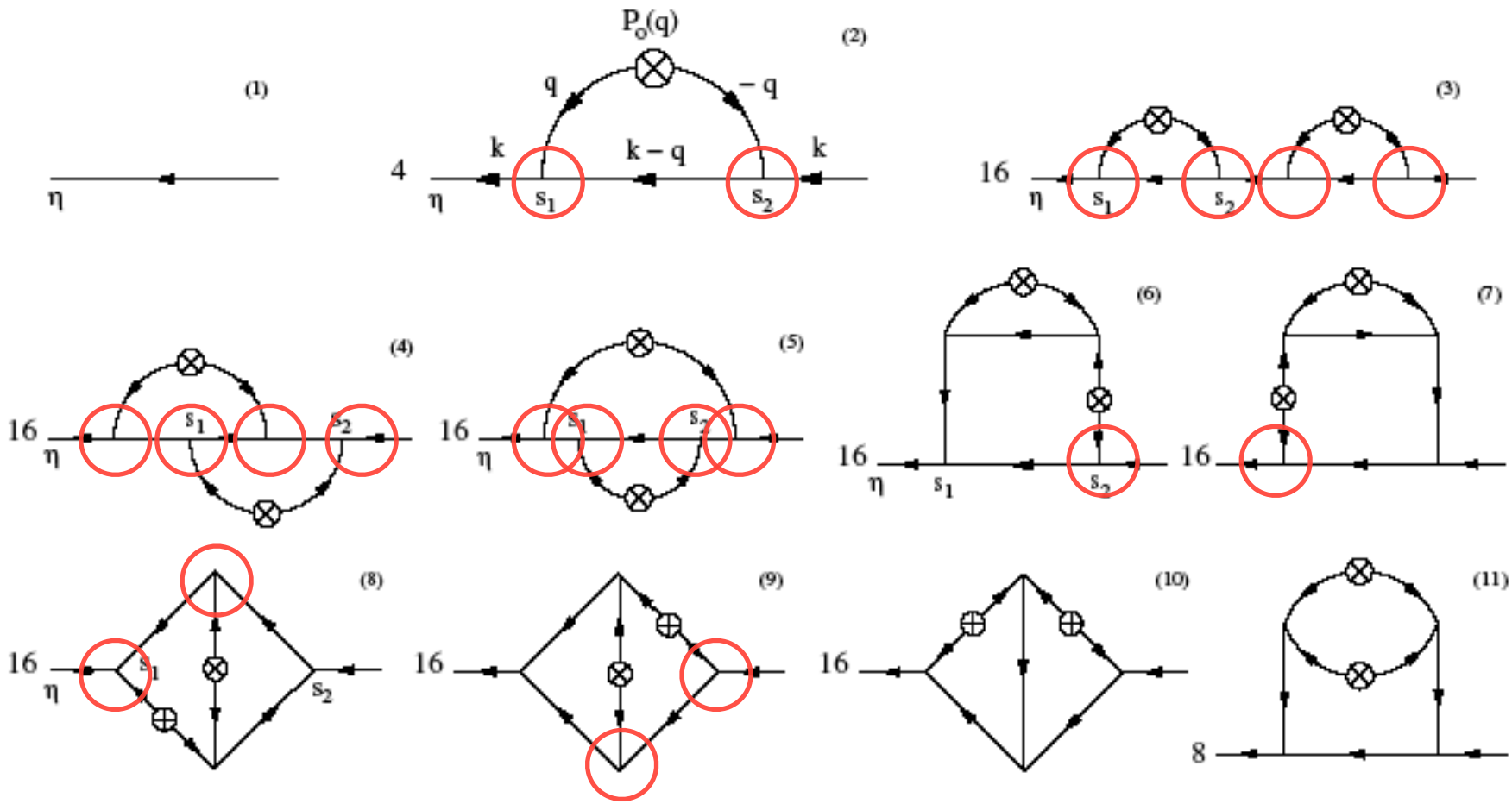

FIG. 2: Diagrams for the non linear propagator $G(k, \eta)$ up to two loops.

Let's see how the dominant contributions arise...

The dominant contributions have the *simplest* ramification possible in terms of initial conditions (that's why the cross-correlate the most):

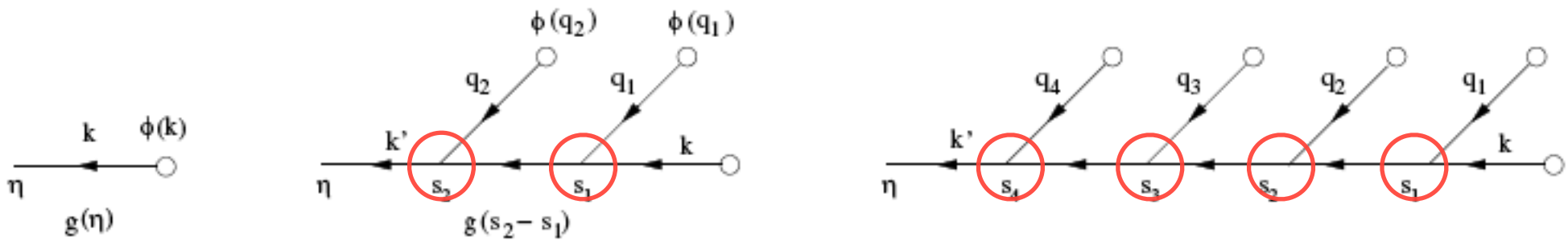

The dominant contributions can be resummed *exactly* in high-k limit!

This is so because in the high-k limit the interaction vertex simplifies, and these diagrams have a very simple time dependence, with all propagators from initial conditions being in the purely growing mode.

These results can be extended for higher-point versions of the propagator.

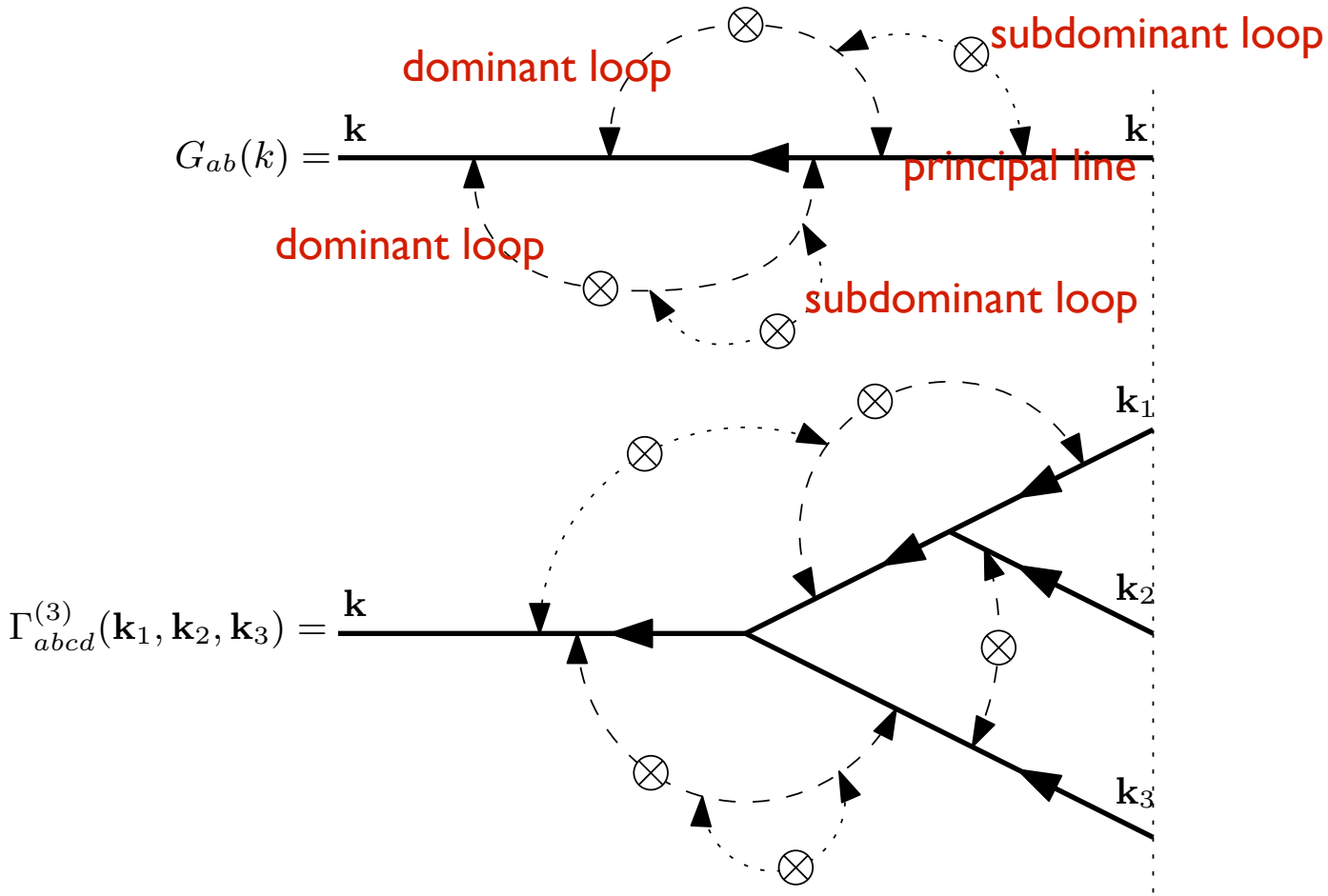

FIG. 2: Example of diagrams contributing to $G_{ab}(k)$ (top) and $\Gamma^{(3)}_{abcd}(\mathbf{k}, \mathbf{k}_1, \mathbf{k}_2, \mathbf{k}_3)$ (bottom). The dominant contribution after resuming all possible configurations is expected to come from those diagrams where all loops are directly connected to the principal line (top) or principal tree (bottom). The principal line and tree are drawn with a thick solid line. A symbol $\otimes$ denotes a power spectrum evaluated at initial time $\eta_{\rm in}$. The dominant loops are those drawn by dashed lines, while the sub-dominant loops are those in dotted lines.

For $k\,\sigma_v D_+ \gg 1$

$$G(k,z) \simeq D_+(z)\,\exp\Big[-\frac{1}{2}k^2\sigma_v^2\Big(D_+(z)-1\Big)^2\Big],$$

$$\sigma_v^2 \equiv \frac{1}{3}\int \frac{P_0(q)}{q^2}d^3q,$$

$$[D_+(z)\sigma_v]^{-1} = 0.15, 0.24, 0.46\,h\,\mathrm{Mpc}^{-1} \qquad \text{at} \quad z = 0, 1, 3$$

Notice this scale is rather large (thanks to the shape of CDM spectrum), so scales much smaller than this have exponentially small influence on large scales.

This ``separation of scales'' is crucial for successful modeling of BAO.

In order to recover the propagator for all scales, we match this asymptotic result to the low-k limit (one-loop correction) by regarding the one-loop propagator as the power series expansion of a Gaussian.

Comparison between predicted G(k) and N-Body Simulations

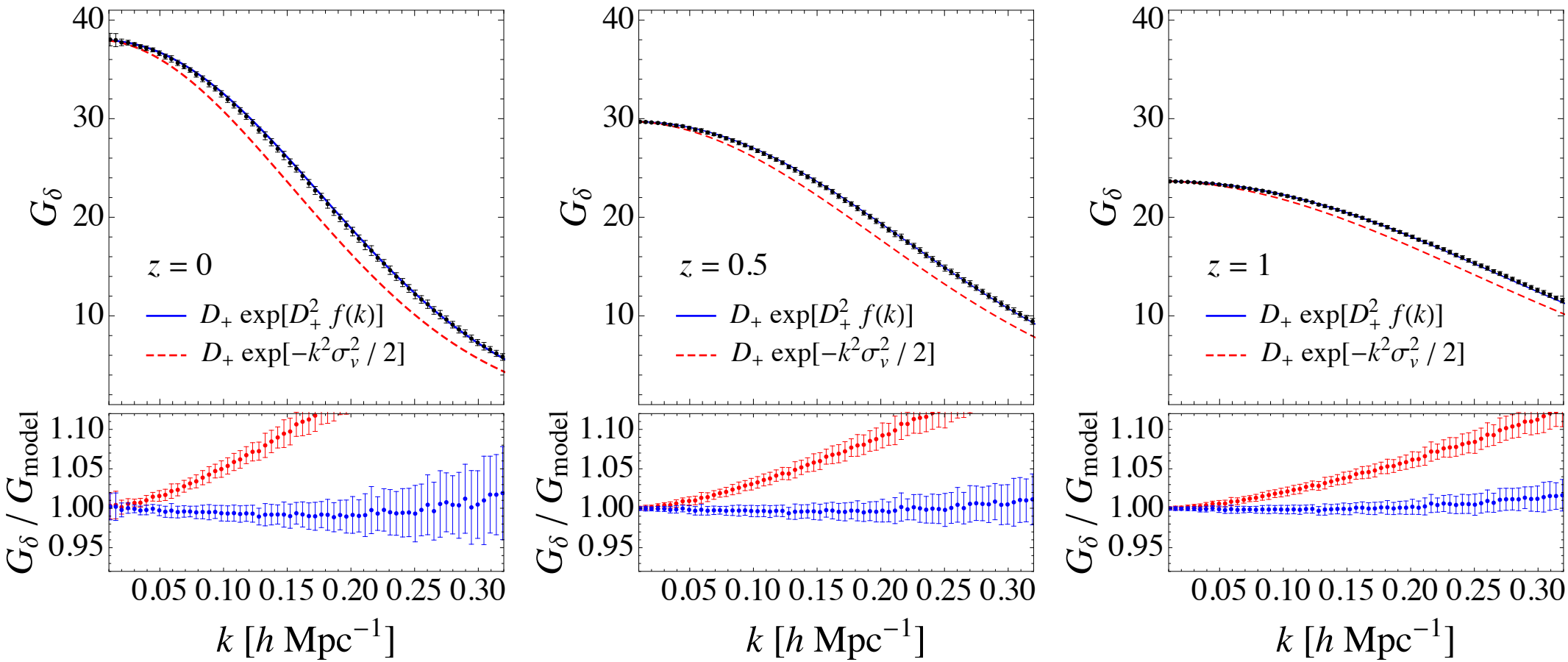

In std N-body simulations (with ICs set in the growing mode, phi+ ~ (1,1)) we can only measure the following combinations,

$$G_{ab}\phi_b \equiv \{G_\delta, G_\theta\}$$

To measure the each matrix element we must set initial conditions for density and velocities using different (uncorrelated) random Gaussian fields.

Testing the fundamentals of Propagator Resummation

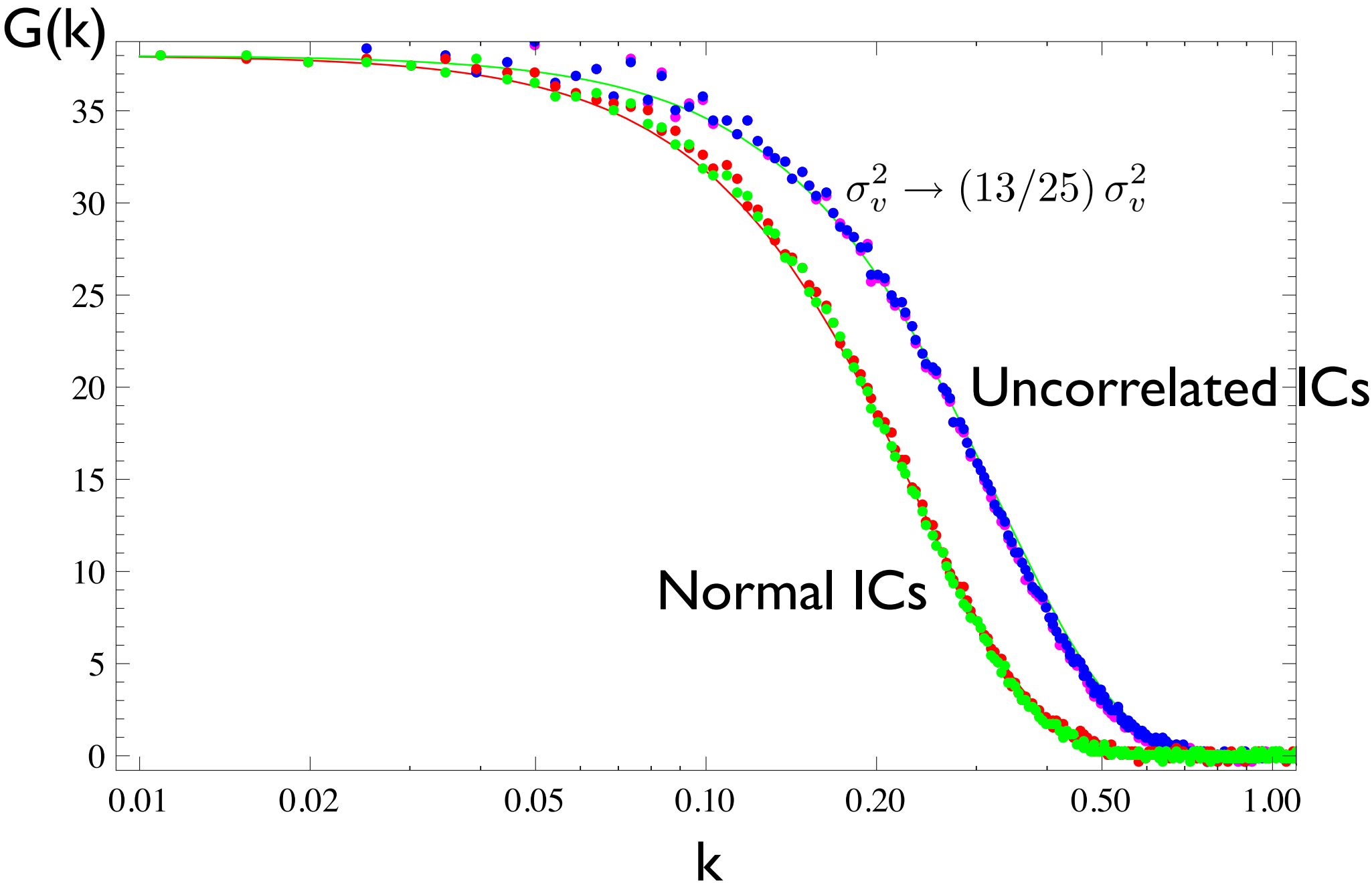

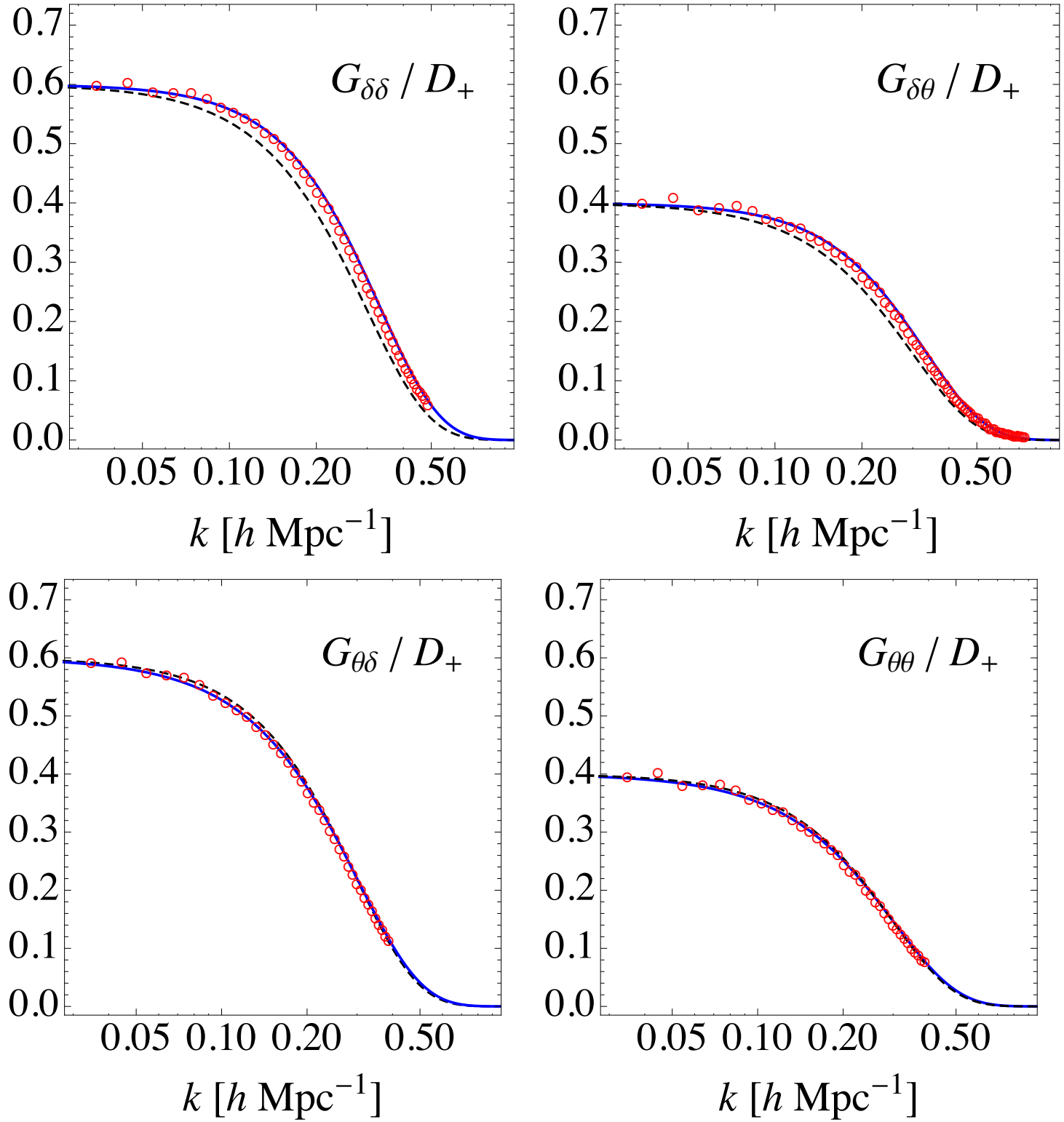
$G_{\delta\delta} / D_+$
$G_{\delta\theta} / D_+$
$G_{\theta\delta} / D_+$
$G_{\theta\theta} / D_+$
0.0
0.1
0.2
0.3
0.4
0.5
0.6
0.7
0.05
0.10
0.20
0.50
k [h Mpc^{-1}]

Comparison between predicted G(k) and N-Body Simulations
Cosmology dependence

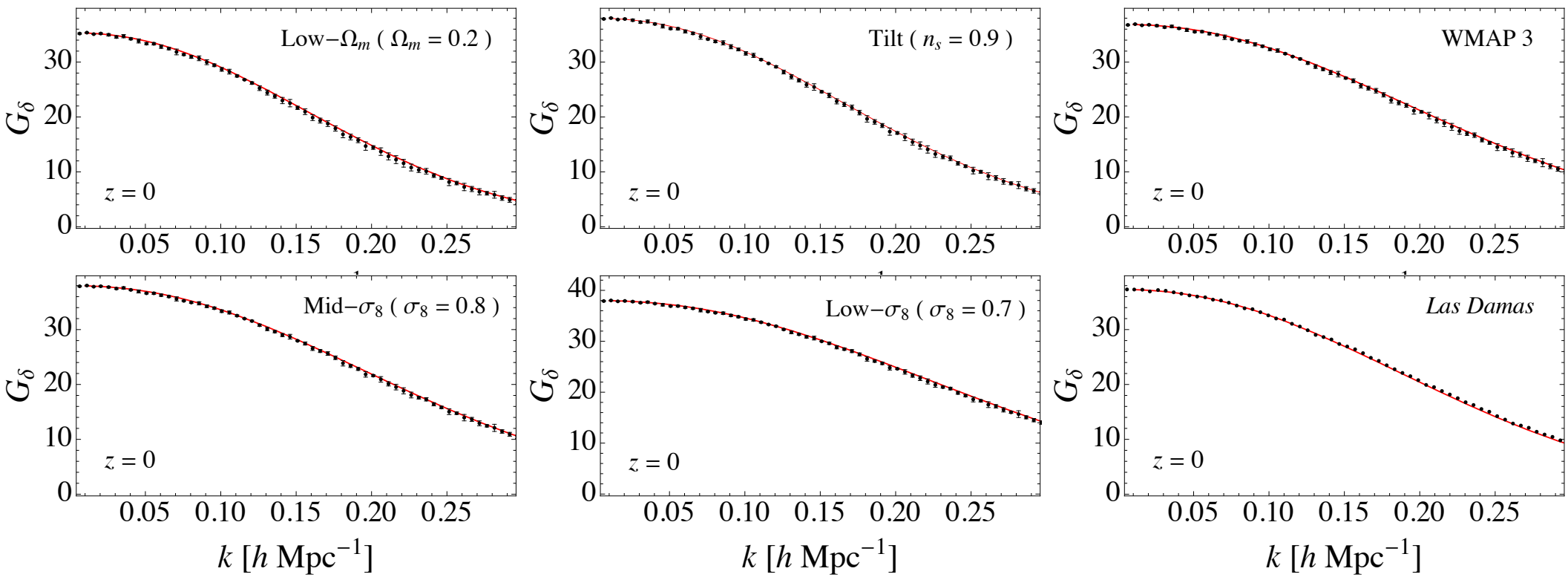

For the power spectrum, RPT reorganizes the PT expansion,

$$P(k,z) = D_+^2(z)\,P_0(k) + P_{1\mathrm{loop}}(k,z) + P_{2\mathrm{loop}}(k,z) + \ldots$$

into,

$$P(k,z) = G^2(k,z)\,P_0(k) + P_{\mathrm{MC}}(k,z)$$

with,

$$P_{\mathrm{MC}}(k,z) = P_{\mathrm{MC}}^{1\mathrm{loop}}(k,z) + P_{\mathrm{MC}}^{2\mathrm{loop}}(k,z) + \ldots$$

Thus, non linear effects can be divided (exactly) into two classes,

- those that are proportional to the initial power at same k.
- those that create power at k even if there was no power to begin with (mode-coupling)

The two-pt function can be written as,

$$\xi(r,z) = [G^2 \otimes \xi_0](r,z) + \xi_{\mathrm{MC}}(r,z),$$

The Power Spectrum in RPT

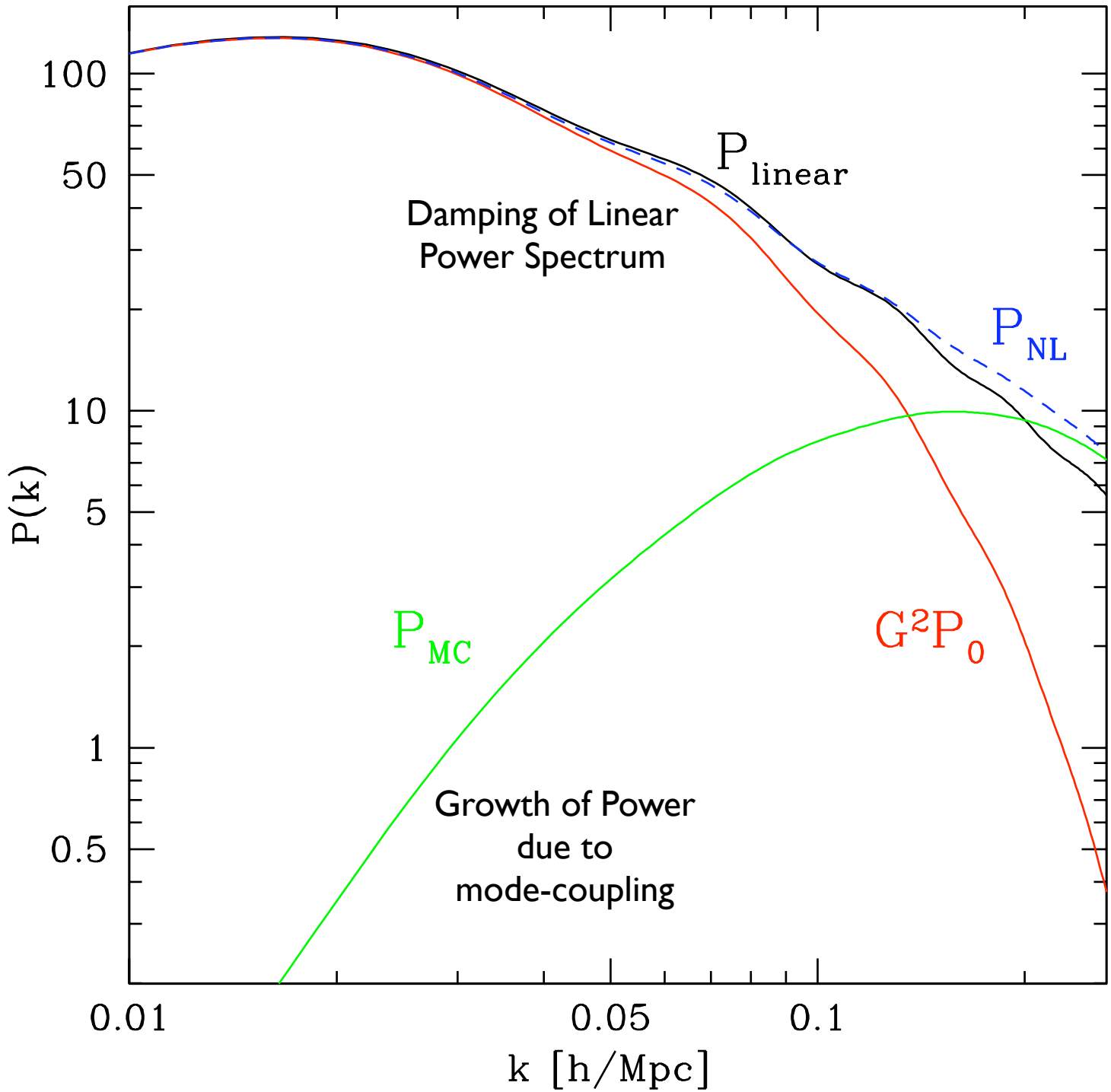

The Two-Point Function in RPT

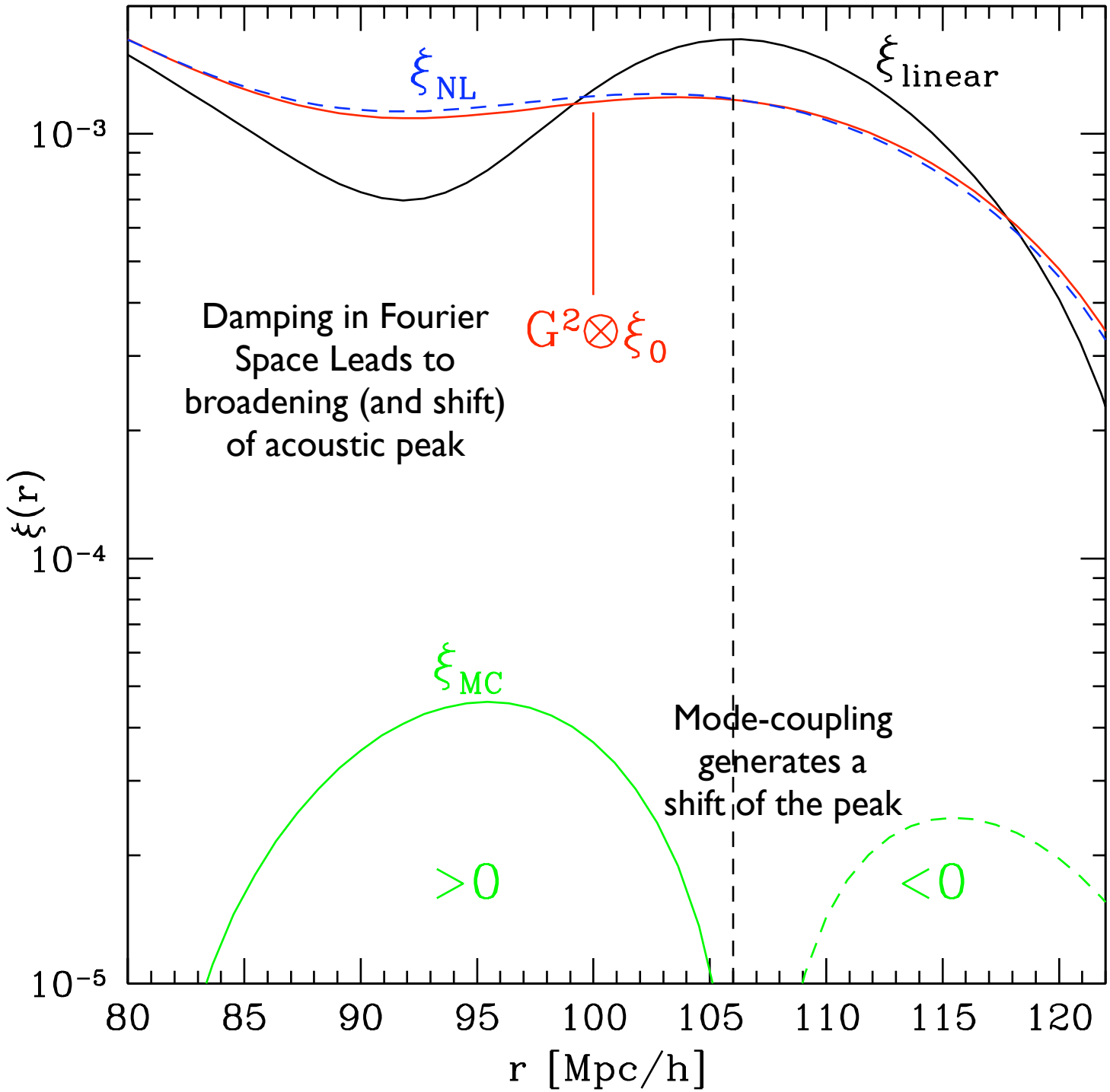

PT expansion (schematic)

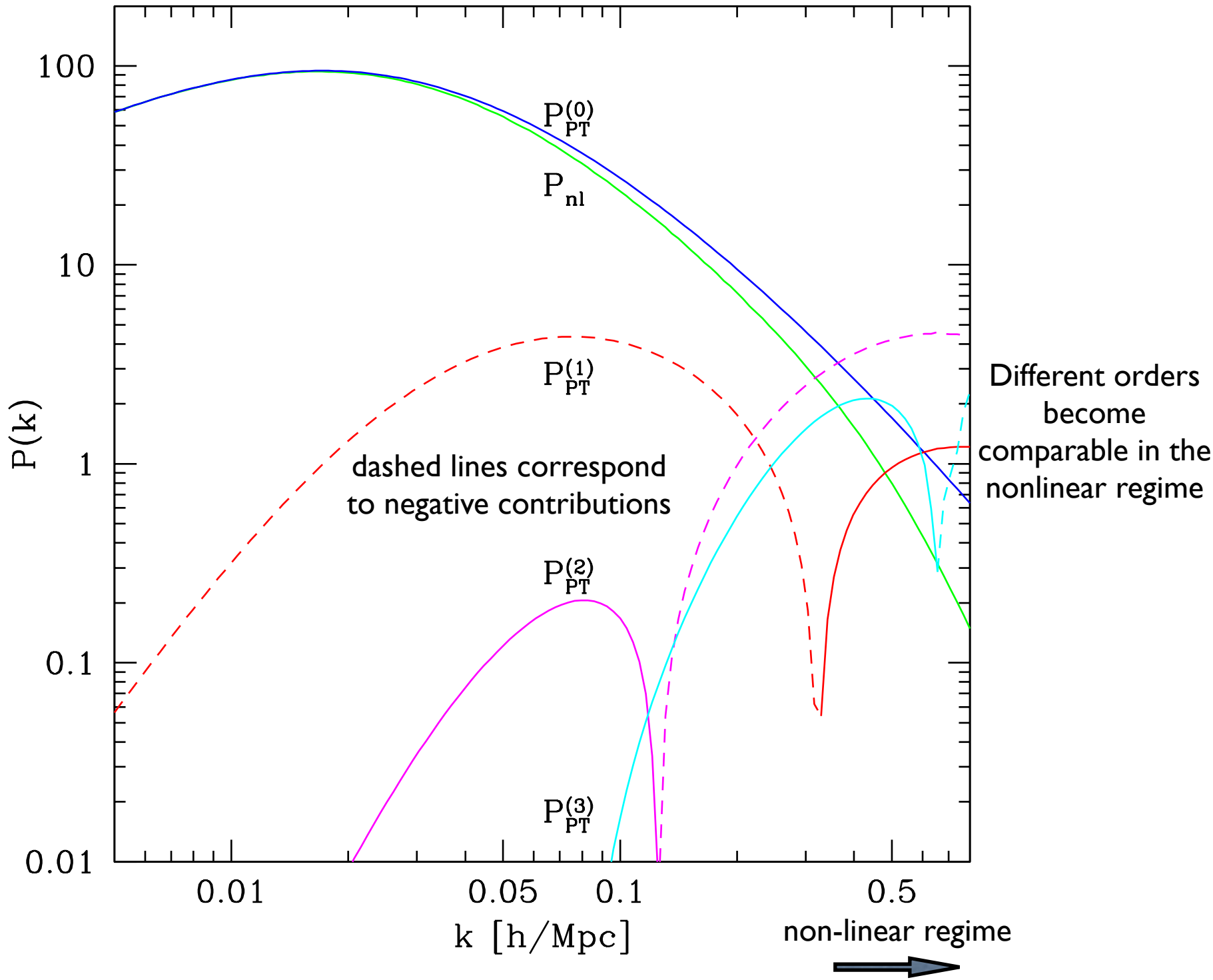

RPT expansion (schematic)

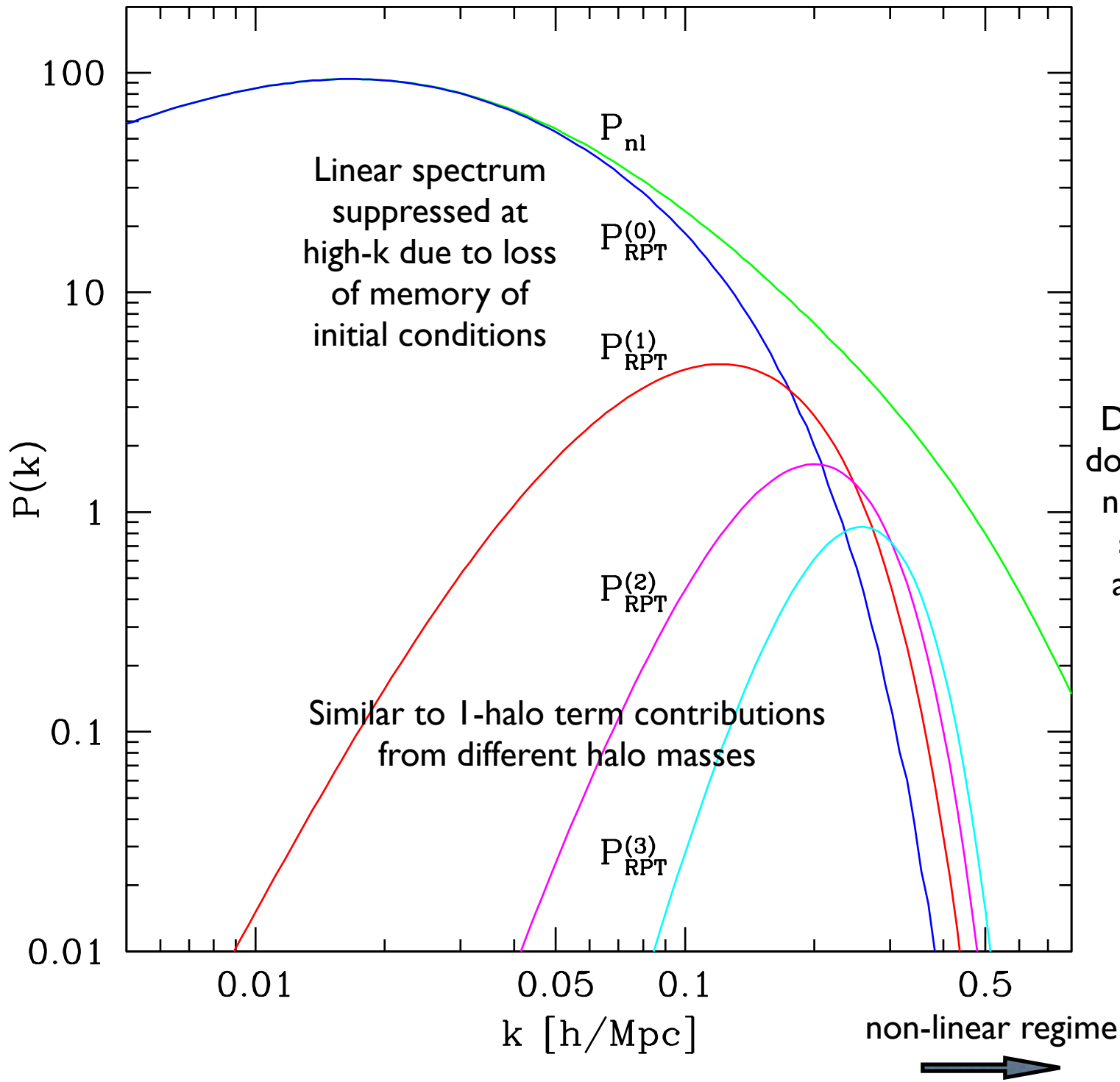

Different orders dominate only in a narrow range of scales and are always positive

Explicit calculation of Mode-Coupling power to 2-loops in RPT

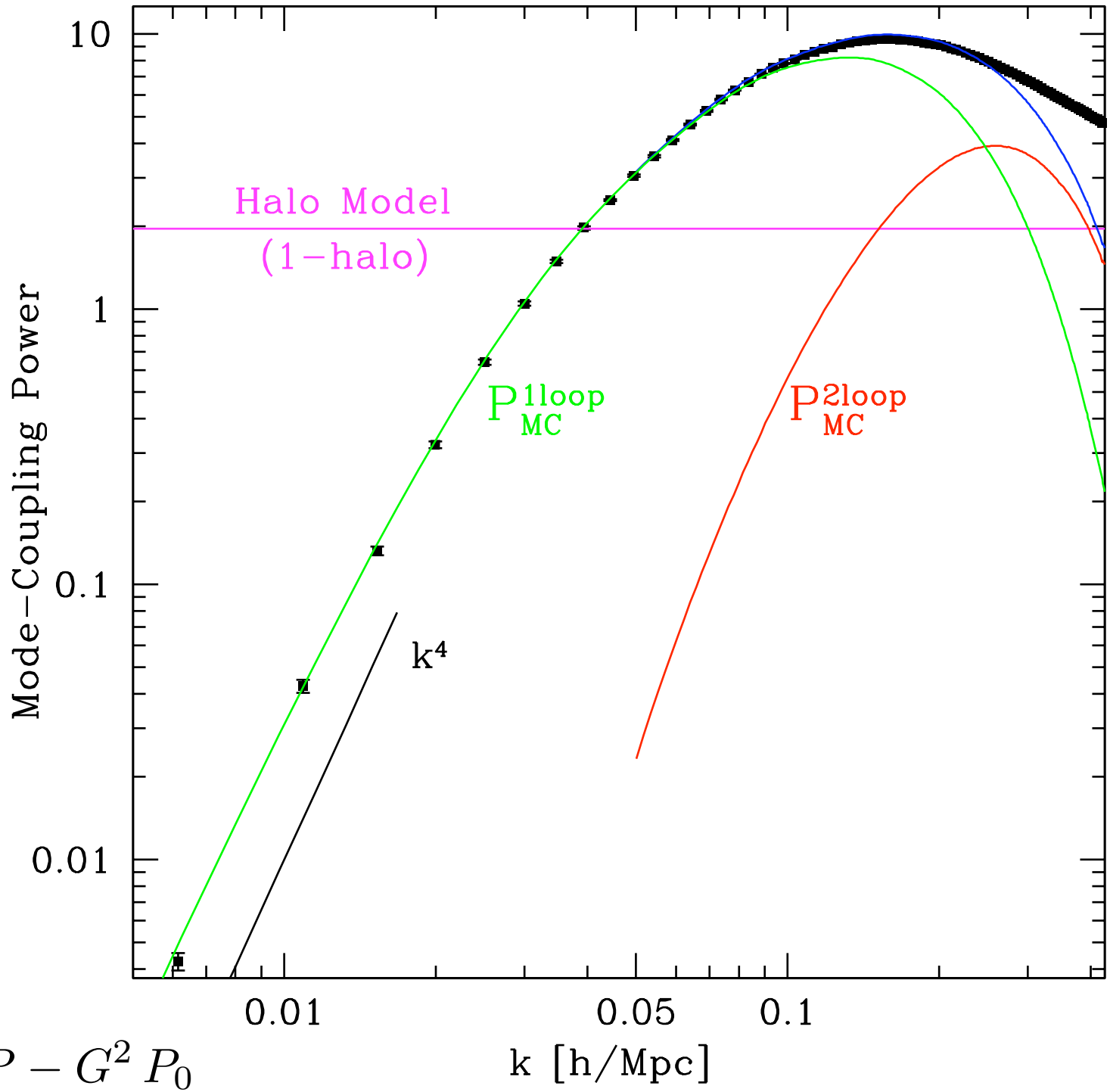

$$P_{\rm MC} \equiv P - G^2\, P_0$$

Nonlinear Evolution of the Power Spectrum and Acoustic Oscillations

- Can use acoustic oscillations imprinted in the dark matter power spectrum as a probe of expansion history (to get to dark energy / modified gravity).

- This "ruler", however, gets modified due to nonlinearities

Challenge: 1% error on sound horizon (~wiggle positions)
induces about 5% error on w

Nonlinear Evolution of Acoustic Oscillations

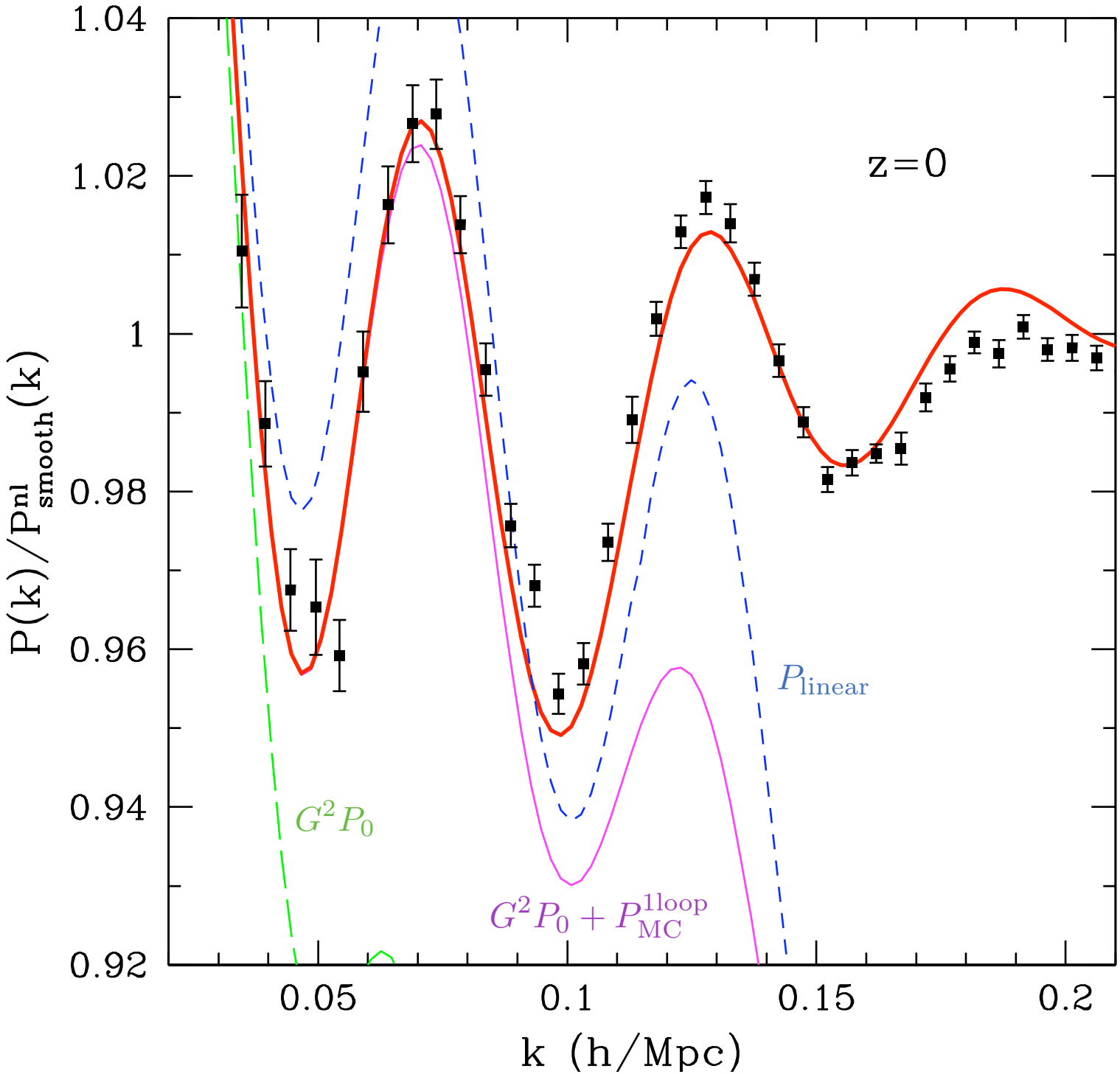

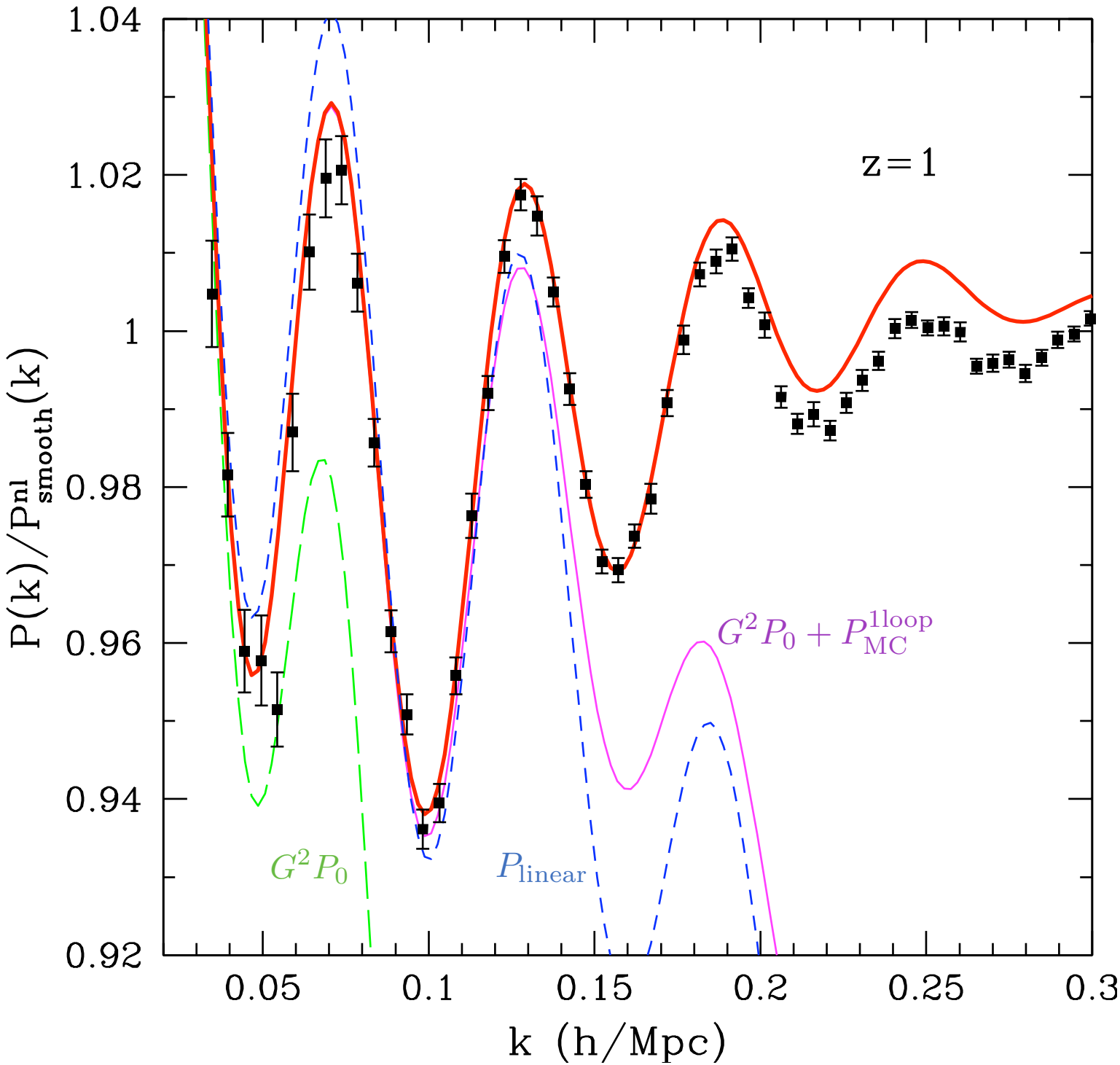
1.04
1.02
1
0.98
0.96
0.94
0.92
0.05
0.1
0.15
0.2
0.25
0.3
k (h/Mpc)
P(k)/P^nl_smooth(k)
z=1
$G^2 P_0 + P_{\rm MC}^{\rm 1loop}$
$G^2 P_0$
$P_{\rm linear}$

Power Spectrum: Dependence on Cosmology

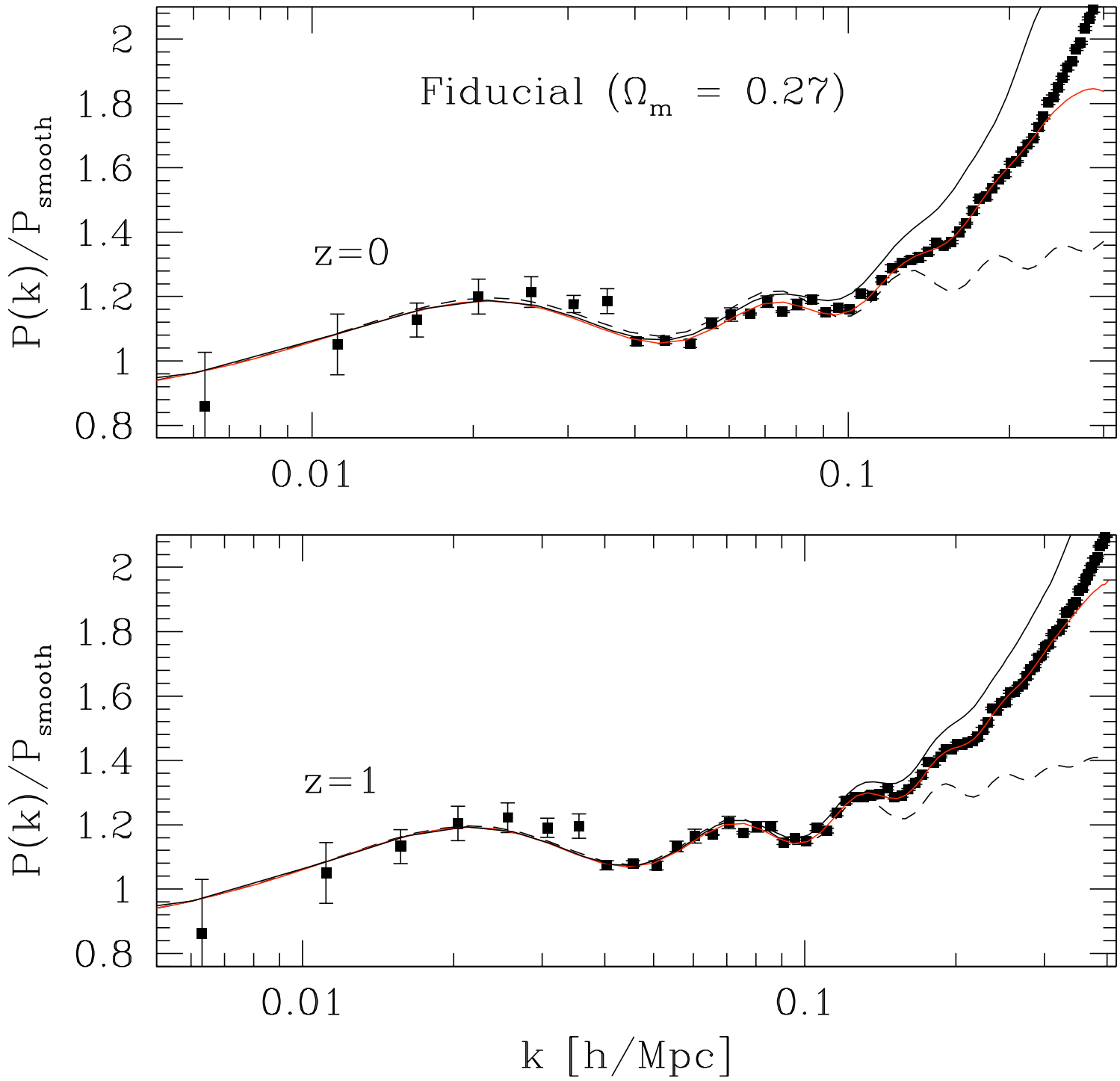

Power Spectrum: Dependence on Cosmology

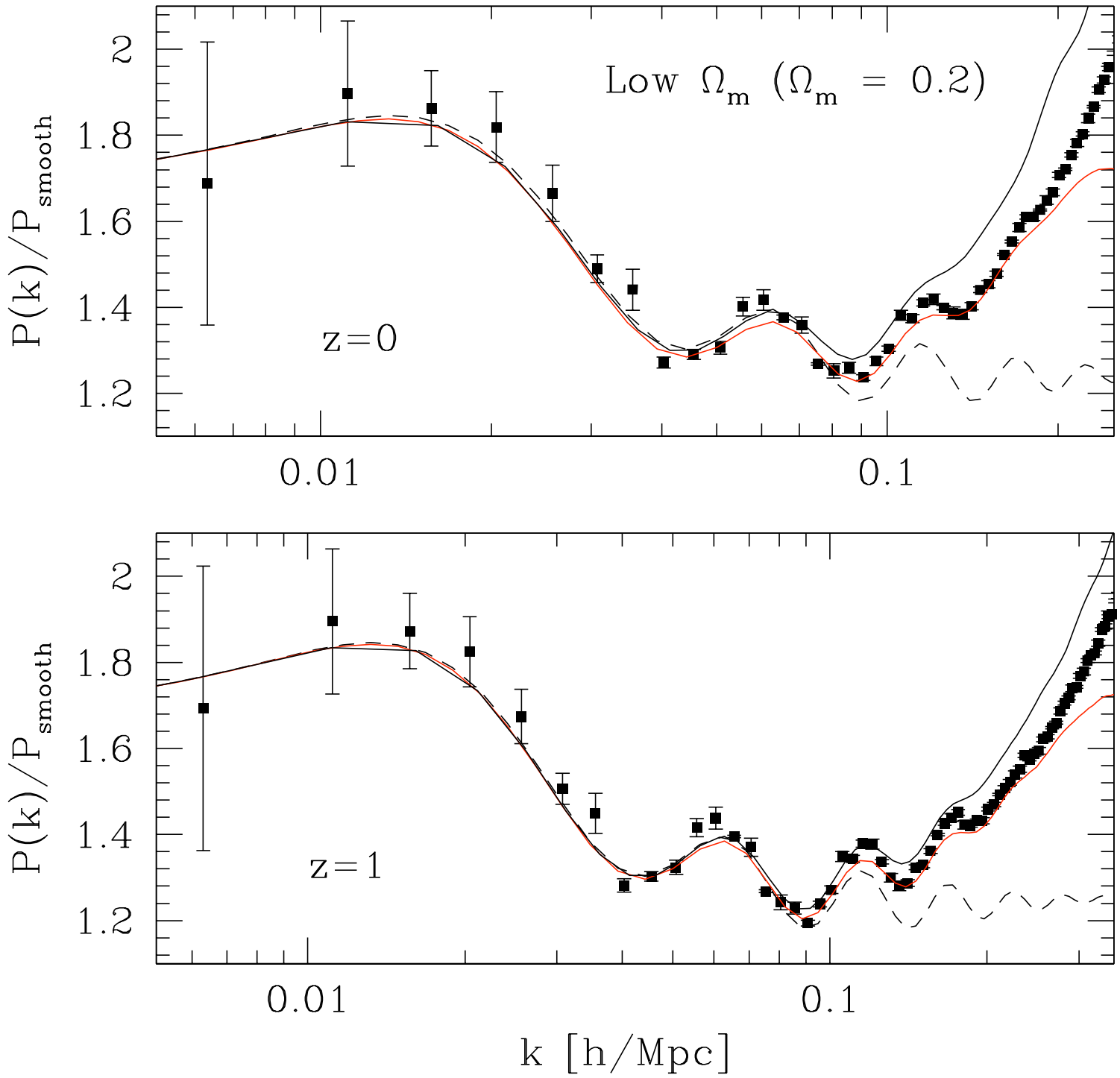

Power Spectrum: Dependence on Cosmology

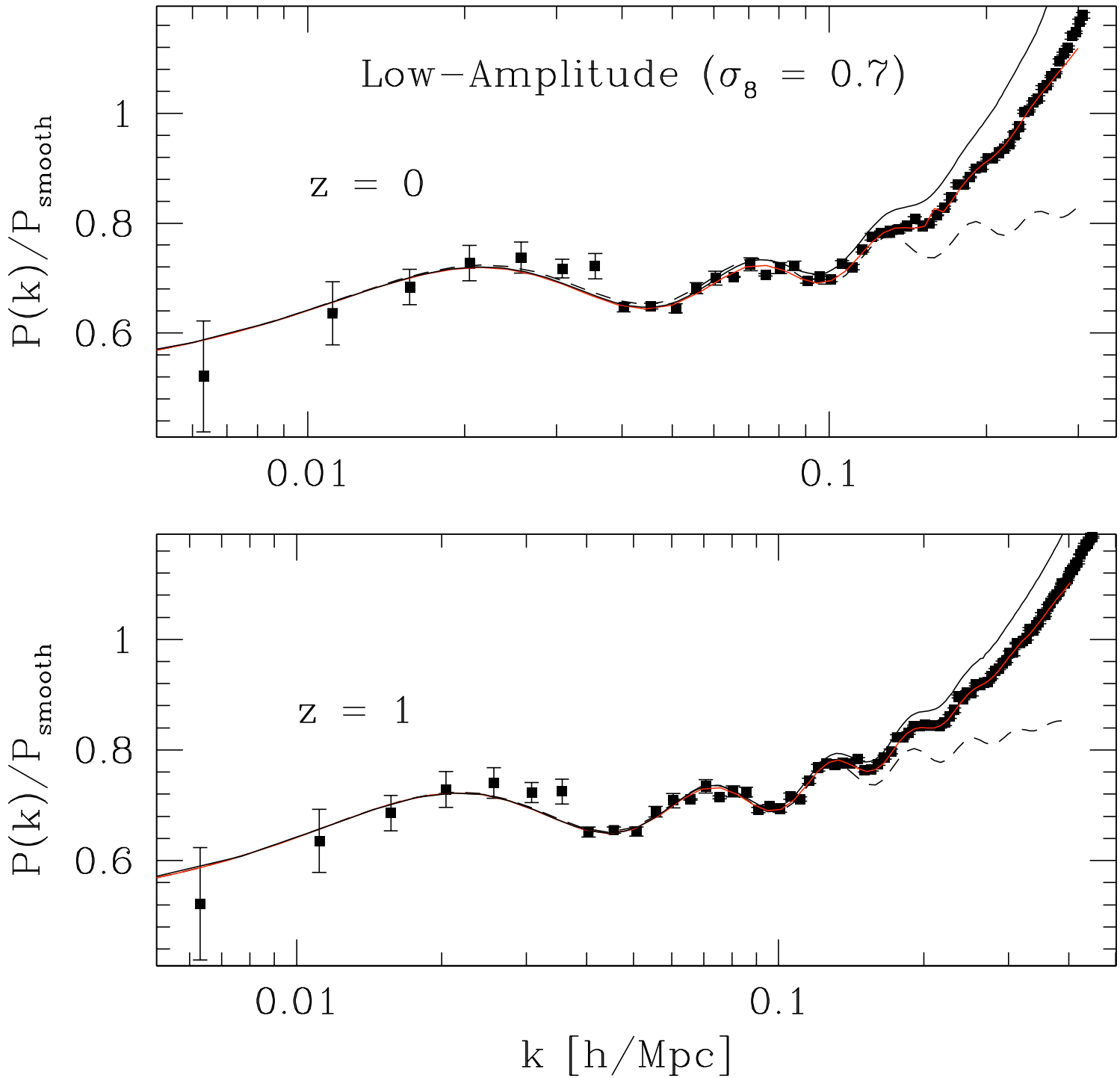

Power Spectrum: Dependence on Cosmology

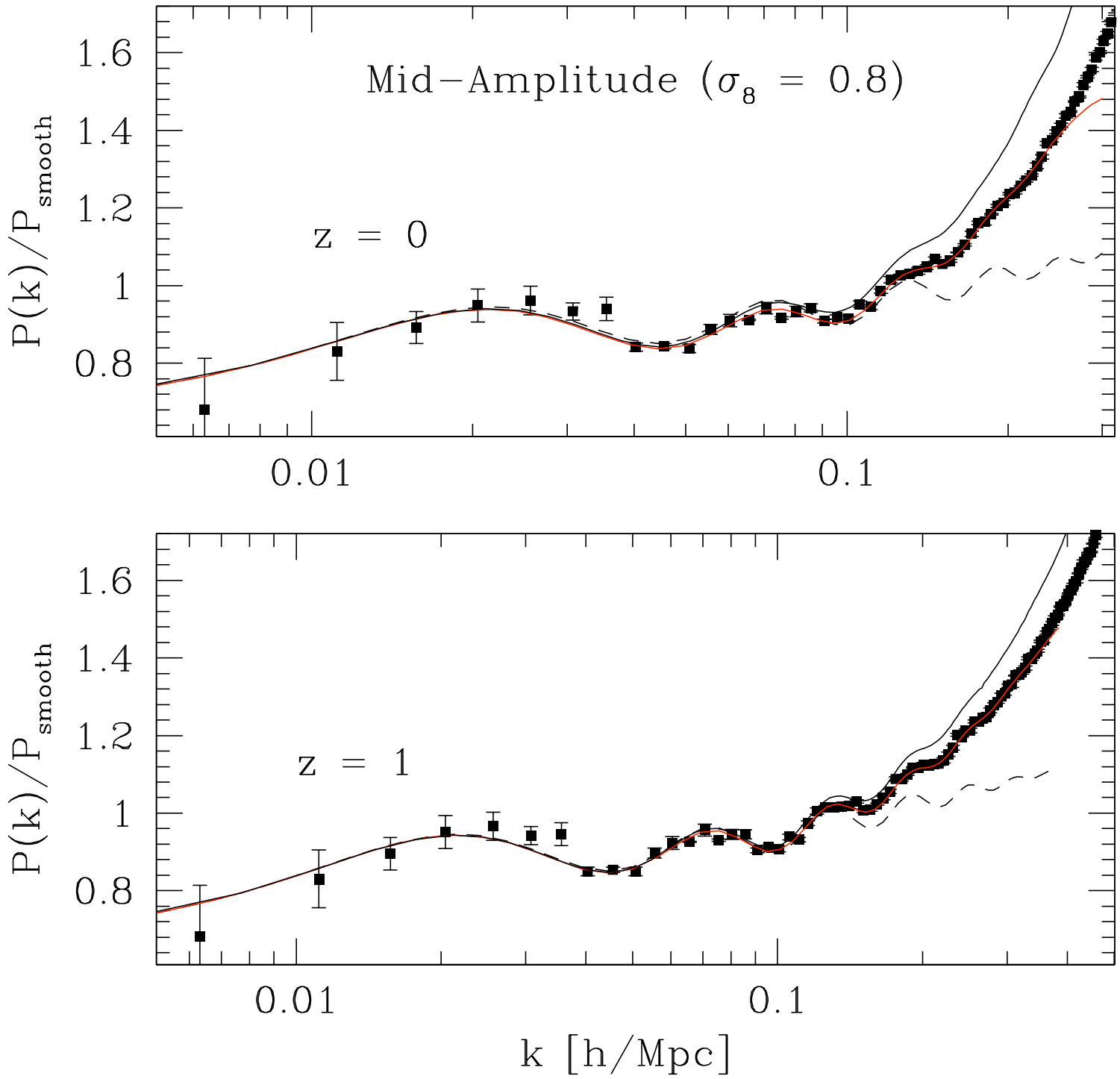

Power Spectrum: Dependence on Cosmology

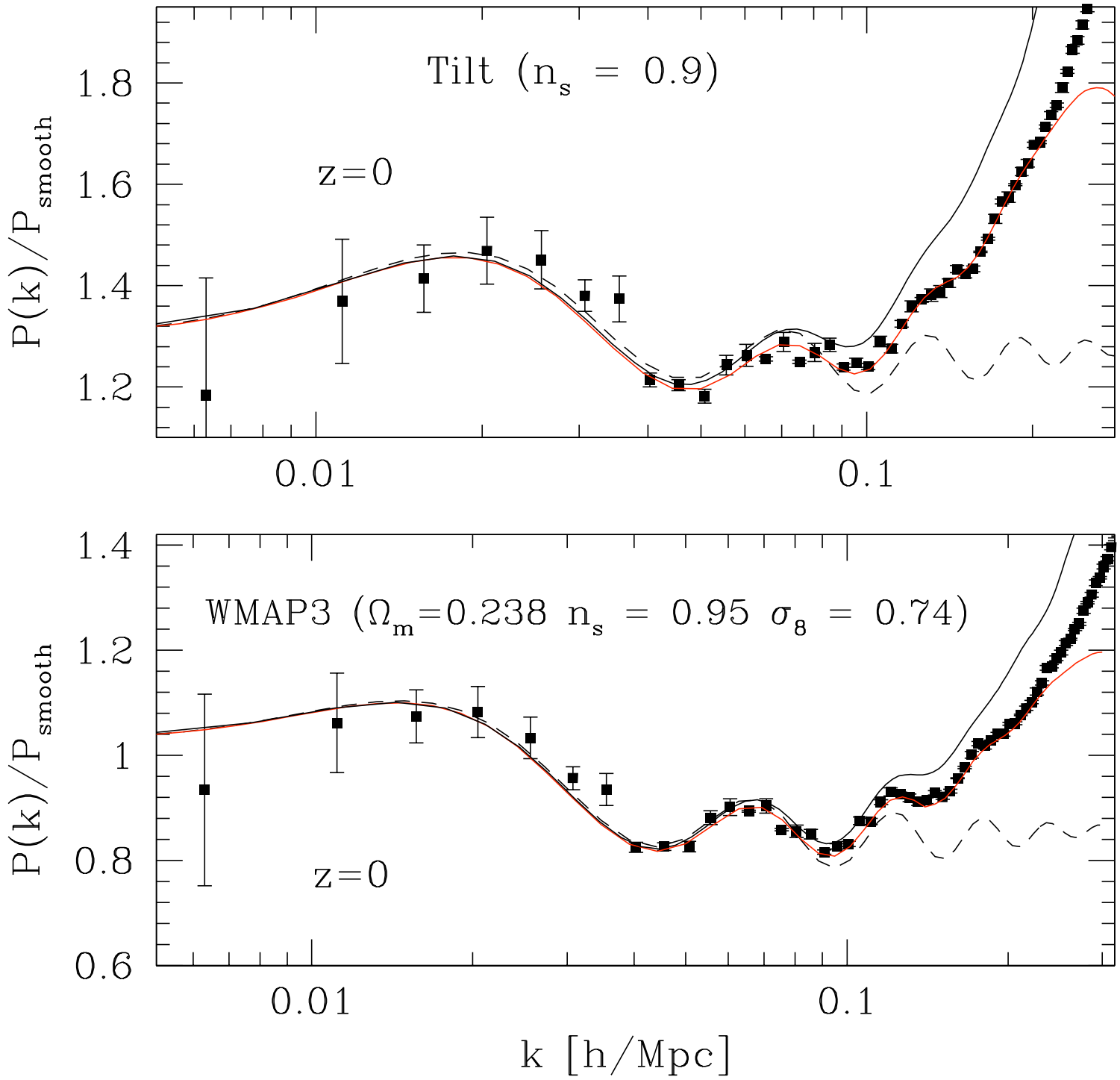

Beyond the pressure-less perfect fluid approximation (PPF)

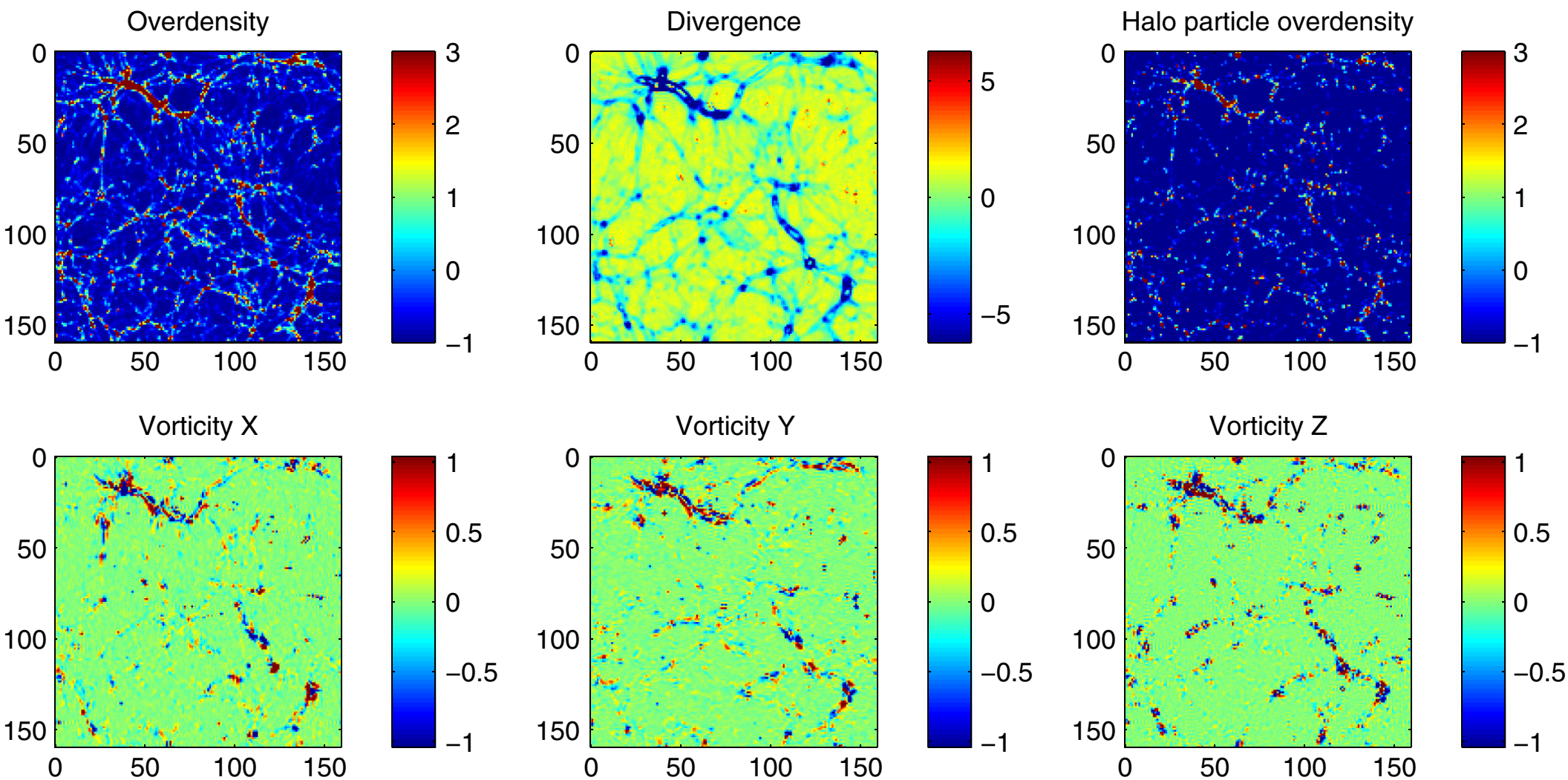

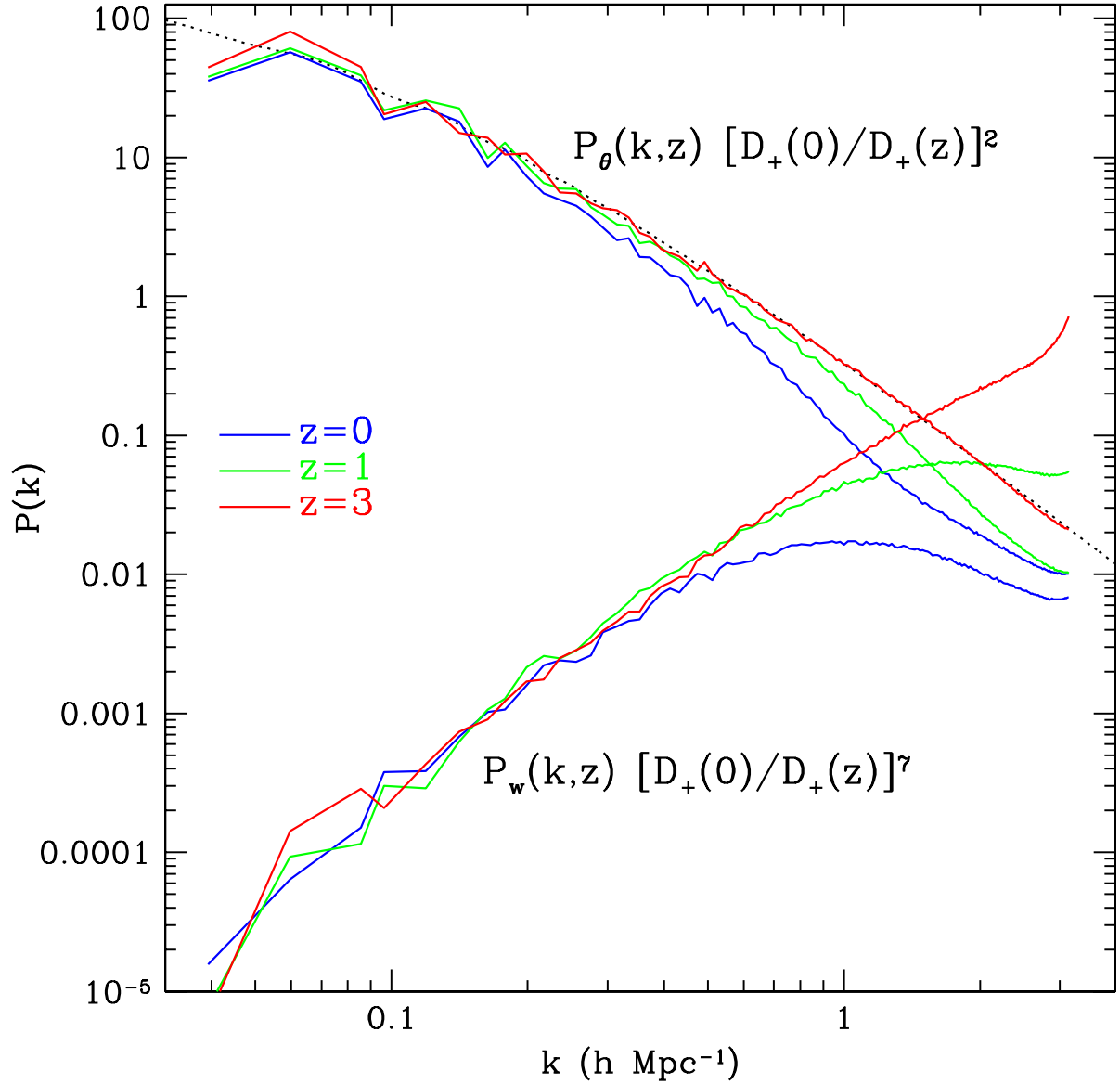

Divergence versus Vorticity Power

FIG. 4 (color online). Time dependence of the divergence and vorticity power spectra. The divergence power spectrum at $z = 1$ and $z = 3$ are linearly extrapolated to $z = 0$ for comparison. The vorticity power spectrum was similarly scaled using Eq. (3) with $n_w = 7$. In the nonlinear regime, both divergence and vorticity grow slower than the large-scale extrapolation.

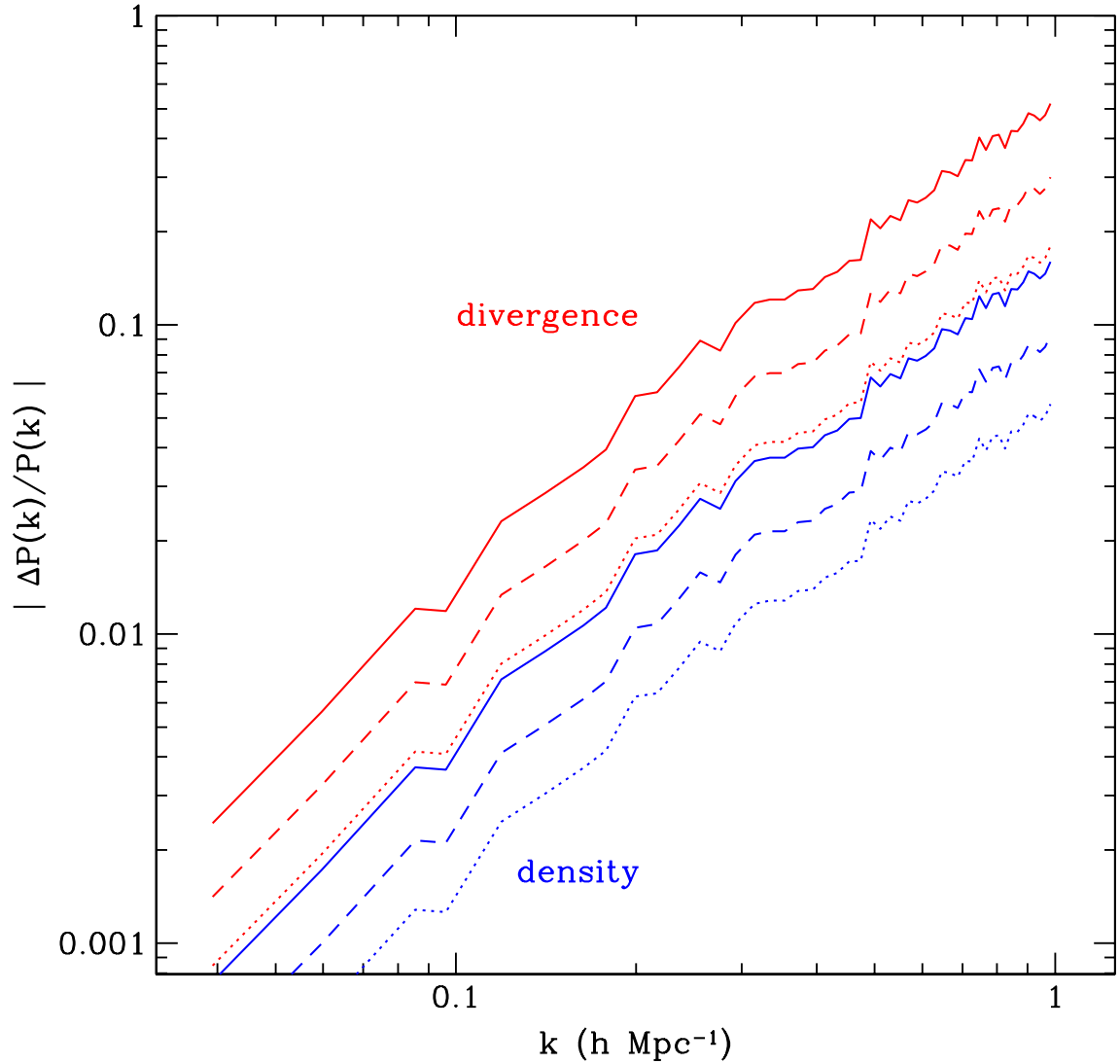

Impact of scalar modes in stress tensor (beyond PPF) on density P(k)

FIG. 9 (color online). Correction to the PPF approximation for the velocity divergence (three top lines) and density power spectrum (three bottom lines) due to velocity dispersion at redshifts $z = 0$ (solid lines), $z = 0.5$ (dashed lines) and $z = 1$ (dotted lines). Note that the actual correction is negative in all cases, we plot their absolute values. These corrections are computed in linear theory, Eqs. (45) and (48), thus extrapolation well beyond $k \sim 0.1h$ Mpc^{-1} is only illustrative.

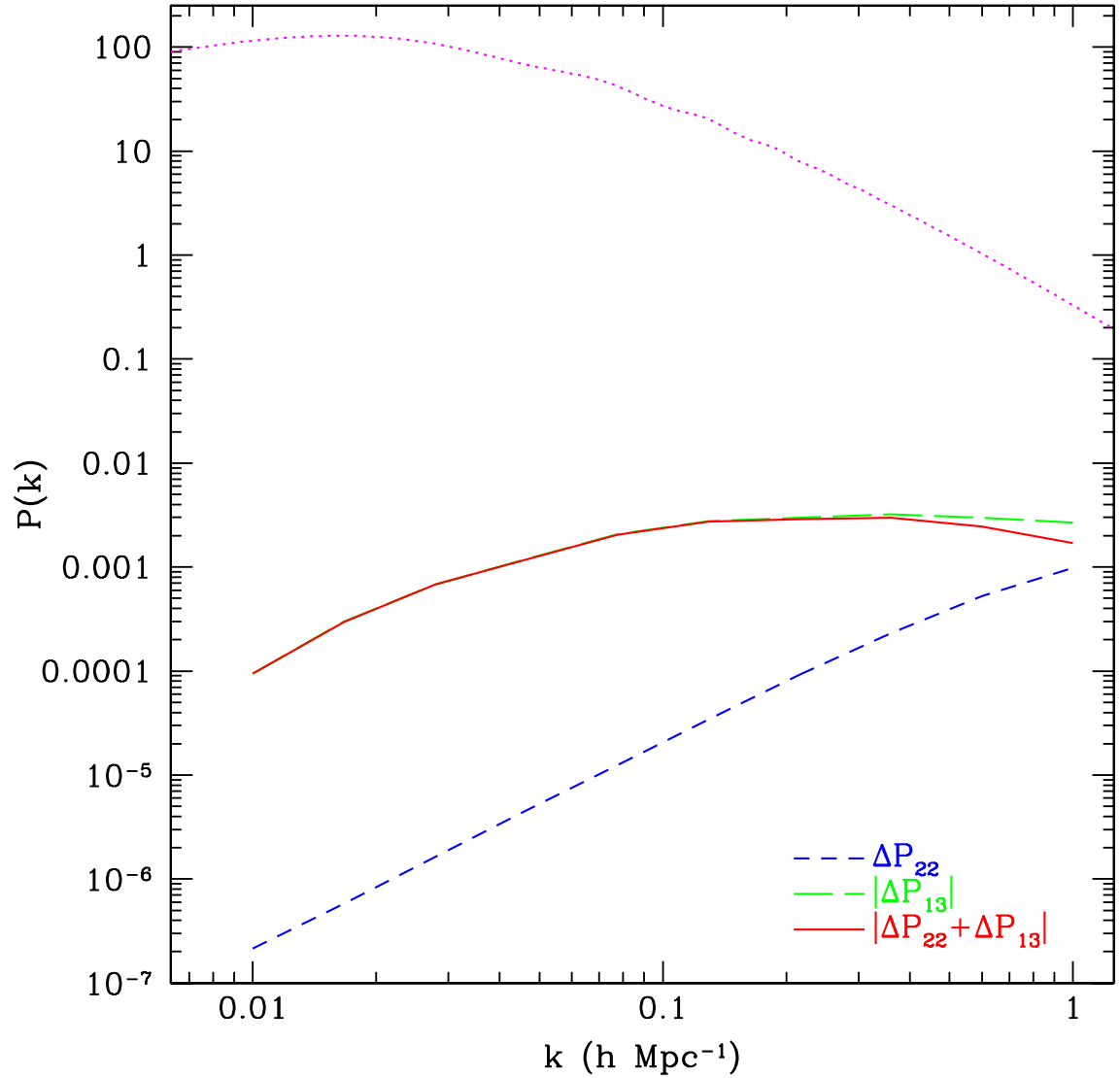

Impact of vector modes in stress tensor (beyond PPF) on density P(k)

FIG. 11 (color online). Corrections to the density power spectrum at $z = 0$ due to stress tensor vector modes (vorticity effects); see Eqs. (67) and (68). Note that the ΔP_{13} contribution (long dashed lines) is negative and larger in magnitude than the ΔP_{22} contribution (short dashed lines). The total correction (solid lines) is negative and reaches 1% of the *linear* spectrum (top dotted lines) at $k \sim 1h$ Mpc^{-1}, where further nonlinear effects not included here should become important.

Bias: From Dark Matter to Galaxies

The process that gives rise to the luminous galaxies we see in galaxy surveys is complicated and not yet fully understood, involving nontrivial effects from hydrodynamics and radiative transfer, among other things.

However, for the purpose of studying galaxy clustering there are many details of galaxy formation that are not needed, particularly if one is interested in the distribution at large scales (since gravity is the only long-range force).

- How different is the clustering of galaxies observed in surveys from the dark matter clustering we measure in numerical simulations?

Galaxy bias

a low-k arbitrary linear bias amplitude has been used to match amplitudes.

Hamilton & Tegmark (2001)

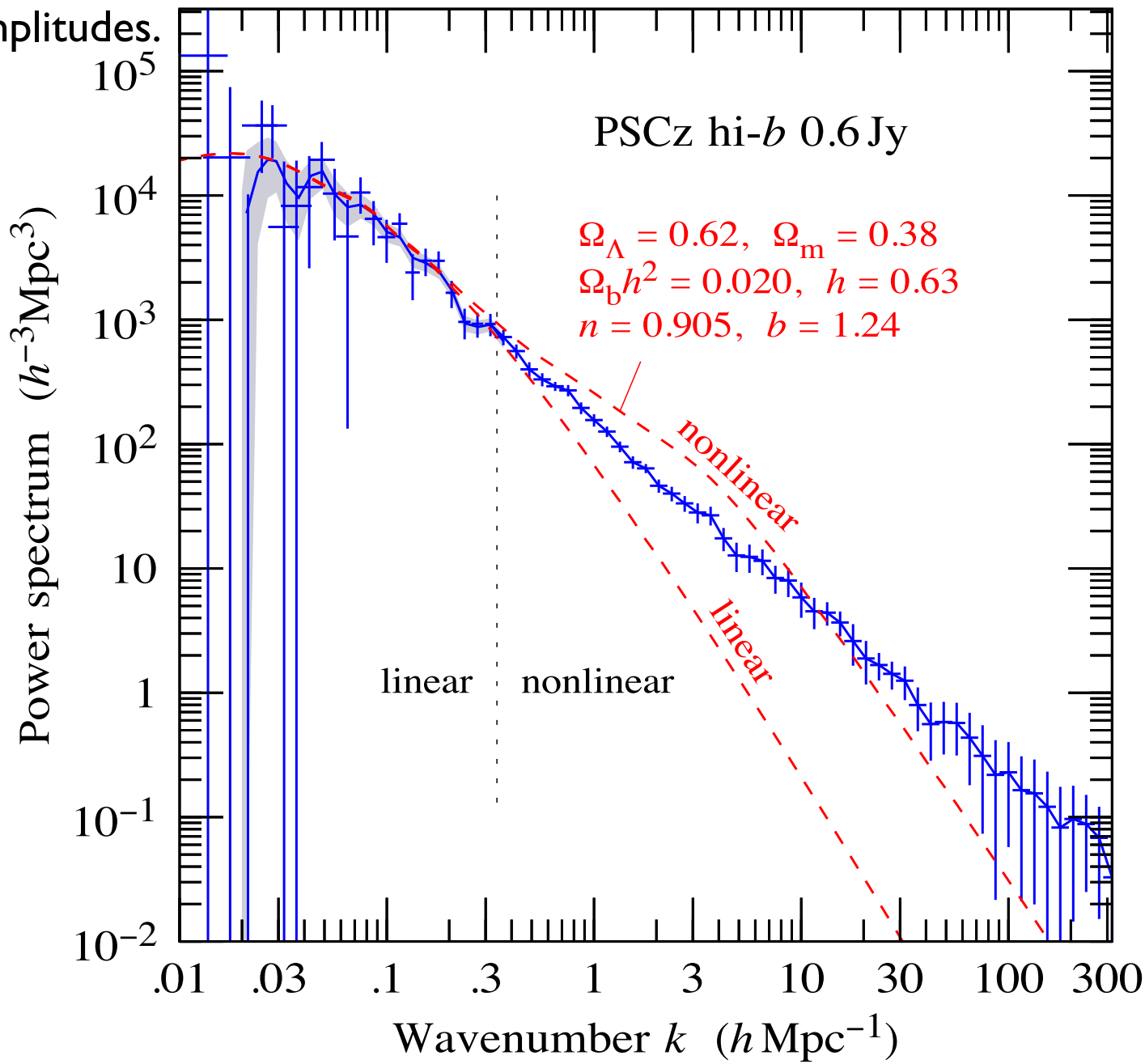

The Local Bias Model

When smoothed on sufficiently large scales R the relationship between galaxies and dark matter becomes a local mapping of fluctuations

$$\delta_g^R(x) = f(\delta^R(x))$$

Thus at large scales the relationship between galaxies and dark matter can then be approximated by,

$$\delta_g \approx b_1\delta + \frac{b_2}{2!}\delta^2 + \frac{b_3}{3!}\delta^3$$

and then one can use this to calculate galaxy correlation functions, e.g. the power spectrum,

$$P_g(k) = b_1^2 P(k) + \ldots$$

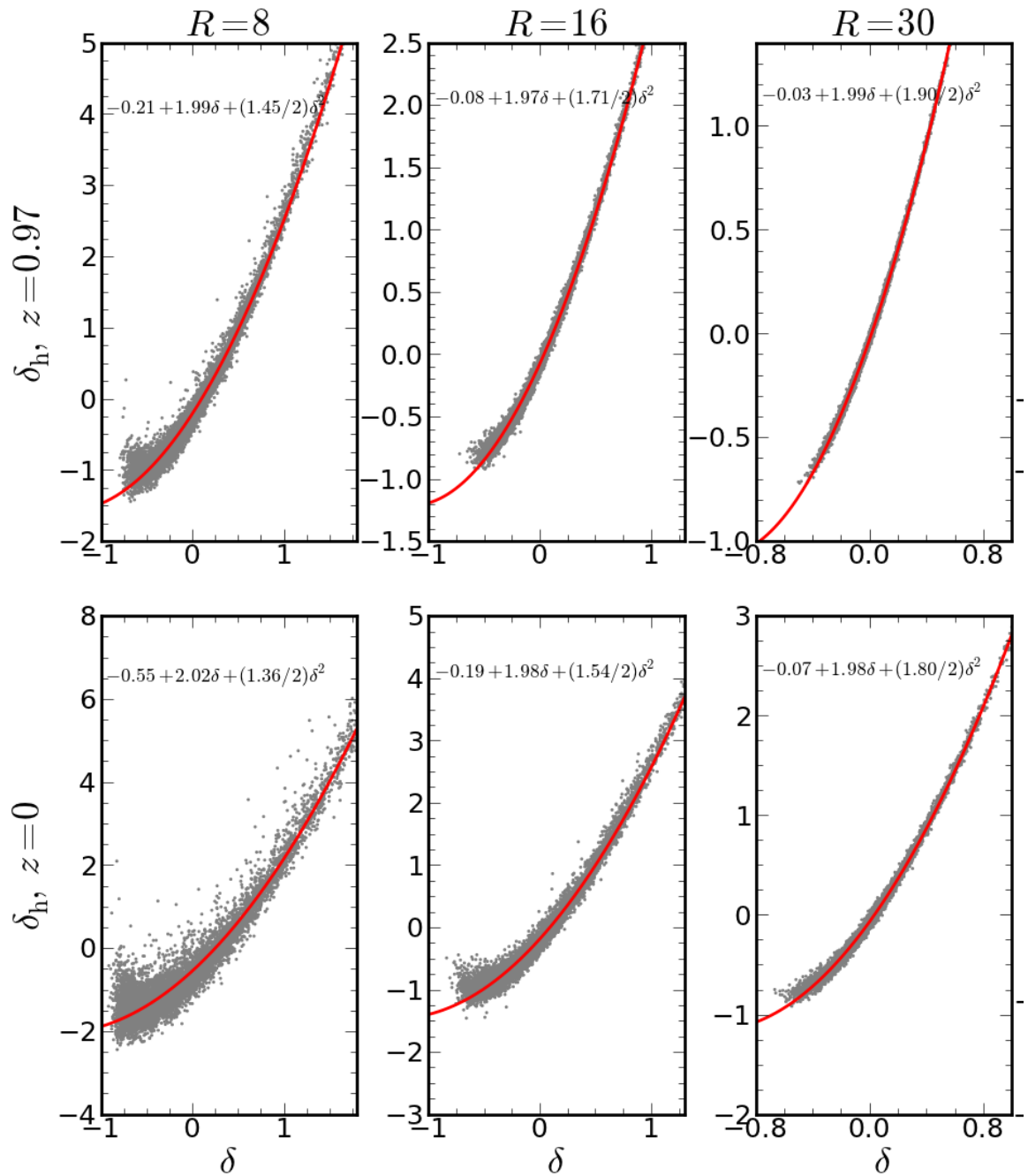
$R=8$
$R=16$
$R=30$
$\delta_{\rm h},\ z=0.97$
$\delta_{\rm h},\ z=0$
$-0.21+1.99\delta+(1.45/2)\delta^2$
$-0.08+1.97\delta+(1.71/2)\delta^2$
$-0.03+1.99\delta+(1.90/2)\delta^2$
$-0.55+2.02\delta+(1.36/2)\delta^2$
$-0.19+1.98\delta+(1.54/2)\delta^2$
$-0.07+1.98\delta+(1.80/2)\delta^2$
δ

Bias parameters measured from halo-matter scatter plots:

- go to constants in the large-scale (large R) limit

- "run" with R at small scales

Alternatively, one can measure the bias parameters in Fourier space, by using higher-order correlations (comparing the tracer bispectrum to the matter bispectrum)

This is more practical than scatter plots for observations (where no scatter plot can easily be constructed)

Bias Parameters from Large-Scale Correlations

One can use higher-order correlation functions to determine the bias parameters. The three-point function (bispectrum) can be estimated by,

$$B_{123} \propto \int d^3x \; \delta_{k_1}(\mathbf{x})\delta_{k_2}(\mathbf{x})\delta_{k_3}(\mathbf{x})$$

When suitably normalized, it depends only on galaxy bias and spectral index,

$$Q_B = \frac{B_{123}}{P_1 P_2 + P_2 P_3 + P_3 P_1}$$

$$Q_B^g = \frac{1}{b_1} Q_B + \frac{b_2}{b_1^2}$$

Bispectrum

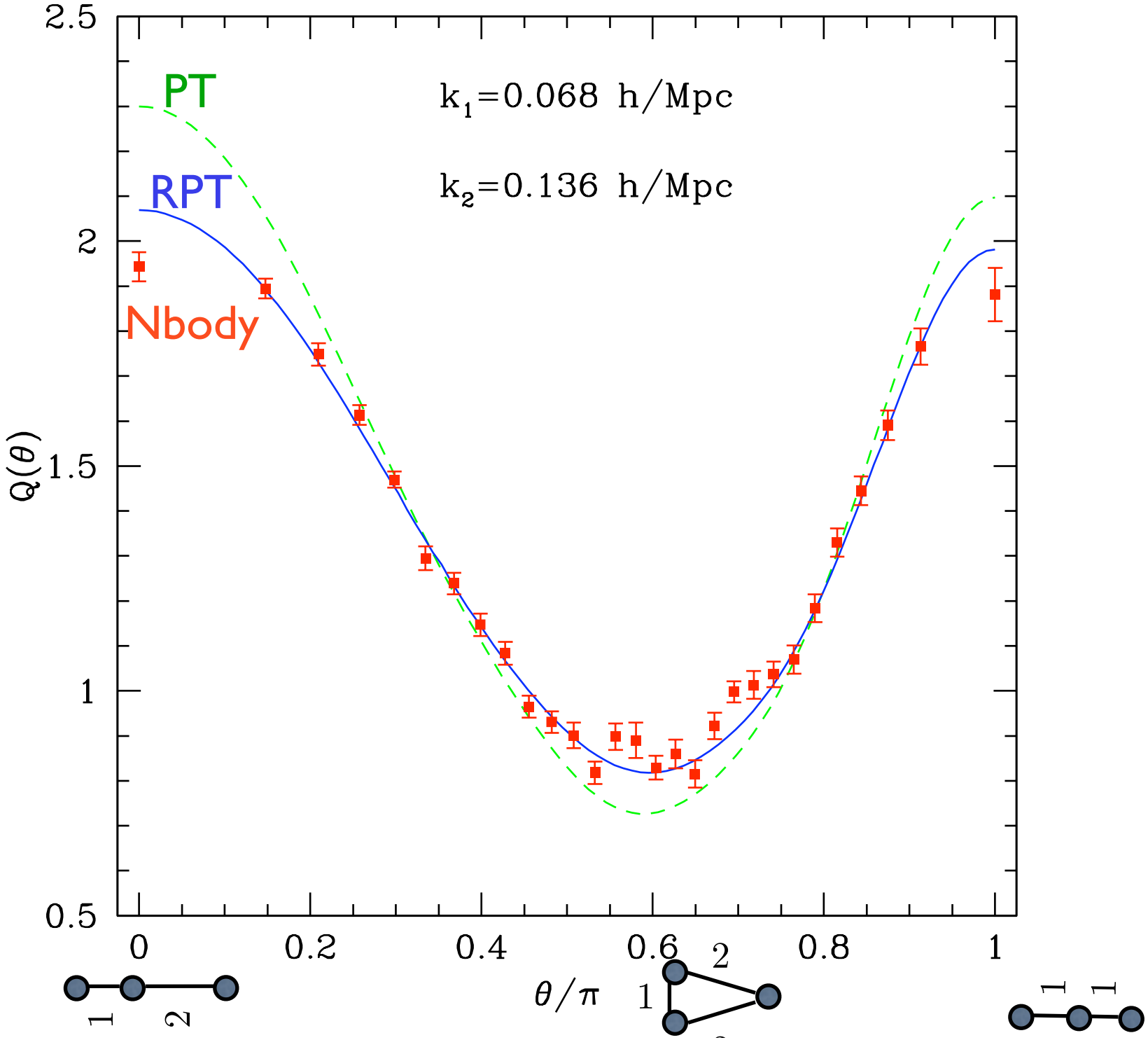
PT
RPT
Nbody
k_1=0.068 h/Mpc
k_2=0.136 h/Mpc
$Q(\theta)$
θ/π
2.5
2
1.5
1
0.5
0
0.2
0.4
0.6
0.8
1
1
2
2
1
1
1

Bispectrum analysis of local bias

TABLE II. Local Eulerian bias parameters b_1 and b_2 obtained from halo-matter-matter bispectrum fits for all triangles with $k < 0.1\,h\,\mathrm{Mpc}^{-1}$. We also include the large-scale bias $b_\times$ obtained from the halo-matter power spectrum, to be compared with b_1. The last column indicates the goodness of the fit assuming a diagonal covariance matrix ($N_{\mathrm{dof}} = 148$).

Sample	$b_\times$	b_1	b_2	χ^2/dof
LMz0	1.43	1.42 ± 0.01	-0.91 ± 0.03	1.86
MMz0	1.75	1.71 ± 0.01	-0.55 ± 0.03	1.29
HMz0	2.66	2.37 ± 0.02	2.98 ± 0.07	3.74
LMz0.5	1.88	1.77 ± 0.01	-0.15 ± 0.03	0.91
MMz0.5	2.26	2.13 ± 0.01	0.67 ± 0.03	0.87
HMz0.5	3.29	2.84 ± 0.03	5.89 ± 0.10	3.77
LMz1	2.43	2.22 ± 0.01	1.27 ± 0.04	0.89
MMz1	2.86	2.62 ± 0.02	2.77 ± 0.06	1.07
HMz1	3.99	3.41 ± 0.05	9.98 ± 0.14	3.42

Is local bias stable under time evolution?

Suppose at some time t*, objects form with local bias,

$$\delta_{\rm g}^* = b_1^* \, \delta_* + \frac{b_2^*}{2!} \, \delta_*^2 + \frac{b_3^*}{3!} \, \delta_*^3 + \ldots$$

As time goes on, does bias stay local?

The answer is (a resounding) no!

$$\begin{aligned}
\delta_{\rm g}^{\rm Nloc} &= \gamma_2 \, \mathcal{G}_2 \, (\Phi_{\rm v})(1 + \beta \, \delta) \\
&\quad + \gamma_3 \left(\mathcal{G}_3(\Phi_{\rm v}) + \frac{6}{7} \, \mathcal{G}_2(\Phi_{\rm v}^{(1)}, \Phi_{\rm 2LPT}) \right) + \ldots \\
\mathcal{G}_2(\Phi_{\rm v}) &= (\nabla_{ij} \Phi_{\rm v})^2 - (\nabla^2 \Phi_{\rm v})^2, \\
\mathcal{G}_3(\Phi_{\rm v}) &= (\nabla^2 \Phi_{\rm v})^3 + 2 \nabla_{ij} \Phi_{\rm v} \nabla_{jk} \Phi_{\rm v} \nabla_{ki} \Phi_{\rm v} - 3 (\nabla_{ij} \Phi_{\rm v})^2 \nabla^2 \Phi_{\rm v}.
\end{aligned}$$

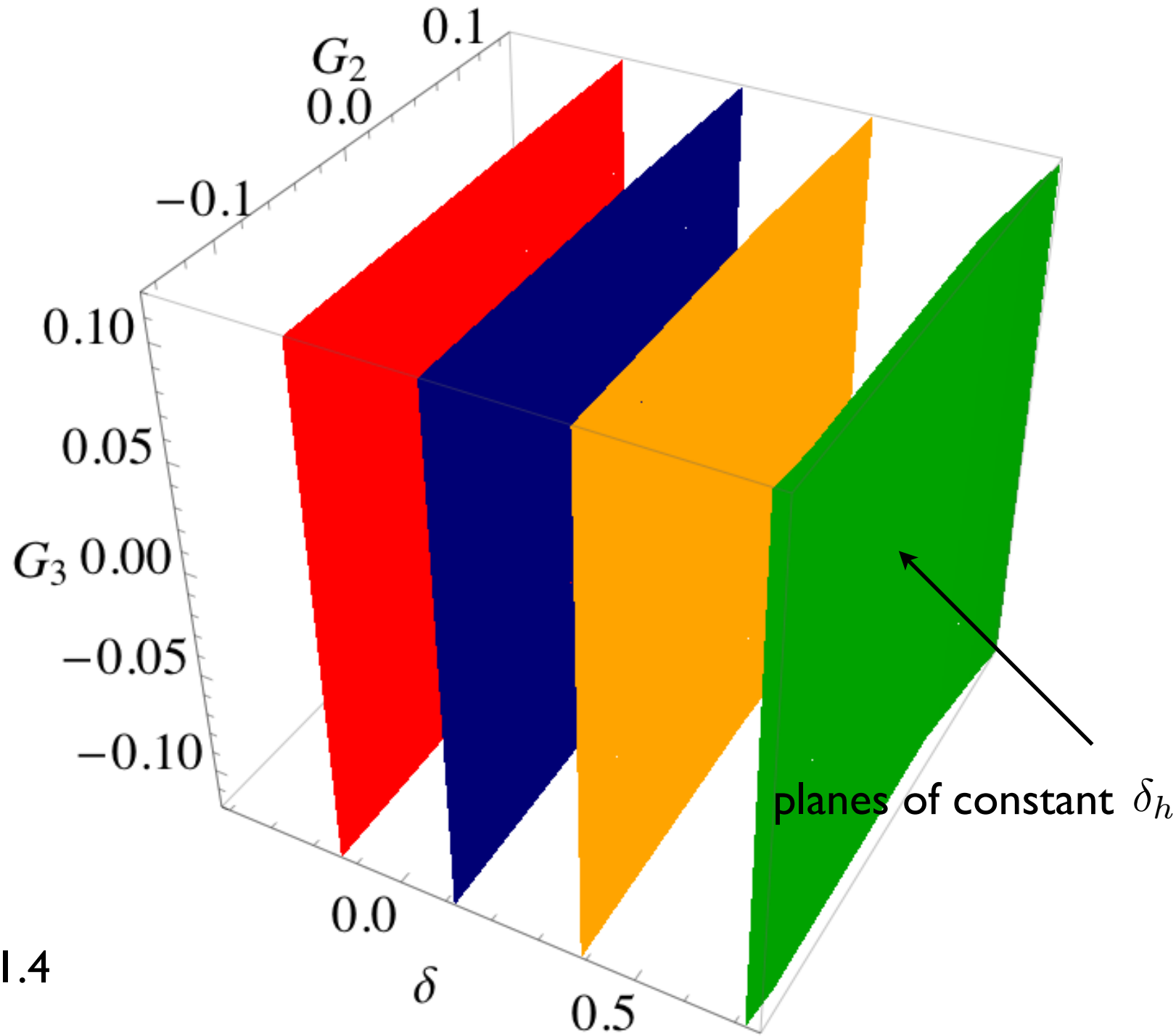

linear bias ~ 1.4

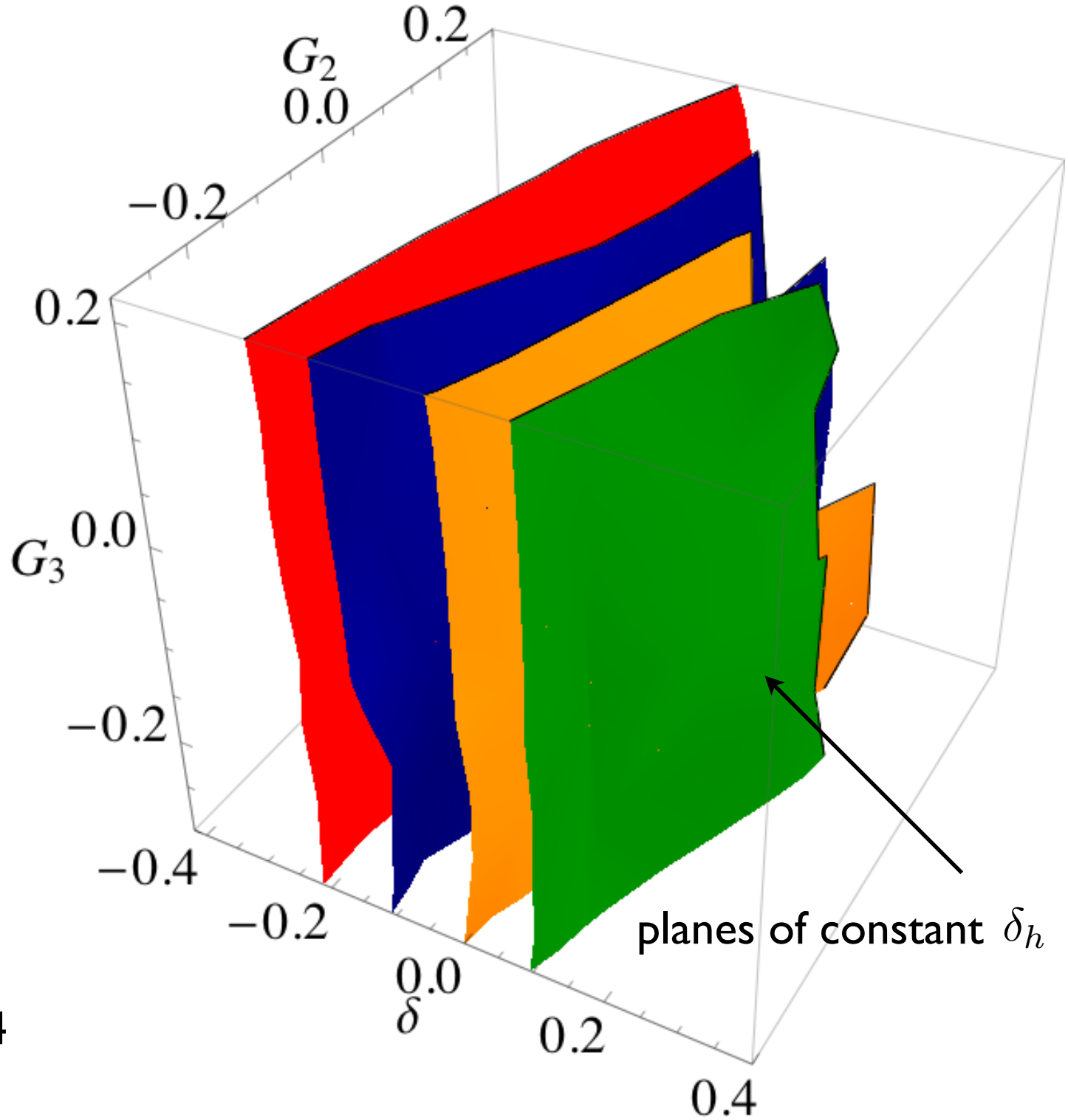

linear bias ~ 4

Bispectrum analysis of non-local bias

TABLE IV. Eulerian bias parameters b_1 and b_2 and non-local γ_2 parameter obtained from doing a quadratic non-local bias model fit to the bispectrum. For comparison purposes, note that a non-zero γ_2 gives an effective $-(4/3)\gamma_2$ contribution to b_2 (see top panel in Fig. 8). Here $N_{\rm dof} = 147$.

Sample	$b_\times$	b_1	b_2	γ_2	χ^2/dof
LMz0	1.43	1.42 ± 0.02	-0.92 ± 0.08	-0.01 ± 0.03	1.87
MMz0	1.75	1.76 ± 0.02	-0.81 ± 0.08	-0.10 ± 0.03	1.19
HMz0	2.66	2.61 ± 0.04	1.71 ± 0.18	-0.48 ± 0.06	2.74
LMz0.5	1.88	1.83 ± 0.02	-0.46 ± 0.09	-0.12 ± 0.03	0.84
MMz0.5	2.26	2.24 ± 0.02	0.05 ± 0.09	-0.24 ± 0.03	0.67
HMz0.5	3.29	3.16 ± 0.06	4.10 ± 0.28	-0.70 ± 0.10	2.91
LMz1	2.43	2.35 ± 0.03	0.57 ± 0.13	-0.28 ± 0.05	0.74
MMz1	2.86	2.80 ± 0.03	1.70 ± 0.16	-0.42 ± 0.06	0.80
HMz1	3.99	3.84 ± 0.08	7.55 ± 0.41	-0.96 ± 0.16	2.73

Impact of non-local bias on the power spectrum

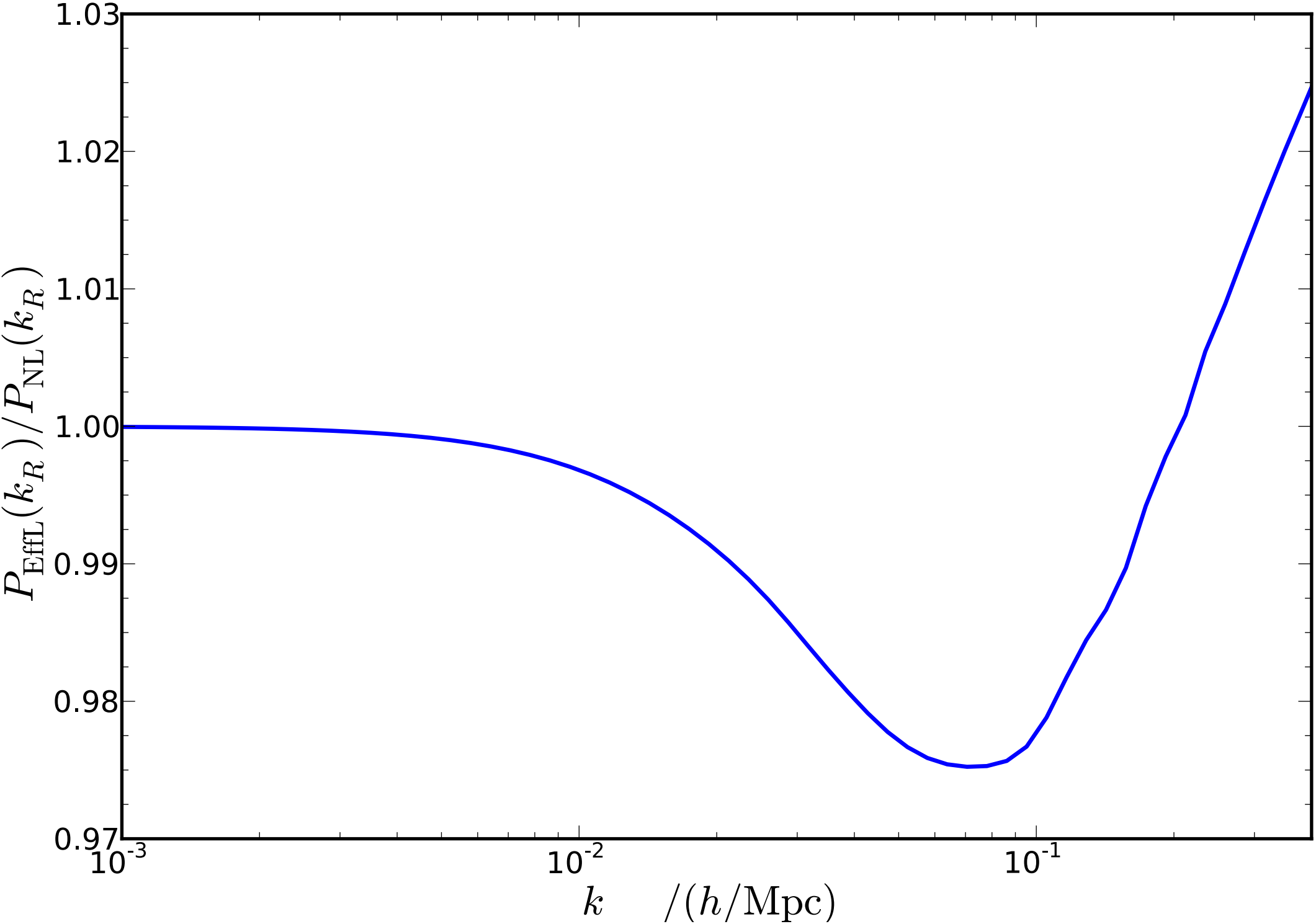

Redshift Distortions

Velocity-Dispersion Effect
(aka Finger of God)
effects small scales ~ few Mpc

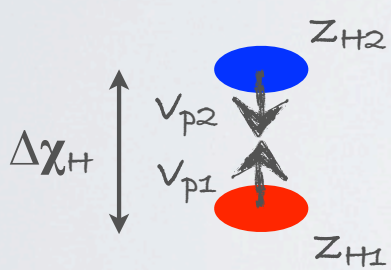

Real Comoving Space

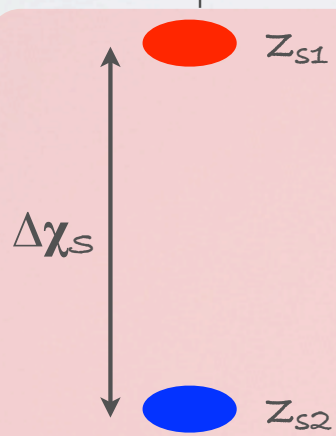

Redshift Space

Squashing Effect
effects large scales ~10'sMpc

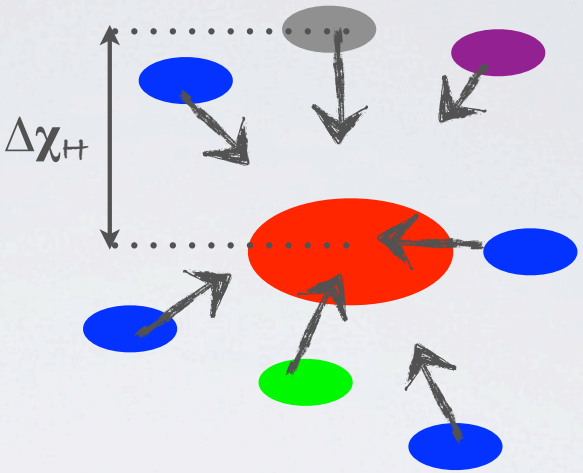

Real Comoving Space

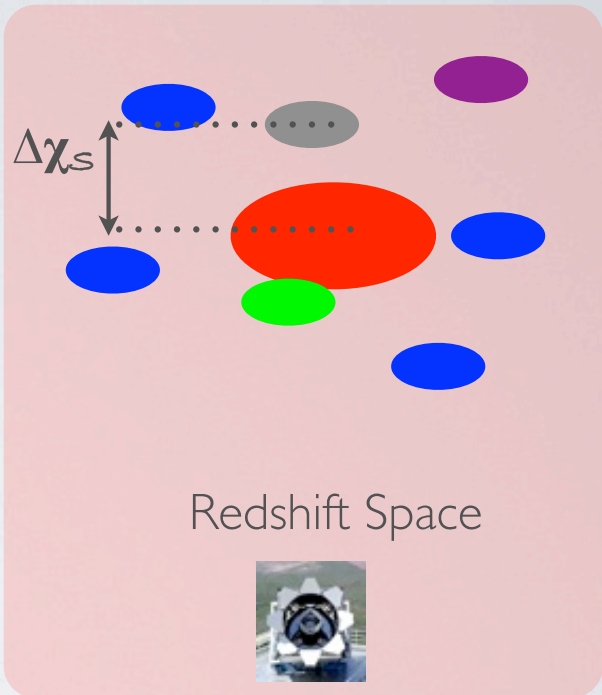

Redshift Space

clustering in redshift-space is anisotropic!

Anisotropy has info on velocities, thus gravity

Fig. by Eyal Kazin

An exact relationship between real and redshift-space clustering:

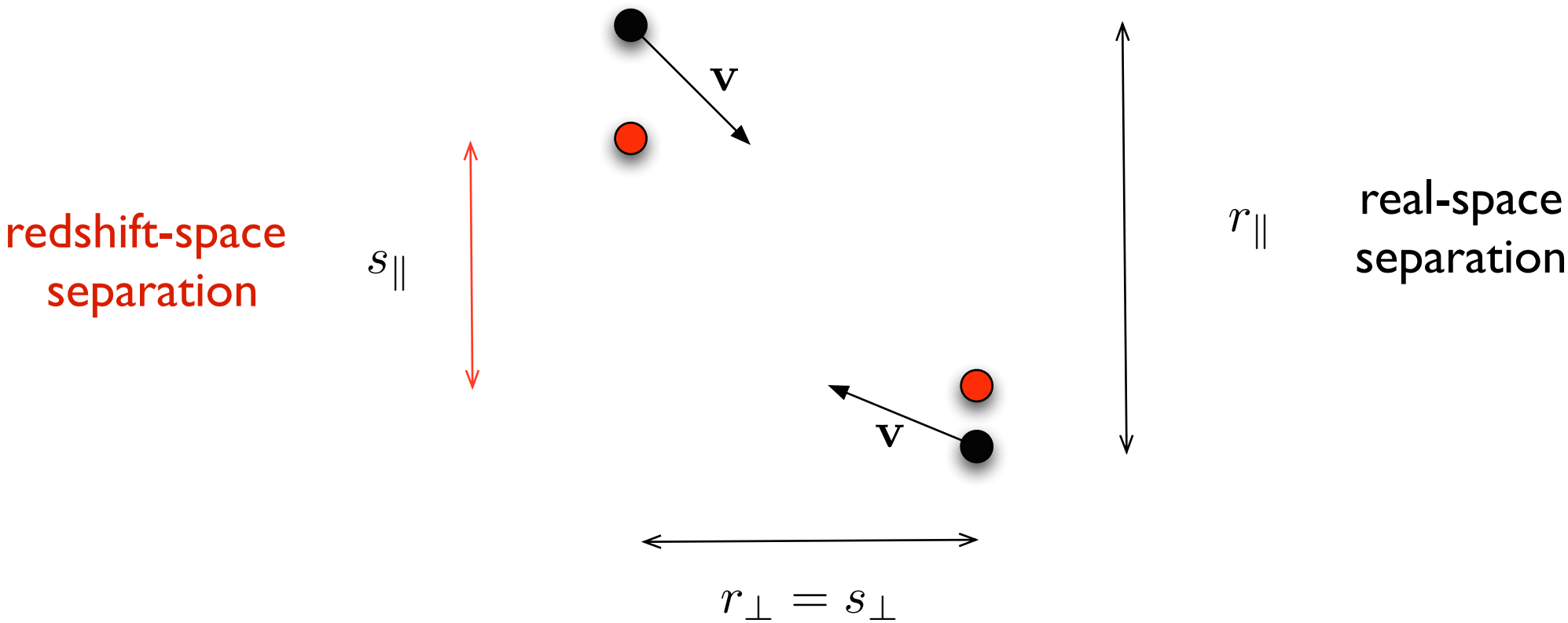

$$1 + \xi_s(s_\parallel, s_\perp) = \int_{-\infty}^{\infty} dr_\parallel \, [1 + \xi(r)] \, \mathcal{P}(\underbrace{r_\parallel - s_\parallel}_{\mathbf{v}_p}, \mathbf{r}),$$

R.S. (2004)

Everything is encoded in the pairwise velocities PDF.

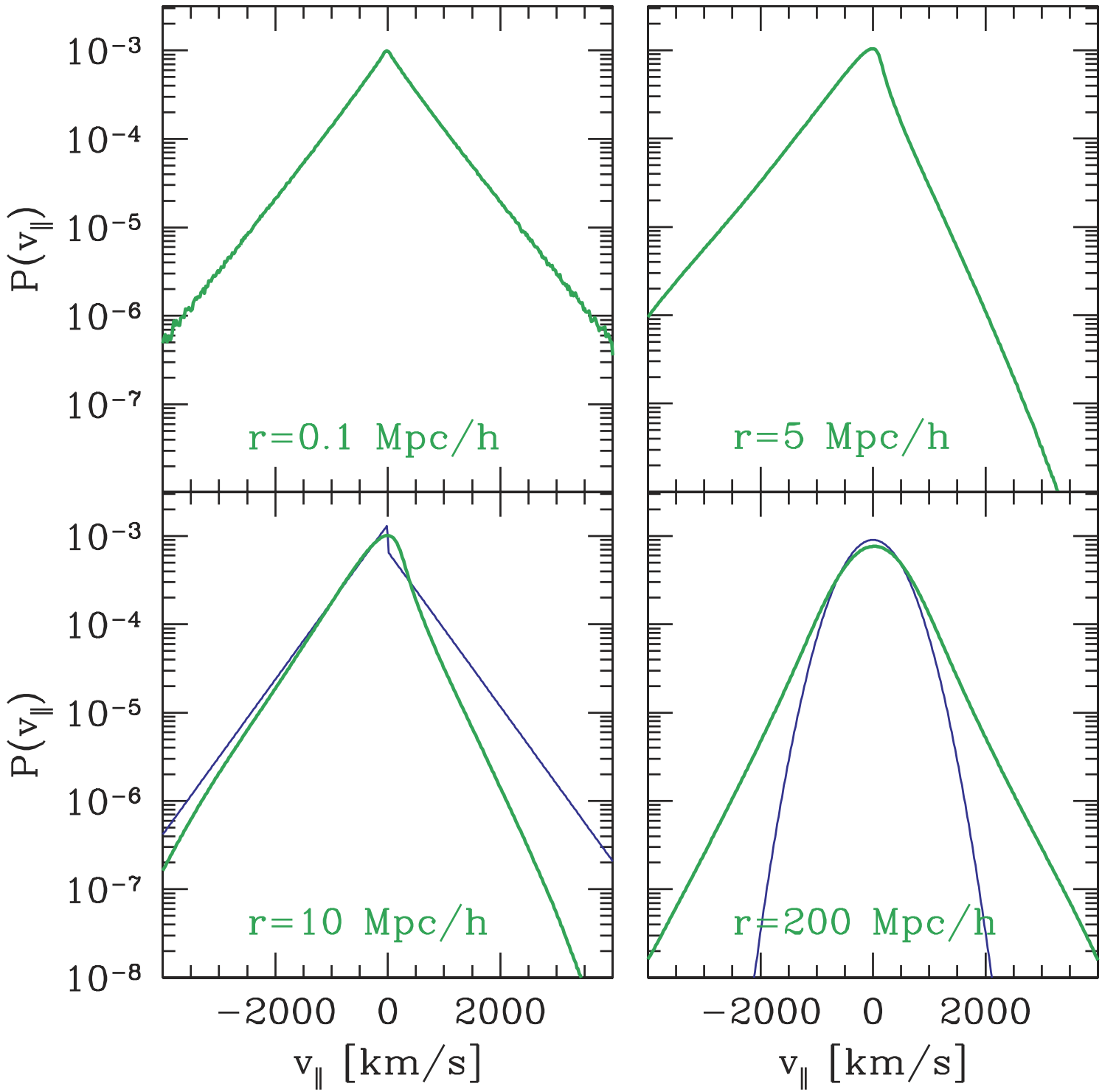
10^{-3}
10^{-4}
10^{-5}
10^{-6}
10^{-7}
10^{-8}
$P(v_\parallel)$
r=0.1 Mpc/h
r=5 Mpc/h
r=10 Mpc/h
r=200 Mpc/h
−2000
0
2000
$v_\parallel$ [km/s]

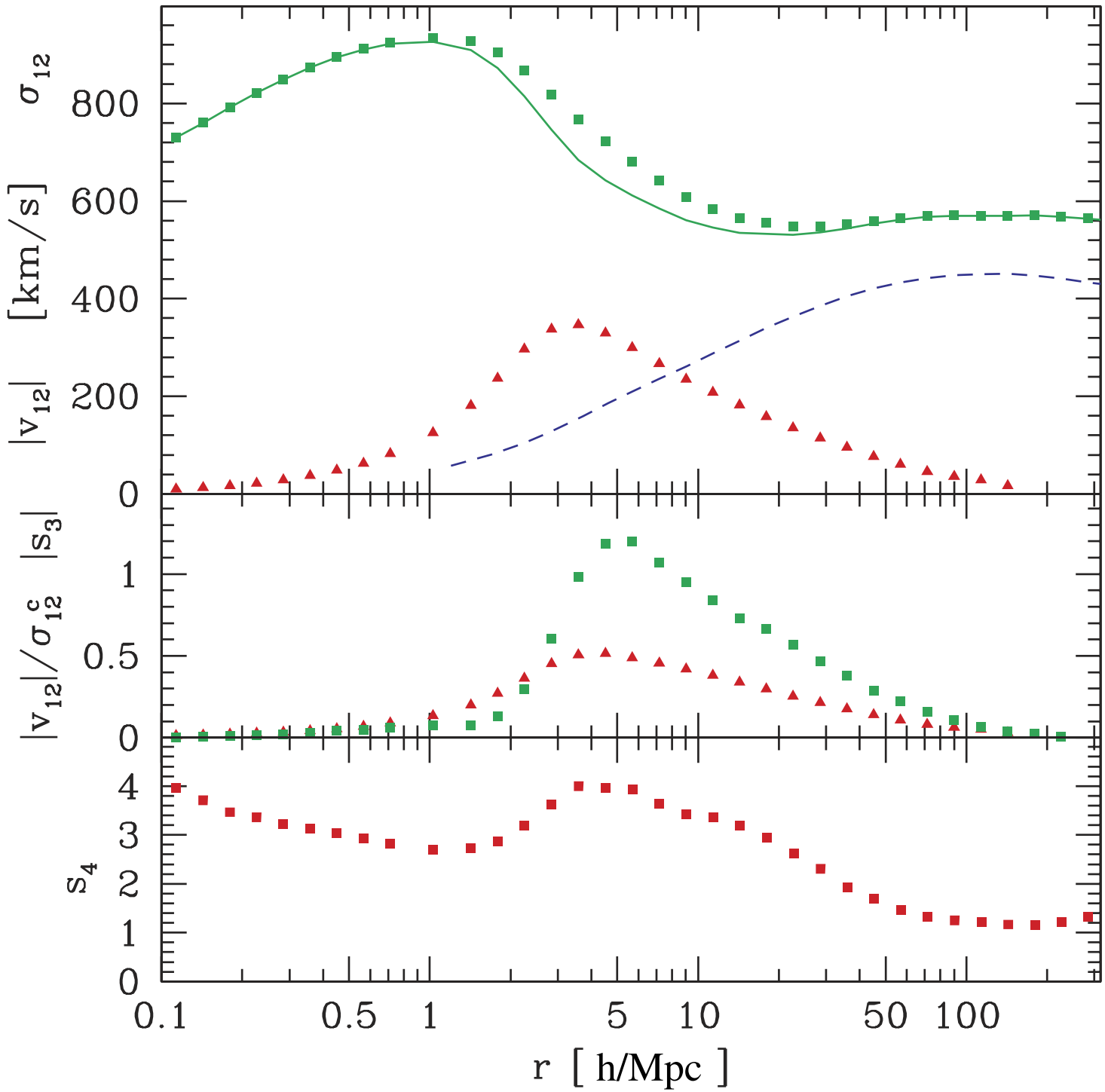
σ_{12}
$|v_{12}|$ [km/s]
800
600
400
200
0
$|s_3|$
$|v_{12}|/\sigma_{12}^c$
1
0.5
0
s_4
4
3
2
1
0
0.1
0.5
1
5
10
50
100
r [h/Mpc]

These are incorporated into the so-called "dispersion model", for the power spectrum,

$$P_s(k,\mu) = P_g(k)\ (1+\beta\mu^2)^2\ \frac{1}{1+k^2\mu^2\sigma_p^2/2},$$

which is used to constrain cosmological parameters from redshift surveys. Anisotropy depends on degenerate combination, at large scales

$$\beta = \frac{f}{b_1}, \qquad k\mu = k_z, \qquad \sigma_p^2 = \text{pairwise velocity dispersion}$$

- f is the most interesting part: it depends on gravity (but not only!), e.g.

$$f = \Omega_m^\gamma, \qquad \gamma \approx 0.56\ (\text{GR}),\ 0.68\ (\text{DGP})$$

- b1 is the linear bias (that relates matter to galaxy clustering). From latest BOSS data, after using CMB, f=0.41+-0.03 (z=0.57) consistent with LCDM+GR: f =0.45+-0.02 (Reid et al 2012)

Redshift-space power spectrum contours

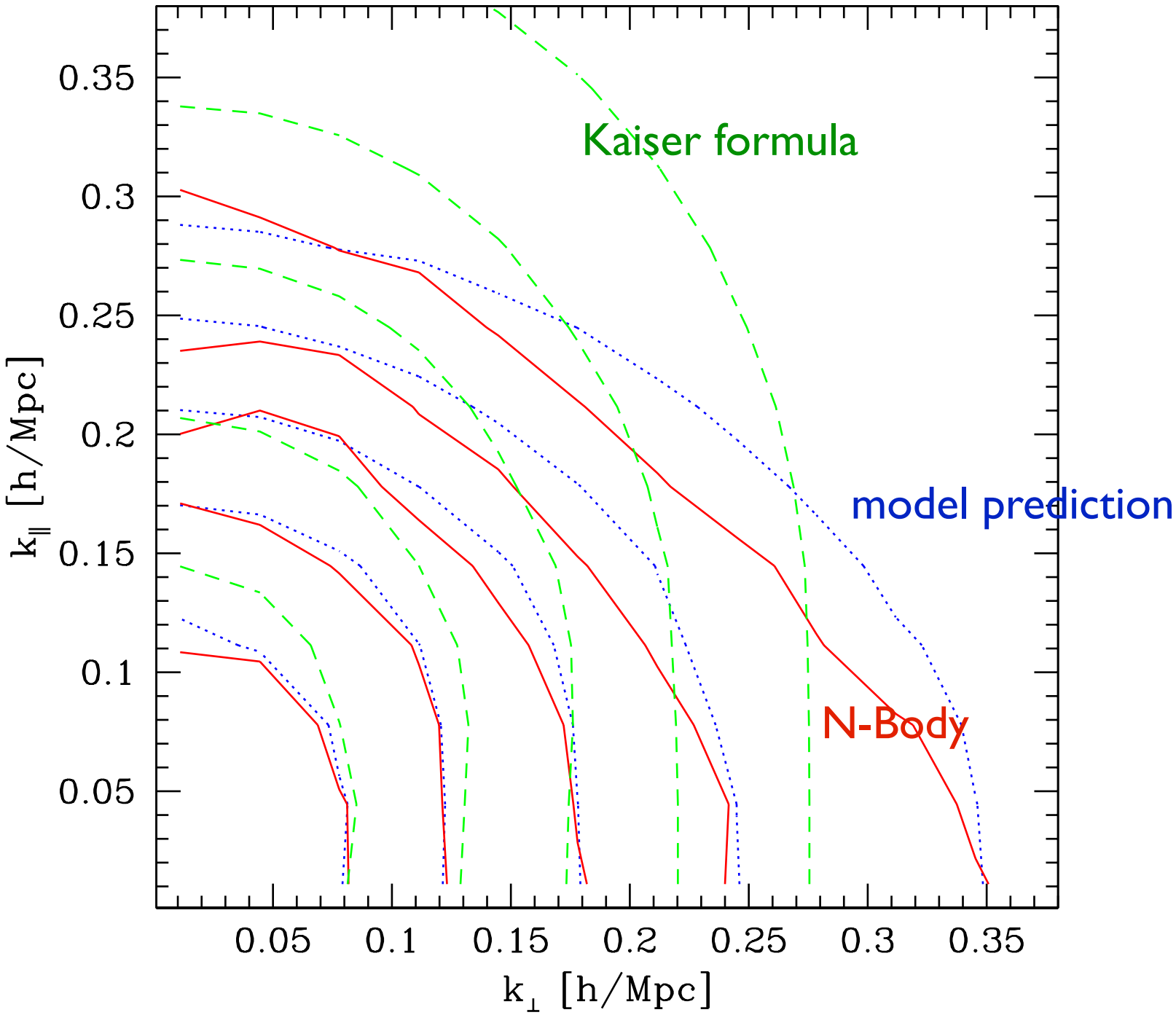

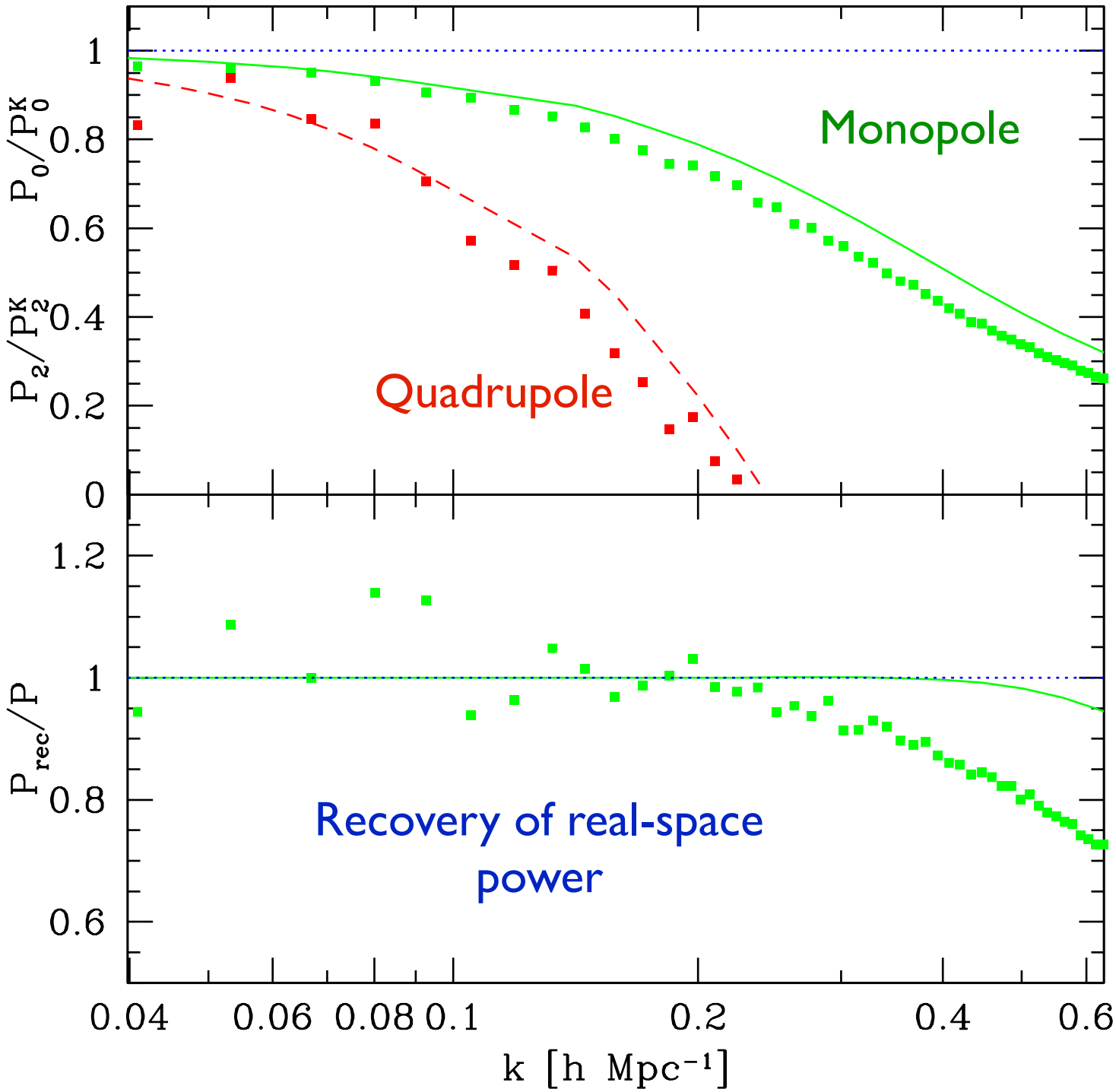
Monopole
Quadrupole
Recovery of real-space power
P_0/P_0^K
P_2/P_2^K
P_{rec}/P
k [h Mpc^{-1}]
0.04
0.06
0.08
0.1
0.2
0.4
0.6
0
0.2
0.4
0.6
0.8
1
1.2

effect of redshift-space distortions on higher-order moments